Master's thesis

NTNU
Norwegian University of Science and Technology
Faculty of Engineering
Department of Civil and Environmental Engineering

Diponkar Adhikari

Establishing Methodologies for Seismic Design in Norway

Master's thesis in Geotechnics and Geohazards
Supervisor: Gudmund Reidar Eiksund
June 2023

NTNU
Norwegian University of
Science and Technology

Diponkar Adhikari

Establishing Methodologies for Seismic Design in Norway

Master's thesis in Geotechnics and Geohazards
Supervisor: Gudmund Reidar Eiksund
June 2023

Norwegian University of Science and Technology
Faculty of Engineering
Department of Civil and Environmental Engineering

NTNU
Norwegian University of
Science and Technology

Preface

The master's thesis was done at the Norwegian University of Science and Technology's (NTNU), Department of Civil and Environmental Engineering as a requirement for a master's degree in geotechnics and geohazards. The thesis is credited worth 30 ECTS and was performed over a period of 28 weeks in the spring semester of 2023. The thesis is related to seismic design methodologies used in Norway. The problem was formulated by numerical simulation using PLAXIS 2D and DEEPSOIL, supplemented by design guidelines Eurocode 1998-1 and 5.

_____

Diponkar Adhikari

Trondheim, 29 June 2023

Acknowledgment

I want to start by expressing my gratitude to my wife Pushpa for being with me in all my hardships, joys, and some irrational outbursts while studying.

I would like to express my sincere gratitude to my supervisor, Gudmund R. Eiksund for his technical advice, continuous support and professional support throughout the period of thesis and my specialization project. Additionally, he has been patiently guiding me and has always made the effort to respond to my inquiries.

I would also like to thank everyone for all the assistance I got throughout the process. Finally, many thanks to my family and friends for their continued support and love during this period.

Abstract

The seismic response of a structure situated on soil with relatively low stiffness is influenced by the material properties of the soil and the type of foundation employed, such as shallow or deep foundations. This thesis aims to assess the response of soil type designated as S_1 as per Eurocode 8-1 to various recorded time histories, scaled to recommended ground acceleration, and evaluate the soil-structure interaction at the same ground condition. The shear force induced at the shallow and pile foundation is determined using the finite element program PLAXIS 2D and Eurocode and compared. This study aims to perform a site response analysis of the site and perform soil-structure interaction on the same site considering shallow and deep foundations.

A representative soil model is constructed with appropriate boundary conditions. For dynamic analysis in PLAXIS 2D, a soil column has been adopted for site response, while a full-scale model of size 150m x 25 is used for seismic analysis on foundations. The choice of boundary condition was based on an extensive literature review, previous experiments, and tests performed during the thesis where input motion and motion registered at the model's base were tallied. The site response analysis was performed on three input motions; Imperial Valley, Friuli, and Nahanni, which were scaled as per recommendations. The results from PLAXIS were compared to a one-dimensional response analysis from DEEPSOIL, and an agreeable observation was noted.

The soil model is then used for free vibration analysis of the buildings considered in the study. The results from PLAXIS and theoretical solutions were tallied and later confirmed with Eurocode, all in tandem with each other. Results from dynamic analyzes show that in all cases of the input motion, the choice of foundation type significantly influences the base shear registered in PLAXIS 2D. The base shear and shear forces on piles are more than when a pile foundation is used, highlighting the need for better design guidelines, as piles could lead to fatal design scenarios. However, it should also be noted that since Eurocode estimations of base shear were extremely high or rather conservative, risk could be somewhat averted. Yet again, in the case of shallow foundations, the results proved that Eurocode overestimated the base shear by three times, leading to extremely uneconomical designs. Likewise, parametric studies performed on the soil strata proved that the ground response was not dependent on the thickness of soil clay or stiffness of stiff clay beneath the soft clay.

Table of Contents

List of Figures

List of Tables

Abbreviations

α	Rayleigh co-efficient
α	Normalized side friction of clay
β	Rayleigh coefficient
β	Lower bound factor for horizontal spectrum design
γ	Shear strain
$\gamma 1$	Seismic class
δ	Logarithmic decrement
δt	Time discretization
η	Viscosity
η	Modification factor
ν	Poisson's ratio
ξ	Damping ratio
ρ	Density
$\sigma 1'$	Major effective principal stress
$\sigma 3'$	Minor effective principal stress
σv	Vertical effective stress
τ	Shear stress
φ	Friction angle
ψ	Dilatancy angle
ω	Angular frequency
a	Attraction
ag	Ground acceleration
agR	Reference peak ground acceleration
A	Cross-sectional area of pile
c	Cohesion
C	Damping matrix
cu	Undrained shear strength
D	Diameter of pile
E	Young's modulus
Ed	Dissipated energy
E50	Triaxial stiffness

E_{oed}	Oedometer modulus
E_{ur}	Unloading/reloading stiffness
EA	Axial stiffness
EI	Inertial stiffness
f	Frequency
f_n	Natural frequency
F_b	Base shear
F_{max}	Maximum tip resistance of pile
g	Acceleration due to gravity
G_0	Shear modulus for small strain
G	Shear modulus
G_s	Secant shear modulus
G_t	Tangential shear modulus
G_{ur}	Unloading/reloading shear modulus
G*	Complex shear modulus
I	Moment of inertia
k*	Complex wave number
K	Stiffness matrix
$l_{spacing}$	Out of plane spacing of the piles
m	Mass
M	Mass matrix
n	Number of nodes
P_u	Later skin resistance of pile
q	Behavior factor
r	Roughness ratio
R_S	Axial spring stiffness
S	Soil factor
S_D	Maximum deformation
S_A	Pseudo acceleration
SV	Pseudo velocity
S_d (T)	Design elastic response spectra
T	Period of vibration

T_d	Damped natural period
T_n	Natural period of vibration
T_{skin}	Axial skin resistance of pile
T_{lat}	Lateral resistance of pile
V_S	Shear wave velocity
$V_{S,30}$	Shear wave velocity of uppermost 30m
z	Depth

1 INTRODUCTION

On a global scale, Norway is categorized as an area with low to intermediate seismic activity. Based on historical data, NORSAR has determined that earthquakes with a Richter magnitude of 5 or greater have a return period of 10 years. Earthquakes of six or higher magnitude are expected to occur once every 100 years. The updated design code has been formulated concerning a seismic event of magnitude 6.5 on the Richter scale and incorporates a 10% probability of surpassing a 50-year threshold, yielding a recurrence interval of 475 years.

Presently, numerous design instances in Norway seem to be primarily influenced by seismic loads instead of conventional wind and misalignment stresses. In 2010, Norway implemented the Eurocode 8 design standard, which comprehensively covers seismic action design, incorporating relevant national values. In cases where earthquake hazards and structure types require earthquake design, it would be advantageous to employ modeling and analytical methodologies that effectively depict the structural characteristics (Rønnquist et al., 2012).

Enhancing structural design reliability was among the driving factors behind developing the updated standards in 2004. This encompassed both updated load factors and modified load actions. Incorporating a seismic action component into the structural design guidelines for low seismic regions like Norway represents a novel development relative to previous design codes. Incorporation of the low-probability load action into the design requirements can facilitate the accommodation of significant structural damage. This design type can be used in conjunction with rigorous analysis for structural engineering purposes. The seismic measures employed in Norway are designed to guarantee that newly constructed edifices can endure earthquakes measuring at least 6.5 on the Richter magnitude scale. Thus far, the prevailing trend in Norwegian design practice seems to prioritize the creation of non-dissipative structures rather than exploring the potential of dissipative systems within the medium ductility classification (Rønnquist et al., 2012)

Eurocode 8 offers streamlined seismic design and computations methodologies, rendering it appropriate for implementation by a wide range of designers. Eurocode 8, in contrast to other codes, adopts a simplified approach and tends to prioritize overstrength in its design methodology. Despite the availability of advanced analytical techniques, options for their implementation are seldom exercised in the design field owing to the employment of rudimentary guidelines. This, in turn, results in substantial heterogeneity in the documentation of seismic design practices across the industry.

1.1 Problem Formulation

Norway adheres to the Eurocode 8-1 and 8-5 regarding seismic design and dimensioning and is complemented by its own Norwegian National Annex, which addresses the local conditions. Due to strict guidelines and rules, there are few options for innovative design thinking regarding seismic design. Almost all the ground types are assigned specific design values; thus, there is little to explore apart from ground type S_1 and S_2, which requires particular site investigation and analysis.

This might be of interest as local site conditions within Norway can match particular soil types. This thesis analyzes models with soft clay that match ground type S_1. The EN 1998-1:2004, 3.1.2(4)P mentions that special attention is required for ground type S_1, as they have low shear wave velocity values, low internal damping, and an abnormally extended range of linear behavior. It could lead to extreme seismic site amplification and soil-structure interaction effects.

Thus, the thesis will investigate the dependence of the response spectrum on the thickness and shear wave velocity of the soft clay/silt layer and the stiffness difference between this layer and the underlying layer. Along with that, the evaluation of directly grounded and embedded foundations in such soil.

1.2 Research Questions

The seismic design protocols for diverse geotechnical constructions in Norway are established per Eurocode8. However, these guidelines are somewhat rudimentary and oversimplified. Consequently, the master's thesis must address the research inquiries formulated after a comprehensive review of the literature:

a) What is the soil's capacity to absorb or amplify seismic load?
b) What is the soil structure interaction is sites with soil type S_1?
c) What are the differences in foundation constructions directly grounded and embedded deep in the soil (pile)?

1.3 Research Objectives

The objectives of the study are listed below, out of which the first two are the main objectives:

1. Evaluate the soil's capacity to damp or amplify and soil structure interaction effects
2. Perform the above evaluations for directly grounded foundations and foundations embedded

deep in the soil.

3. Perform a parametric study of soil strength and stiffness for seismic design for soil type S1
4. Calculate base shear forces of shallow foundation and raft-pile foundation

1.4 Approach

This study aims to employ the Finite Element Methods, which are widely accessible, to analyze models and attain the study's objectives. The study aims to quantitatively validate these objectives using alternative analytical or numerical methods in all scenarios, such as theoretical and analytical solutions, and software such as DEEPSOIL. Initially, a numerical analysis will be performed on the Finite Element Method (FEM). Subsequently, assuming its validity, additional analytical or numerical techniques will be employed to corroborate the findings.

1.5 Research Boundaries

As delineated in the preceding section, this thesis aims to perform seismic response analysis on ground type S_1 and structures with shallow and deep foundations. The study of earthquakes encompasses a wide range of subjects, with Eurocode 8 providing a comprehensive framework for consideration. Establishing a boundary is crucial in light of practical limitations, such as time constraints. Furthermore, it is essential to acknowledge the presence of various assumptions and limitations in the calculations that require discussion. The primary research constraints are enumerated as follows:

1. This thesis uses only three recommended input motions for earthquake analysis and one soil type. More input motions would be suitable when analyzing such critical soil conditions.
2. The pile foundations are modeled as 2D elements using embedded beam row elements, assuming they are elastic.
3. Liquefaction and ground water flow have not been taken into account.
4. In a plain-strain PLAXIS model, geometric damping is avoided, and Rayleigh damping has been utilized.
5. All the structural elements are elastic.
6. The soil layers have been reduced to two such that soil material parameters represent a particular soil condition. This simplifies the analysis but might not be entirely realistic.

1.6 Thesis Outline

The thesis consists of six chapters, which are as follows:

Chapter 1 - Introduction: The chapter overviews the research topic and its significance. It outlines the comprehensive overview of the thesis. The text includes the background, problem formulation, research questions, objectives, approach, and constraints.

Chapter 2 – Literature Review: The chapter provides a concise overview of the pertinent literature and prior research that has been examined to conduct the analysis. The examination of existing literature can be categorized as scholarly literature about the field of geotechnical earthquake engineering, existing literature, and research regarding the finite element analysis method and associated software program and Eurocode 8 that has been utilized as the basis of the analysis.

Chapter 3 - Methodologies: This chapter provides an overview of the model construction process in PLAXIS and DEEPSOIL and the material properties of soil and structural components utilized for simulating the problem. This part outlines the methodology for constructing a detailed model for dynamic analysis.

Chapter 4 - Results: This section presents the results obtained from all the analyses. The analyses can be categorized as site response analysis, analysis of free vibration, analysis of seismic response, and determination of shear force and parametric studies. The findings from each section are discussed.

Chapter 5 - Discussion and Conclusion: In this chapter, a comprehensive overview, analysis, and conclusion of the thesis are presented, focusing on the attainment of its stated objectives.

Chapter 6 - Recommendations for Future Research: This chapter discusses the recommended areas for further study.

2 LITERATURE REVIEW

2.1 Geotechnical Earthquake Engineering

Tectonic forces give rise to fractures in the earth's crust, resulting in seismic activity known as earthquakes. The immense forces are responsible for forming mountains, valleys, ridges, and oceans. The movement of tectonic plates in the Earth's crust generates elastic stresses in the bedrock, which can lead to the development of fractures in areas of geological weakness when the rock's capacity to withstand these stresses is exceeded. The process of fracturing alleviates the significant quantity of elastic strain energy accumulated within the rocks in the Earth's crust. In addition, energy propagation occurs as a wave directed towards the Earth's surface originating from the fault, ultimately resulting in seismic activity. The seismic waves generated by earthquakes induce ground motion and stimulate surface structures. Therefore, it is crucial to utilize various analytical methods to comprehend and assess the characteristics to mitigate the risk of structural failure caused by seismic activity (Aki, 1972).

2.1.1 Seismic Wave Propagation

Various seismic waves are generated by the fault located beneath the Earth's surface, including body and surface waves. Body waves propagate through the interior of the Earth and can be classified into two distinct categories: primary waves (P-waves) and secondary waves (S-waves). The illustration depicted in Figure 1 exhibits p-waves, which are commonly referred to as primary or longitudinal waves. These waves propagate through both solids and fluids, much like sound waves. In contrast, S-waves are classified as secondary or transverse waves. S-waves induce shear deformations in materials and propagate in vertical and horizontal planes. However, due to the negligible shear deformation of fluids, these waves cannot propagate through them. Furthermore, the geological substances exhibit rigidity under compression, and p-waves indicate greater velocity than s-waves.

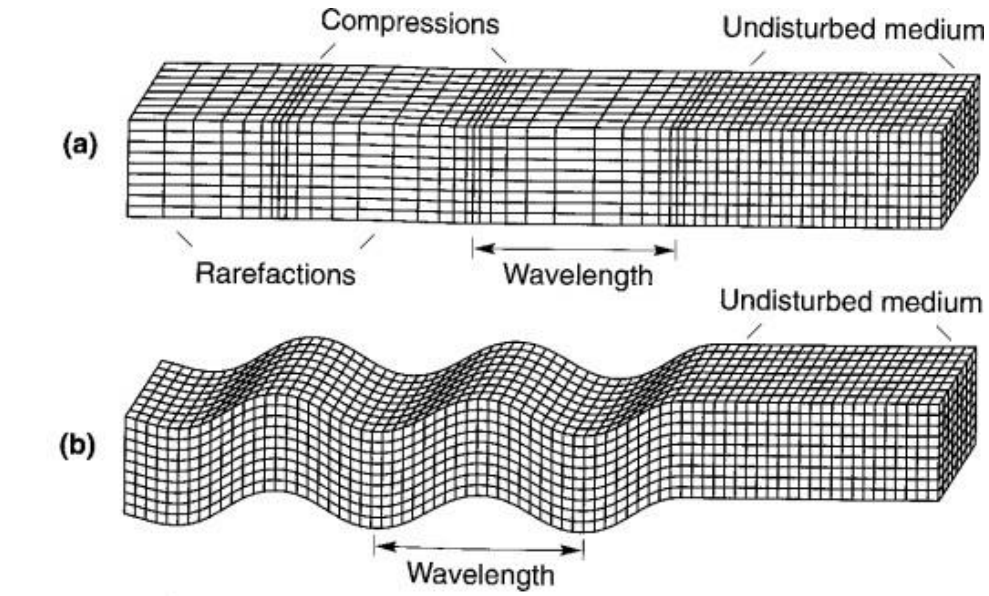

Figure 2- 1 Deformation due to body waves: a) p-waves and b) s-waves (Kramer, Geotechnical Earthquake Engineering, 1996)

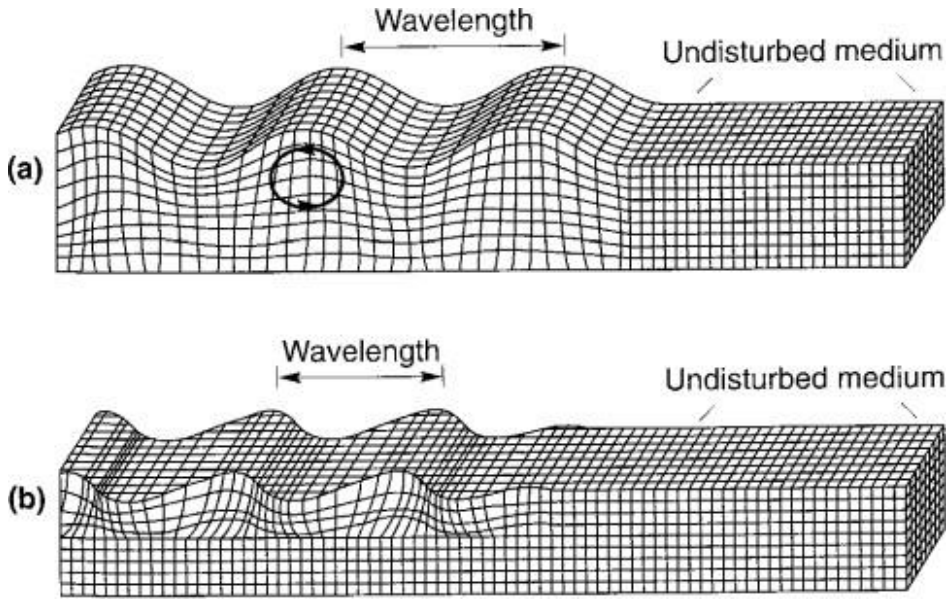

Figure 2- 2 Deformations due to surface waves: a) Rayleigh wave and b) Love wave (Kramer, Geotechnical Earthquake Engineering, 1996)

Surface waves arise due to the interplay between body waves and the surface strata of the earth, and their magnitude diminishes approximately with increasing depth. In earthquake designs and analysis, the two types of surface waves typically considered are Rayleigh waves and Love waves. Rayleigh waves are generated through the surface interaction of p-waves and the vertical component of s-waves with the earth's crust. Love waves are caused by the interaction

between the horizontal component of s-waves and the soft surface of the Earth (Kramer, Geotechnical Earthquake Engineering, 1996).

2.1.2 Boundary Effect on Wave Propagation

Comprehending the behavior of body waves as they propagate through heterogeneous media, such as soil with multiple subsurface layers, is a fundamental requirement. The impact of boundaries on the incident body waves is crucial owing to the potential amplification response that may manifest on the surface. The interface separating two distinct materials must adhere to two fundamental criteria, namely, the preservation of displacement continuity and the fulfillment of equilibrium:

$$A_I + A_R = A_T \tag{2. 1}$$

$$\sigma_I + \sigma_R = \sigma_T \tag{2. 2}$$

AI, AR, and AT are displacement amplitudes of the incident, reflected, and transmitted waves, respectively, and σ_I, σ_R, and σ_T are stress amplitudes of the incident, reflected, and transmitted waves, respectively. Now through the compatibility and equilibrium conditions:

$$A_R = \frac{1-\alpha_z}{1+\alpha_z} A_I, \sigma_R = \frac{\alpha_z - 1}{\alpha_z + 1}\sigma_I \tag{2. 3}$$

$$A_R = \frac{1-\alpha_z}{1+\alpha_z} A_I, \sigma_R = \frac{\alpha_z - 1}{\alpha_z + 1}\sigma_I \tag{2. 4}$$

$$A_T = \frac{2}{1+\alpha_z} A_I, \sigma_T = \frac{2\alpha_z}{\alpha_z + 1}\sigma_I \tag{2. 5}$$

$$\alpha_2 = \frac{\rho_2 v_2}{\rho_1 v_1} \tag{2. 6}$$

The equations above delineate the impedance ratio, the proportion between the product of density and wave velocity of two successive layers of material that the waves traverse. A significant impedance ratio would result in a clamped boundary condition, resulting in zero displacement amplitude at the boundary and a doubling of the stress. Similarly, a state of zero impedance denotes a free boundary, resulting in a complete dissipation of stresses and a twofold increase in displacement amplitude. This phenomenon is of utmost significance as most structures are on free surfaces. Usually, propagating waves come across a boundary that is not perpendicular, resulting in a modification of the wave's type and a change in the direction

of both reflected and transmitted waves. Empirical observations have indicated that seismic activity originating from a fault undergoes refraction towards a near-vertical propagation path due to increased wave velocity as depth increases. This phenomenon serves as a fundamental principle for various forms of site response analysis (Kramer, Geotechnical Earthquake Engineering, 1996).

2.1.3 Earthquake Excitation

The equation of motion for the multi-degree of freedom (MDOF) system is shown in the equation below:

$$m\ddot{u} + c\dot{u} + ku = p(t) \tag{2.7}$$

The system under consideration involves the mass matrix denoted by m, the damping matrix denoted by c, and the stiffness matrix denoted by k. Additionally, the system is subject to external excitation, p(t), while the acceleration, velocity, and displacement of the system are represented by $\ddot{u}$, $\dot{u}$, and $and\ u,$ respectively (Chopra A. K., 1995).

The occurrence of an earthquake results in the initiation of motion at the base of the system. This motion denoted as $\ddot{u}_b(t)$, induces acceleration to the system, in conjunction with the acceleration stemming from the relative motion between the ground and the structure, u(t) (Chopra A. K., 1995). Thus, we get a total acceleration to the system given by:

$$\ddot{u}_t(t) = \ddot{u}(t) + \ddot{u}_b(t) \tag{2.8}$$

The equation of motion for the system becomes:

$$\boldsymbol{m\ddot{u}} + \boldsymbol{c\dot{u}} + \boldsymbol{ku} = -\boldsymbol{m\ddot{u}}_b(t) \tag{2.9}$$

2.1.3.1 Damping

Damping refers to the gradual reduction in the magnitude of free oscillations. To clarify, the energy of the oscillating system undergoes dissipation via one or more mechanisms (Chopra A. K., 2007). The equation involves the coefficient of damping denoted by c and the velocity function represented by u(t). Rayleigh damping is a helpful method for measuring damping in dynamic analysis. This approach combines the damping effect with the mass and stiffness of the system, resulting in a simplified measurement. The damping matrix C, according to

Rayleigh, comprises the α component of the mass matrix M and the β component of the stiffness matrix K. The formula can be expressed as follows, wherein α and β denote the Rayleigh coefficients (Bentley, 2022)

$$[c] = \alpha[M] + \beta[k] \tag{2.10}$$

The α parameter is a factor that considers the impact of mass on the damping of a given system. As the alpha value increases, lower frequencies experience greater damping. The β parameter is a factor that incorporates the impact of stiffness on the damping characteristics of the system. As the value of beta increases, a greater number of higher frequencies experience damping. The damping measurement is conducted considering both material and geometric damping, which is quantified by the damping ratio ξ. The values of coefficient α and β can be derived from the given equation, which is dependent on the damping ratio ξ and the angular frequency of vibration ω.

$$\alpha + \beta\omega_i^2 = 2\omega_i\xi_i \tag{2.11}$$

This equation's resolution can be achieved by establishing a minimum of two objective frequencies that correspond to two distinct damping ratios.

$$\alpha = \frac{2\omega_1\omega_2(\omega_1\xi_2 - \omega_2\xi_1)}{\omega_1^2 - \omega_2^2} \tag{2.12}$$

$$\beta = \frac{2(\omega_1\xi_2 - \omega_2\xi_1)}{\omega_1^2 - \omega_2^2} \tag{2.13}$$

Various authors have proposed distinct approaches for determining suitable Rayleigh parameters. The literature review will present the methodology proposed by (Hudson et al., 1994). The initial target frequency pertains to the mean inherent frequency of the soil deposit, while the subsequent target frequency corresponds to the next odd integer of the ratio between the fundamental frequency of the input motion and the natural frequency of the soil. Beyond this specific range, the input signal exhibits overdamped behavior. The inherent frequency of the soil can be expressed as:

$$f_1 = \frac{v_s}{4H} \tag{2.14}$$

Where, v_s is the shear wave velocity of the soil, and H is the thickness of the soil layer.

As seismic waves propagate through a soil system, a portion of their energy is dissipated. A soil-structure system's damping characteristics impact its response's shape and magnitude. Even minor deformations can cause irreversible changes in the behavior of soil. Damping is a phenomenon that arises due to multiple contributing factors. Several factors have been identified by (Kramer, Geotechnical Earthquake Engineering, 1996).

- Damping due to soil radiation
- Damping at the interface of soil and structure
- Damping due to soil material property (stiffness/ strength properties)
- Refraction

2.1.3.2 Free Vibration

Free vibration of a structure is defined as the occurrence in which the system undergoes disturbance from its static initial state due to an external load and subsequently experiences free vibration without any external intervention. This provides a foundation for ascertaining the inherent frequency of oscillation and level of damping exhibited by a single degree of freedom (SDOF) system (Chopra A. K., 2007).

In the case of a single-degree-of-freedom structure with viscous damping and no external load, equation (2.7) can be expressed as follows:

$$m\ddot{u} + c\dot{u} + ku = 0 \tag{2.15}$$

Also,

$$\ddot{u}(t) + \omega_n^2 u(t) + 2\xi\omega_n \dot{u}(t) = 0 \tag{2.16}$$

Here, natural frequency, $\omega_n = \sqrt{\frac{k}{m}}$ and damping ratio, $\xi = \frac{c}{c_{cr}} = \frac{c}{2m\omega_n}$, c_{cr} is the critical damping coefficient of the system. When $\xi \geq 1$, the system does not oscillate long and returns to the initial state, but when ξ<1, the system oscillates and returns to the original state with a gradual amplitude decline. This is an underdamped system, and this replicates almost all of the structural systems.

The natural period of the damped system T_D is related to the natural period T_n as:

$$T_D = \frac{T_n}{\sqrt{1-\xi^2}} \tag{2.17}$$

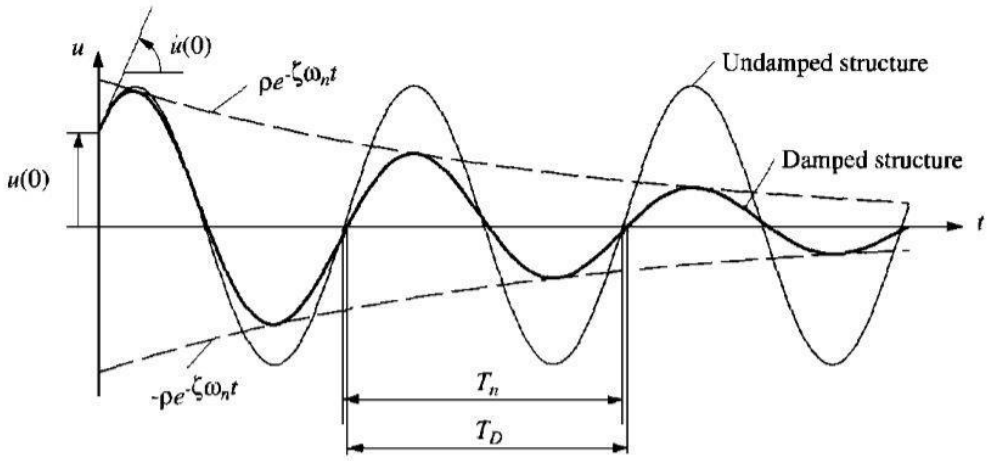

Figure 2- 3 Damping effect in free vibration

The relation can further be used to find the undamped natural period by determining logarithmic decrement, δ using the logarithmic ratio of two successive peaks as shown in the relation below:

$$\delta = \ln\frac{u_i}{u_i + 1} = \frac{2\pi\xi}{\sqrt{1-\xi^2}} \tag{2.18}$$

Then over n cycles, the displacement decreases gradually from u_1 to u_{n+1} then the equation above becomes:

$$\delta = \frac{1}{n}\ln\frac{u_1}{u_{n+1}} \cong 2\pi\xi \tag{2.19}$$

2.1.3.1 Fourier Transformation

The seismic activity within the earth is characterized by non-periodic and transient vibrations, commonly referred to as earthquake motion. To derive the seismic response of the ground to an earthquake, it is necessary to formulate the beats in a manner that facilitates linear analysis. The Fourier transformation is a commonly used tool for this purpose.

The Fourier transform converts a signal, p(t), to a series of harmonic functions that constitutes

the initial signal.

$$\hat{p}(\mathrm{i}\omega) = F[p(t)] = \int_{-\infty}^{\infty} \mathrm{e}^{\mathrm{i}\omega t}\ p(t)dt \tag{2.20}$$

The above equation shows the first step, where $\hat{p}(\mathrm{i}\omega)$ is the amplitude of the harmonic signal for a given frequency.

The determination of the system response is carried out in the frequency domain, where each frequency û(iω) is evaluated based on the $\hat{p}(\mathrm{i}\omega)$ functions. The temporal response can be obtained by performing inverse integration of the frequency response over all frequencies, as illustrated in the following equation:

$$u(t) = \frac{1}{2\pi}\int_{-\infty}^{\infty} H(\mathrm{i}\omega)\hat{p}(\mathrm{i}\omega)\mathrm{e}^{\mathrm{i}\omega t}p(t)\,\mathrm{d}\omega \tag{2.21}$$

The variable $H(\mathrm{i}\omega)$ represents the response of the system to a specific frequency of excitation. The equations presented pertain to the process of continuous Fourier transformation. However, it is worth noting that the discrete Fourier transformation is more commonly utilized, with the Fast Fourier Transform (FFT) being a popular algorithm for its computation (Chopra A. K., 2007).

2.1.4 Response Spectrum Analysis

Response Spectrum Analysis (RSA) is a valuable technique in earthquake engineering due to its implicit and filtered depiction of a potent ground motion. The RSA method is utilized to determine the ultimate response of a single-degree-of-freedom (SDOF) structure to a specific earthquake time history based on the structure's inherent natural period. The damping ratio-dependency of the response spectrum results in the production of varying spectra for different damping ratios (Chopra A. K., 1995). Figure 3 shows the mechanism of Response Spectrum Analysis, which shows the acceleration response spectrum obtained from the response analysis of five different SDOF systems (Kramer, Geotechnical Earthquake Engineering, 2014).

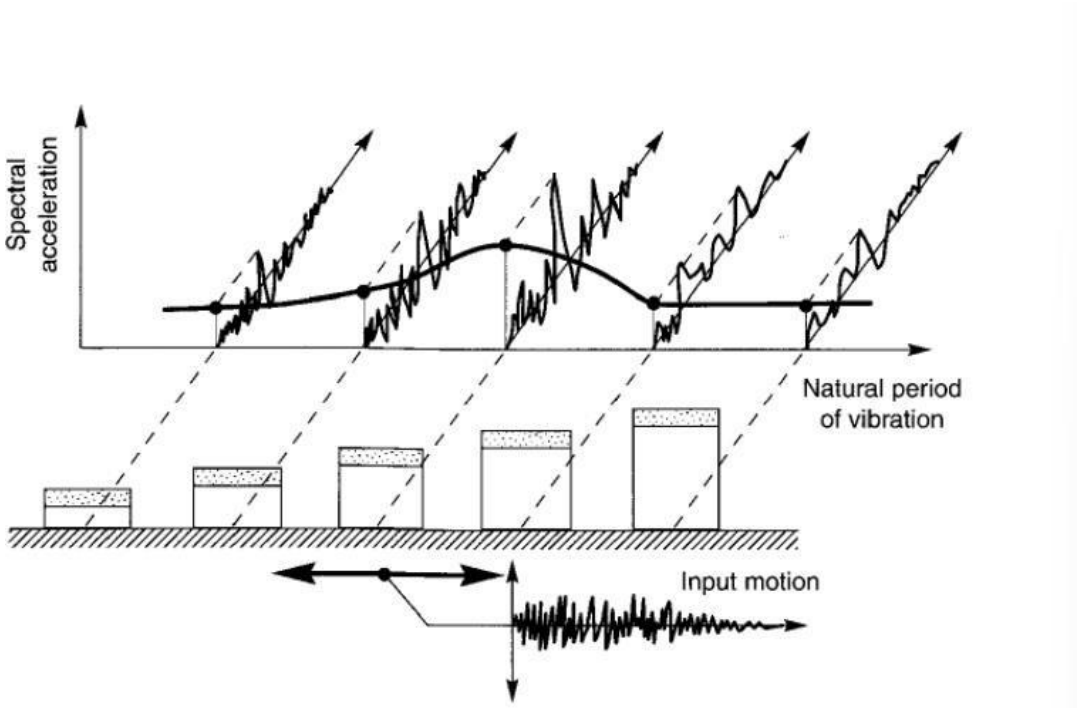

Figure 2- 4 Maximum acceleration amplitudes for different SDOF systems plotted versus natural period (Kramer, Geotechnical Earthquake Engineering, 2014)

The different kinds of response spectra used in the analysis are:

1. Deformation response spectrum, SD (T, ξ) = max |SD (t, T, ξ)|

The deformation response spectrum furnishes data for the computation of the maximum potential deformation SD (T, ξ)≡ u0 and inertial forces. The maximum static force is achieved by multiplying the maximum displacement and stiffness of the product.

2. Pseudo-velocity response spectra, Sv (T, ξ) = max |Sv (t, T, ξ)|

V is defined from the peak deformation of the linear elastic SDOF system with the natural frequency ω_n given by:

V = Sv (T, ξ) = ω_nSD (T, ξ) = $\frac{2\pi}{T_n}$ SD (T, ξ), and V is peak pseudo-velocity and gives maximum kinetic energy within the system for a mass, m, during an earthquake, E = $\frac{1}{2}m[S_v(T,\xi)]^2$.

3. Pseudo-acceleration response spectra, SA (T, ξ) = max |SA (t, T, ξ)|

A is defined from the peak deformation of the linear elastic SDOF system with the natural frequency ω_n, given by:

A = SA (T, ξ) = ω_n^2SD (T, ξ) = $\left(\frac{2\pi}{T_n}\right)^2$ SD (T, ξ), and A is peak pseudo-acceleration and gives

maximum base shear of the system for a mass, m, during an earthquake, V_b = mA= $\frac{1}{2}m[S_v(T,\xi)]^2$.

2.1.4 Earthquake in Norway

Norway is in a region characterized by low seismic activity, and no recent earthquakes of significant magnitude have resulted in substantial damage to buildings or structures. According to historical records, the earliest documented earthquake occurred in 1647, with its epicenter believed to have been situated in the outer Oslofjord region. The earthquake was estimated to have had a magnitude of 5 on the Richter scale. Seismic activity has been periodically documented; however, no noteworthy seismic event was recorded until 1904. Subsequently, a moderate-magnitude seismic event occurred in Oslo, causing structural harm to numerous edifices, and generating perceptible tremors throughout the Fjord region. The seismic event's magnitude was approximately 5.4 on the Richter scale (Molina & Lindholm, 2005). It has been evaluated that the area has the potential to experience an earthquake of magnitude six or higher based on seismic and tectonic analyses (Bungum et al., 2005). The seismic risk assessment of the Oslo region, the occurrence of an earthquake measuring six on the Richter scale in the vicinity of the eastern rift boundary fault near Oslo would damage 45% of the building mass (Molina & Lindholm, 2005). This is attributed to the existence of soft clays underlying the area. The damages do not encompass consequential impacts such as liquefaction that may have occurred after the earthquake.

Historically, building and structure designs in Norway have been optimized for wind and misalignment loads without incorporating the seismic design considerations recommended by Eurocode 8. Implementing seismic design legislation for existing buildings in Norway is not being considered due to its lack of economic feasibility (Rønnquist et al., 2012a).

2.2 Soil Parameters

The seismic analysis of soil necessitates the consideration of specific soil parameters, namely the cyclic undrained shear strength (τ_{cy}), the pore water pressure (u), and the small-strain shear modulus (G_{max}). Empirical evidence suggests that sand and silt exhibit undrained behavior under seismic loading conditions due to the rapid loading rate. The friction angle primarily determines the strength of large gravel and sand particles, while their drainage characteristics are also considered.

2.2.1 Cyclic Shear Strength

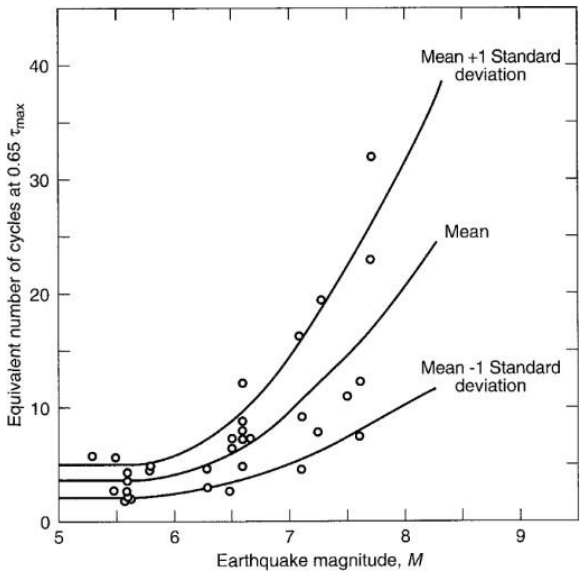

Figure 2- 5 Number of equivalent uniform stress cycles, Neq (Seed et al., 1975)

Determining the undrained shear strength for cyclic loading is contingent upon quantifying the equivalent number of shear stress cycles, denoted as N_{eq}. The determination of N_{eq} is frequently based on the magnitude of the predominant earthquake. The relationship between N_{eq} and the magnitude of an earthquake is illustrated in Figure 2-5 (Seed et al., 1975). The value of the constant stress is equivalent to 0.65 multiplied by the maximum shear pressure. The Figure estimates N_{eq}, which is determined to be 5, 10, and 15 for earthquakes measuring 6, 6.75, and 7.5, respectively. Numerous databases have been developed to document cyclic shear strength; however, it is imperative to establish empirical parameters for prevalent soil types.

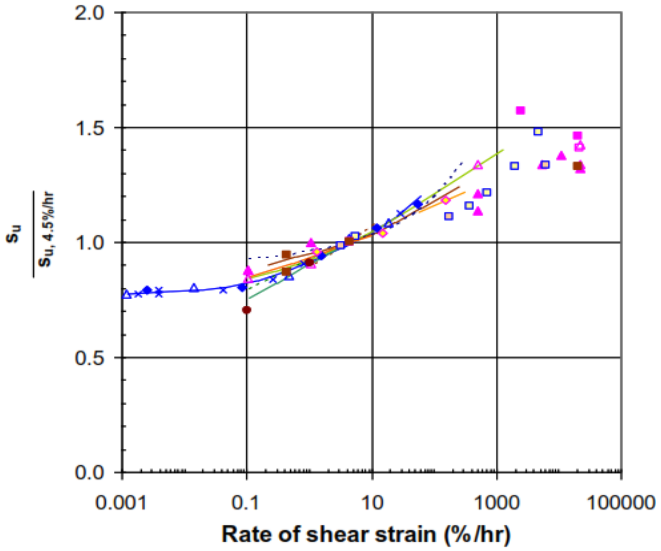

Figure 2- 6 Static shear strength of clays as a function of the rate of shear strain (Lunne & Andersen, 2007)

The loading rate appears to have no discernible impact on the behavior of frictional materials.

Nevertheless, clays' strength significantly rises as the loading rate increases. According to Lunne and Andersen's (2007) findings, a correlation exists between the static shear strength of various clays and the shear strain rate, as depicted in Figure 2-6. The seismic excitation typically observed in earthquakes, ranging from 0.5 to 1 Hz, has significantly enhanced the static shear strength of clay during seismic loading, with potential increases of up to 40%.

2.2.2 Small-strain shear modulus

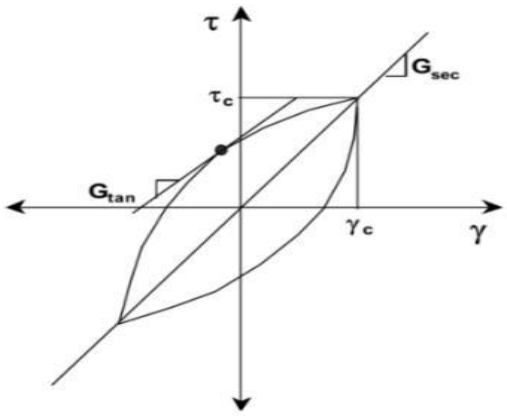

Figure 2- 7 Equivalent linear cyclic shear hysteresis (Kumar et al., 2013)

The shear modulus pertains to the capacity of soil to withstand shear deformation, as determined by the ratio of shear stress to shear strain. Soils undergo a cyclic shear when exposed to s-waves, which can be simplified using hysteretic loops, as illustrated in Figure 2-7.

The determination of shear stiffness can be achieved by calculating the inclination of the tangent to each point of the loop, denoted as G_T. However, for practical purposes, it is more advantageous to calculate the average shear stiffness per cycle by determining the inclination of the secant to the loop, denoted as G_S (Kramer, Geotechnical Earthquake Engineering, 1996). The fundamental principle behind the equivalent linear approximation of soil's non-linear response in the seismic analysis is the estimation of shear stiffness through the secant to the loop. However, in cases where significant deformations and plastic failures occur, utilizing an authentic hysteresis loop becomes necessary.

As illustrated in Figure 2-7, the secant shear stiffness decreases in value as the shear strain and number of cycles increase. By utilizing the backbone curve depicted in Figure 2-8a), one can determine the secant stiffness at the present shear strain. The gradual decline in the proportion of secant stiffness to maximum stiffness is illustrated in Figure 2-8b) as a modulus reduction curve.

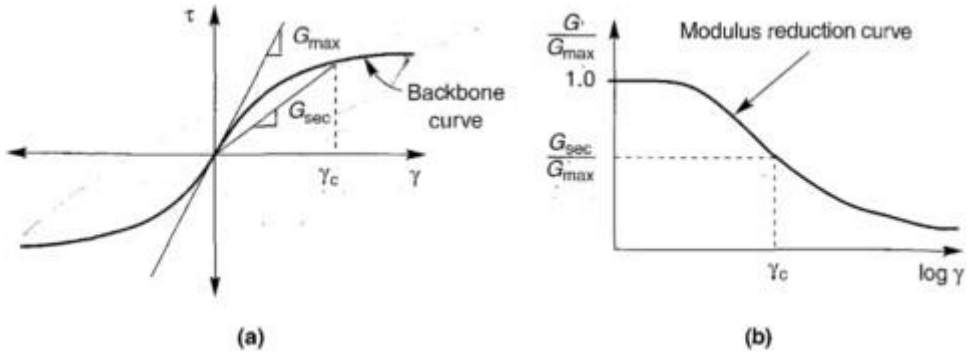

Figure 2- 8 a) Backbone curve and b) Modulus reduction curve
(Kramer, Geotechnical Earthquake Engineering, 1996)

Numerous techniques exist for the assessment of small-strain shear modulus, G_{max}. These include laboratory experiments utilizing bender elements, seismic cone penetration testing (CPT), Spectral Analysis of Surface Waves (SASW), the application of empirical relationships with strength parameters, and field tests utilizing CPT (GEOFUTURE, 2013).
The laboratory experiments involving bend elements, spectral analysis of surface waves (SASW), and seismic cone penetration testing (CPT) are highly dependable methods for determining the shear wave velocity (V_S) of soil. This can be achieved either through analysis of soil samples or through on-site testing. Upon the discovery of V_S, the computation of G_{max} is performed as,

$$Gmax = \rho V_S^2 \tag{2.22}$$

Where ρ is the density of the soil.

Multiple empirical relations are available in the literature that can also be used to find the trustworthy value of G_{max} using standard soil strength parameters.

2.3 Soil Damping

The damping in the dynamic response of a foundation is caused by the energy loss of waves propagating through the soil media during an earthquake. This mainly occurs due to the following kinds of damping:

a. Hysteretic damping

b. Radiation damping

2.3.1 Hysteretic Damping

During the transmission of waves through the soil, a portion of the elastic energy contained within the waves undergoes conversion into heat or permanent deformations, leading to a reduction in the amplitude of the waves. Viscous damping is utilized to represent the dissipation of elastic energy for mathematical convenience and to facilitate explanation. The Kelvin-Voigt solid is used to model soil elements. The material depicted in Figure 2-9 is classified as a slender, linear viscoelastic substance.

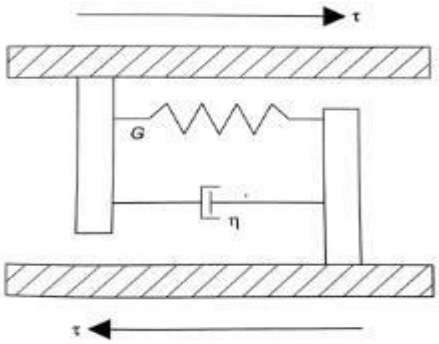

Figure 2- 9 Kelvin-Voigt solid

Then, the stress-strain relationship is:

$$\tau = G\gamma + \eta \frac{\partial \gamma}{\partial t} \tag{2.23}$$

The variables τ, γ, η, and G represent the shear stress, shear strain, viscosity, and shear modulus of the soil material, respectively. Upon each successive cycle, there is a dissipation of elastic energy, which results in a decrement in the shear stiffness of the soil. Hysteretic damping, dependent on soil non-linearity, contributes an average of 5% for low/moderate seismic conditions.

2.3.2 Radiation Damping

The phenomenon of radiation damping is intricately linked to the geometric characteristics of waves as they traverse through the soil medium. The observed phenomenon can be attributed to the propagation of waves across a significant media volume, resulting in the conservation of total elastic energy while causing a decrease in the amplitude of the wave as it moves away from the fault. Consequently, a notable degree of variability is contingent upon the foundation type and soil quality, including but not limited to soft or stiff soil and deep or shallow soil deposits. Studies have proposed charts and formulas for distinct soil-damping soil types and foundations (Gazetas, 1991). Radiation damping can mitigate the dynamic loads exerted on a structure, facilitating cost-effective designs and analyses. Soil damping can exclusively be employed in Soil Structure Interaction (SSI) evaluations conducted in the time domain, which is less prevalent than the response spectrum technique.

2.4 Soil Structure Interaction

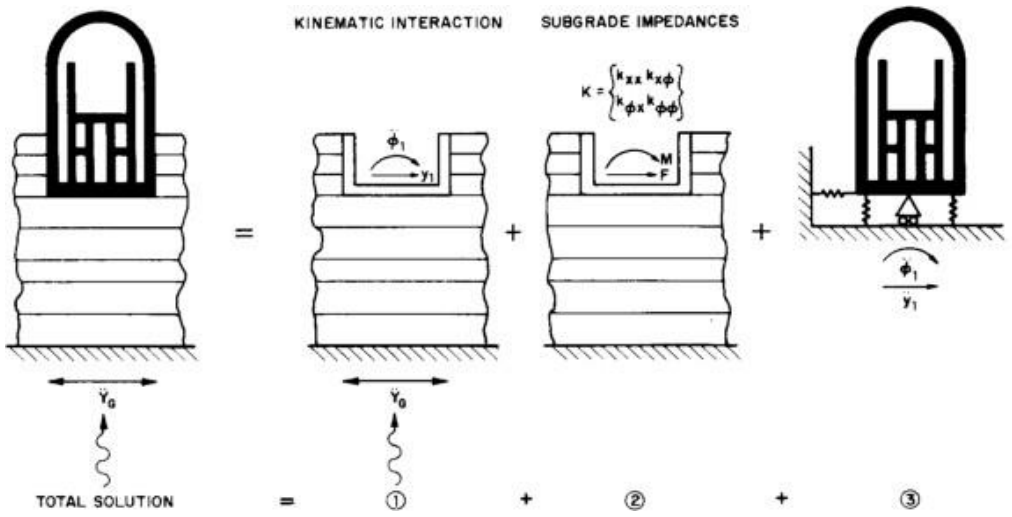

Figure 2- 10 Three-step solution (Kausel et al., 1978)

Comprehending the interaction between the structure and the soil in its vicinity is a crucial element of knowledge acquisition. Placing a foundation within a soil layer can induce soil motion in its area instead of the motion observed in an unobstructed field. The response of a structure is altered from what is anticipated in fixed base analysis and is contingent upon the foundation geometry, embedment, and dynamic properties of the underlying soil. The implementation of SSI is known to cause a reduction in the stiffness of soil and an elevation in the structure's natural period. This contrasts with fixed base analysis, characterized by higher overturning moments and shear forces (Wolf, 1985).

The concept of utilizing soil-structure interaction (SSI) in earthquake analysis to mitigate the foundation and superstructure load was initially disregarded. However, recent occurrences have demonstrated the significance of SSI in identifying critical scenarios, particularly in densely populated regions with tall structures. The more recent codes, such as Eurocode 8, specify circumstances in which SSI should be considered (GEOFUTURE, 2013).

The SSI is carried out in three steps, as Kausel et al. (1978) recommended in the Three-Step method. This procedure breaks SSI into three computation steps, also shown in Figure 2-10:

1. Identifying a reliable base motion entails the utilization of the acceleration input motion at the structure's foundation. Calculating this motion involves the assumption of a foundation and superstructure with negligible mass, commonly known as kinematic interaction analysis. A primary objective during this stage consists of the computation of the free-field ground surface oscillation based on the provided bedrock outcrop oscillation, as illustrated in Figure 11. The phenomenon is commonly known as seismic site response or soil amplification. It is noteworthy that in the case of surface foundations or shallowly embedded foundations relative to the foundation width, the uniform motion of the base is nearly indistinguishable from the motion of the free field, rendering this procedure unnecessary.

2. The objective is to ascertain the foundation impedance that varies with frequency at the structure's base.

3. In the third step, the structure's seismic response supported by the assumed soil springs was calculated. This was done by subjecting the structure to the base motion computed in the second step. The term used to describe this phenomenon is known as inertial interaction analysis.

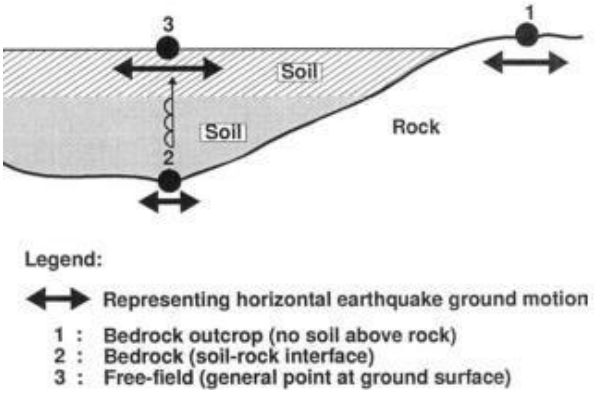

Figure 2- 11 Features in site response analysis (GEOFUTURE, 2013)

2.4.1 Soil Springs

As stipulated in the initial stage, the kinematic interaction phenomenon can be disregarded for most foundations. Hence, the sole data necessary for SSI pertains to soil springs. Determining the average stiffness of soil springs in foundations can be achieved by utilizing Finite Element software, which considers specific soil and foundation parameters. Programs that use P-Y curves, such as Geosuite, can be employed to determine the stiffness of pile foundations. Soil springs refer to matrices with dimensions of 6x6 that are constructed to incorporate the stiffness of a given structure. Straightforward closed-form solutions can be utilized for homogenous soil. Corresponding equations are referenced in Eurocode 8 for rigid circular foundations and single piles. As mentioned in 2.3.2, Gazetas (1991) has also provided extensive sets of equations, charts, and tables for soil springs.

2.4.2 Non-linear Springs

The utilization of linear soil springs is a customary practice in the context of soil-structure interaction (SSI) analyses. However, employing non-linear springs capable of accommodating foundation forces is also feasible. FE programs such as PLAXIS and Geosuite can be utilized to calculate non-linear soil springs comparable to linear soil springs. Appropriate non-linear soil models or Wrinkler springs can also be employed for this purpose. Determining soil stiffness involves an iterative process whereby the secant stiffness is considered at the level of applied loads (Athanasiu et al., 2015).

2.5 Site Response Analysis

Site response analysis is a research endeavor aimed at comprehending the impact of soil deposition on seismic waves at local sites. The propagation of a wave from a fault to the soil layers above alters its behavior, leading to variations in its amplitude and frequency. The ground response is contingent upon the material properties of the soil and wave characteristics, resulting in a deviation from the input wave. The examination may encompass one, two, or three dimensions and may be executed in a linear, equivalent, or non-linear manner. The impact of soil effects on the intensity and frequency of seismic activity is widely acknowledged. Wave propagation analysis is a common technique in geotechnical engineering to consider these effects. This analysis can integrate either equivalent-linear or non-linear soil dynamics. Eurocode8 tackles the issue of soft soil amplification by incorporating diverse response spectra for ground types, which are based on empirical data and may potentially be overly simplified. A noticeable dissimilarity between the design spectra and the modeled soil structure is evident. The code utilizes a rudimentary attribute for softer soil categories, characterized by low stiffness and/or significant thickness, leading to a more level design spectrum (Ziotopolou & Gazetas, 2010).

2.5.1 Amplification Factor

The amplification factor is a metric used to quantify the variation in the intensity of seismic waves that occurs because of the existence of soil and rock strata at a specific location. Assessing soil and rock layer response to seismic waves and designing earthquake-resistant structures are frequently employed practices in geotechnical engineering. The amplification factor is commonly denoted as the ratio between the seismic wave intensity observed at the ground's surface and the wave's intensity at a greater depth, such as the bedrock. A seismic wave's intensity is unaffected by soil and rock layers when its value is 1. However, a value greater than 1 indicates amplification, while a value less than 1 indicates damping (Kramer, Geotechnical Earthquake Engineering, 2014)

In a homogenous linearly elastic soil stratum, the oscillatory horizontal movement of the underlying bedrock results in the vertical propagation of shear waves, as illustrated in Figure 2-11 (Kramer, Geotechnical Earthquake Engineering, 1996). The horizontal displacement equation can be formulated as follows:

$$u(z,t) = A\mathrm{e}^{\mathrm{i}(\omega t+kz)} + B\mathrm{e}^{\mathrm{i}(\omega t-kz)} \tag{2.24}$$

Where ω is the angular frequency of the wave, k is the wave number, and t is time. A and B are the amplitude of waves traveling upward and downward.

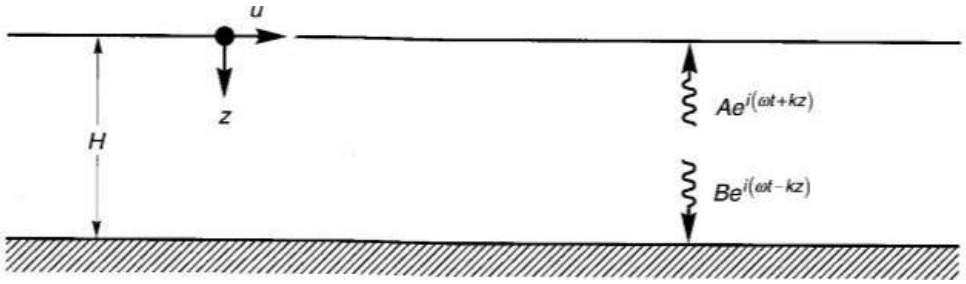

Figure 2- 12 Wave propagation in linear elastic soil

Incorporating damping in the soil layer assumption can yield more realistic results. If the soil exhibits Kelvin-Voigt shearing characteristics, it is possible to express the wave equation as follows:

$$\rho\frac{\partial^2 u}{\partial t^2} = u\frac{\partial u}{\partial \varkappa^2} + \eta\frac{\partial^3 u}{\partial x^2 \partial t} \tag{2.25}$$

Where, $u(z,t) = A\mathrm{e}^{\mathrm{i}(\omega t+kz)} + B\mathrm{e}^{\mathrm{i}(\omega t-kz)}$

Here, complex wave number k* can be obtained through the complex shear modulus, G* = G (1 + i2ξ) and complex shear velocity, $v_s^* = \sqrt{\frac{G^*}{\rho}} = \sqrt{\frac{G(1+2\mathrm{i}\xi)}{\rho}} = v_s(1+2\mathrm{i}\xi)$

Usually, ξ is very small; thus, complex wave number. $k^* = \frac{\omega}{v_s^*}$

These relationships can then be used to confirm a transfer function which is the ratio of the surface and the bedrock motion for a damped soil over rigid rock given by:

$$|F(w)| \approx \frac{u_{max}(0,t)}{u_{max}(H,t)} = \frac{1}{\sqrt{\cos^2\left(\frac{\omega H}{v_s}\right) + \left[\xi\left(\frac{\omega H}{v_5}\right)\right]^2}} \tag{2.26}$$

The amplification factor F(ω) is contingent upon the wave's frequency and attains its highest value when the wave's frequency corresponds to the natural frequency of the soil deposit. The

amplification factor's relationship with frequency at various damping conditions is depicted in Figure 2-12. According to Kramer (1996), the data indicates that the impact of damping is more pronounced on higher frequencies than on lower frequencies. The natural frequency of the soil layer is determined by:

$$\omega_n = \frac{v_s}{H}\left(\frac{\pi}{2} + n\pi\right), \text{N = 0, 1, 2, 3, ...} \quad (2.27)$$

And peak acceleration is registered when n = 0, and the fundamental frequency of the layer of soil becomes, $f_n = \frac{v_s}{4H}$

Various factors, such as the physical properties, composition, and thickness of the soil and rock layers at the site, can influence the amplification factor. The magnitude of seismic activity may be subject to the impact of seismic wave frequency and intensity, in addition to the bedrock's depth.

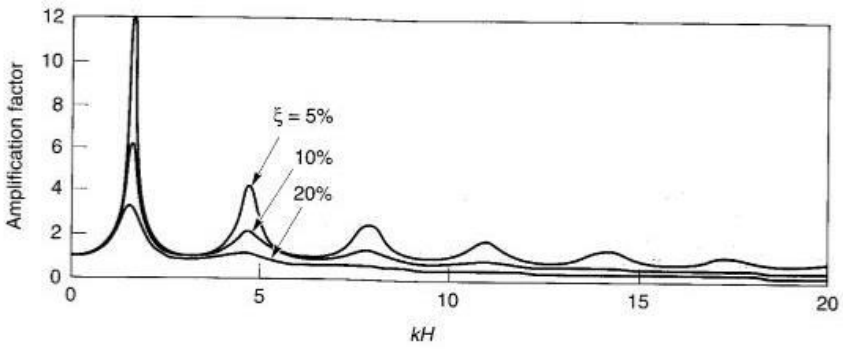

Figure 2- 13 Amplification of a soil layer for different frequencies

2.5.2 One-dimensional Site Response Analysis

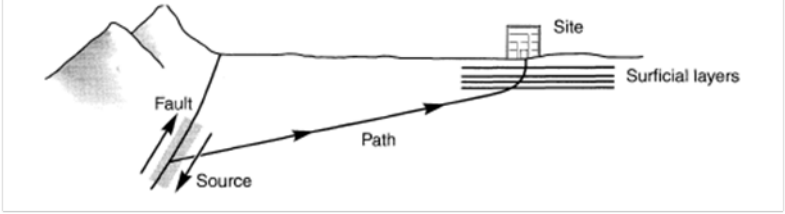

Figure 2- 14 Wave propagation from fault to site (Kramer, Geotechnical Earthquake Engineering, 1996)

When a fault ruptures beneath the Earth's surface, body waves propagate in all directions away from the source. Refraction and reflection occur when waves propagate across the interfaces of dissimilar geological materials. When rays with an inclination hit the boundaries of horizontal layers, they tend to reflect in a more vertical direction. This is because the wave propagation velocities of shallower materials are generally lower than those beneath them. Frequent occurrences of refraction can lead to a significant bending of rays, causing them to approach a vertical direction upon reaching the ground's surface. The fundamental basis of analyzing ground response in one dimension is the assumption that all boundaries are horizontal.

Additionally, it is presumed that the primary cause of a soil deposit's response is due to simple harmonic waves that propagate vertically from the underlying bedrock. In one-dimensional ground response analysis, it is commonly assumed that the soil and bedrock surface have infinite horizontal extension. Numerous studies have shown that in various cases, techniques founded on this assumption can effectively predict soil reactions that are in good agreement with observed reactions (Kramer, Geotechnical Earthquake Engineering, 1996).

2.5.2.1 Linear Approach

The assessment of transfer functions forms the basis of linear soil response analysis. Transfer functions have been established to account for intricate geological and geotechnical scenarios, such as Uniform Undampened Soil on Rigid Rock, Uniform Damped Soil on Rigid Rock, Uniform Damped Soil on Elastic Rock, and Layered Damped Soil on Elastic Rock. The transfer function under periodic loading conditions can be expressed in a standard formulation as follows:

Periodic load: $Q(t) = \sum_{n=-\infty}^{\infty} q_n^* \, e^{i\omega_n t}$

Fourier coefficients q_n^* is determined as follows:

$$q_n^* = \frac{1}{T_f} \int_0^{T_f} Q(t) \mathrm{e}^{-i\omega t} \, \mathrm{d}t \tag{2.28}$$

The equation of motion accounts for the response of a single-degree freedom system loaded in n-harmonics.

$$m\ddot{u}_n(t) + c\dot{u}_n(t) + ku_n(t) = q_n^* e^{i\omega_n t} \tag{2.29}$$

The response of the system: $u(t) = H(\omega n) \, q_n^* e^{i\omega_n t}$

Where $H(\omega n)$ is the transfer function that relates displacement to the external load. Substituting the above equation to the equation of motion results into:

$$H(\omega_n) = \frac{1}{-m\omega_n^2 + \mathrm{i}cw_n + k} = \frac{1}{k(\beta_n^2 + 2\mathrm{i}\beta_n + \xi + 1)} \tag{2.30}$$

However, other transfers could be formulated as well with different relationships. For example, the Fourier amplitude and phase spectra of input signal Q(t) and output displacement u(t) are:

$$F_0(\omega_n) = H(w_n) F_i(\omega_n) \tag{2.31}$$

$$\phi_0(\omega_n) = H(\omega_n) \phi_i(\omega_n) \tag{2.32}$$

2.5.2.2 Equivalent linear approach

The linear methodology employed in site response analysis postulates a homogenous soil layer characterized by a consistent variation in stiffness as a function of depth. Mathematical functions are utilized to represent the geometry and parameters in an idealized manner. Simplistic assumptions are less likely to integrate actual site conditions. Under such circumstances, conducting an equivalent linear approach or finite element analysis to obtain a realistic outcome is possible. It is possible to simulate soil properties, such as shear modulus and damping ratio, that are linearly equivalent to seismic loading.

The concept of equivalent shear modulus is denoted by the secant shear modulus and the damping ratio equivalents, respectively represented by the energy dissipated in a single cycle

of the hysteresis loop. Modulus reduction and damping curves are determined through laboratory experimentation, utilizing the principle outlined in section 2.2.2. The motion of earthquakes is not characterized by harmonic patterns but rather by irregular time histories. To replicate this anomalous phenomenon, a loading reduction factor of 65% is implemented to counterbalance the overestimation of shear strain, as suggested by (Kramer, Geotechnical Earthquake Engineering, 1996). The fundamental principle of the numerical analysis software by programs such as SHAKE, EERA, and DEEPSOIL involves the iterative implementation of equivalent linear analysis. The iteration process is executed until the congruity of the shear modulus and dumping ratio with the strain induced in each layer is achieved.

2.5.2.3 Non-linear approach

The non-linear and inelastic behavior of soil has been extensively recognized in geotechnical engineering. The soil's shear modulus exhibits constant variation due to the non-linear stress-strain behavior of soil in dynamic analyses. The soil exhibits an inelastic behavior, leading to

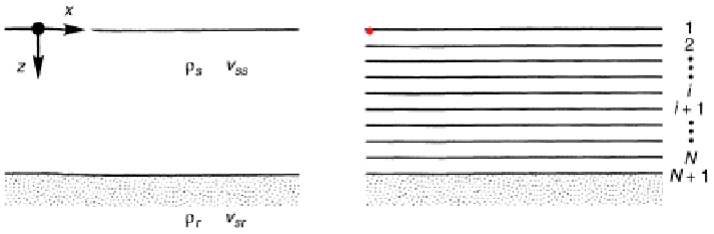

Figure 2- 15 Nomenclature of soil deposit and discretization to N-layers

a deviation in the load release path from the original loading path, resulting in energy dissipation at the inter-particle contact locations. Both time domain and frequency domain analyses account for the non-linear impacts of site response issues. Linear and non-linear methods are employed in both the time and frequency domains for investigating the propagation of shear waves in layered soil media in one dimension. Empirical evidence suggests that non-linear analyses exhibit a higher degree of concurrence with the recorded seismic activity than linear analyses. The equation of motion that governs the non-linear ground response when moving horizontally at bedrock is as follows:

$$\frac{\partial \tau}{\partial z} = \rho \frac{\partial^2 u}{\partial t^2} \tag{2.33}$$

Defining the finite differences of the corresponding differentials in the equation above:

$$\frac{\partial \tau}{\partial z} = \frac{\tau_{i+1,t} - \tau_{i,t}}{\Delta z} \tag{2.34}$$

$$\frac{\partial^2 u}{\partial t^2} = -\frac{\ddot{u}_{i,t+\Delta t} - \ddot{u}_{i,t}}{\Delta t}; \ddot{u} = \frac{\partial u}{\partial t} \tag{2.35}$$

Substituting these equations, the following equation is obtained: \

$$\ddot{u}_{i,t+\Delta t} = \ddot{u}_{i,t} + \frac{\Delta t}{\rho \Delta z}\left(\tau_{i+1,t} - \tau_{i,t}\right) \tag{2.36}$$

A solution for shear stress at rock boundaries was given by Joyner & Chen (1975) as follows:

$$\tau_v \approx \rho_r \overline{v_{sr}}\left(2\ddot{u}_r(t + \Delta t)\right) - \ddot{u}_{N+1,t+\Delta t} \tag{2.37}$$

Similarly, shear strain is given by Kramer (1996) as:

$$\gamma_{i,t} = \frac{\partial u_{i,t}}{\partial z} \approx \frac{u_{i,t+\Delta t} - u_{i,t}}{\Delta t} \tag{2.38}$$

2.6 Material Models

PLAXIS offers a variety of material models that can be utilized for analytical purposes. PLAXIS provides specific models that are recommended for dynamic analysis. The analytical framework employed for subsequent investigation is the Hardening Soil Model with small-strain stiffness, commonly referred to as Hardening Soil Small (HSSmall). The proposed model can incorporate the strain-dependent behavior of stiffness and hysteretic damping of the soil.

2.6.1 Hardening Soil Model with Small Strain Stiffness (HSSmall)

According to Bentley's (2022) research, this model is a variant of the Hardening Soil model that accounts for enhanced soil stiffness at low strains. This feature renders it a viable option for utilization in the dynamic analysis of soil models. The stiffness of soil exhibits a notable increase primarily at low levels of strain compared to the stiffness of other engineering structures. In this phase, the strain-stiffness relationship exhibits non-linear behavior. Consequently, the HSSmall model incorporates two additional parameters to account for this phenomenon. Specifically, these parameters are included to enhance the accuracy of the model:

1. Small-strain shear modulus, G_0^{ref}

2. Shear strain level $\gamma_{0.7}$ at which the secant shear modulus reduces to 70% of G_0^{ref}

The stress dependency of small strain stiffness is given by:

$$G_0 = G_0^{ref}\left(\frac{c\cos\phi - \sigma_3'\sin\phi}{c\cos\phi + P_{ref}\sin\phi}\right)^m \tag{2.39}$$

$$G_0^{ref} = \frac{E_0^{ref}}{2(1+\nu_{ur})} \tag{2.40}$$

Where, E_0^{ref}, G_0^{ref}, c, ϕ, σ'3, P_{ref}, ν_{ur} And m are reference very small strain Young's modulus, reference shear modulus at very small strains, cohesion, friction angle, effective minor principal stress, reference minor principal stress (-σ'_3), Poisson's ratio for unloading-reloading, and power for the stress-level dependency of stiffness. The stress-strain relationship for small strains can be characterized by a hyperbolic function, as proposed by Hardin and Drnevich, 1972.

$$\frac{G_5}{G_0} = \frac{1}{1+\left|\frac{\gamma}{\gamma_{0.7}}\right|} \tag{2.41}$$

Later this was simplified by Dos Santos and Correia (2001):

$$\frac{G_s}{G_0} = \frac{1}{1+0.385\frac{\gamma}{\gamma_{0.7}}} \tag{2.42}$$

This relation is used in the PLAXIS 2D as a basis for the stress-strain curve. Again, Again, according to Vucetic and Dobry (1991), G_s/G_0 - γ curves depend on the plasticity index, PI (usually taken for 50%). The stress-strain relationship for small strains can be characterized by a hyperbolic function, as proposed by Hardin and Drnevich in 1972. Here, unloading-reloading stiffness, $G_{ur} = \frac{E_{ur}}{2(1+\nu_{ur})}$; E_{ur} is the unloading-reloading modulus, and ν_{ur} is Poisson's ratio for loading/unloading. The HSsmall model exhibits enhanced displacement reliability compared

to the HS model and is better suited for dynamic analysis due to its ability to capture cyclic behavior (Bentley, 2022a).

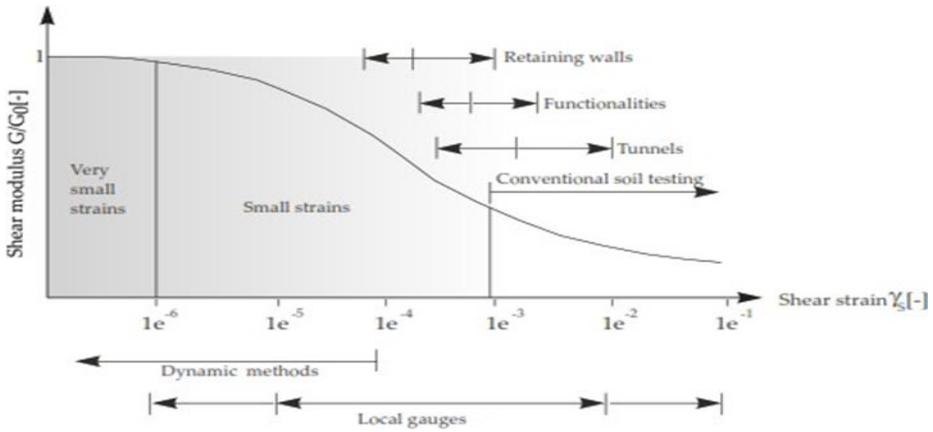

Figure 2- 16 Characteristic stiffness-strain behavior (Bentley, 2022a)

The following equation provides a reasonable estimation of γ0.7:

$$\gamma_{0.7} = \frac{1}{9G_0}[2c'(1+\cos(2\emptyset')) - \sigma_1'(1+K_0)\sin(2\emptyset')] \tag{2.43}$$

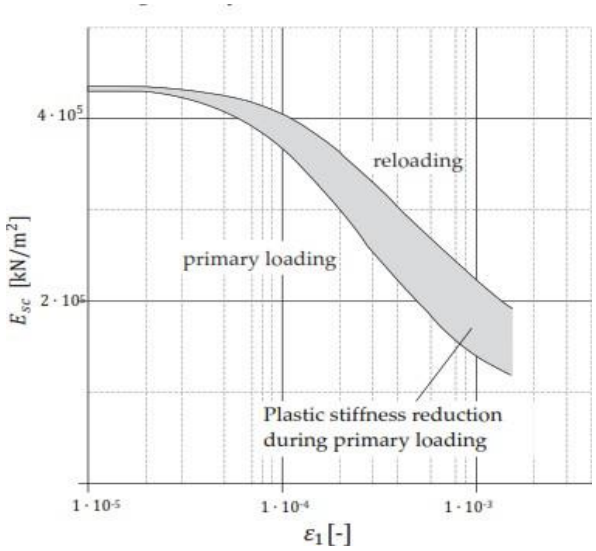

Figure 2- 17 Stiffness reduction during initial loading and unloading/reloading (Bentley, 2022a)

Where K_0 and σ_1' are earth pressure coefficient at rest and effective vertical stress.

According to the material model manual authored by Bentley (2022), the HSSmall model exhibits superior displacement outcomes and is better suited for dynamic analysis due to its incorporation of the cyclic behavior of soil unloading and loading during seismic events.

2.7 Finite Element Method

The Finite Element Method (FEM) is a computational approach to approximate solutions for boundary value problems in engineering. The technique has gained widespread adoption in diverse areas of engineering, such as structural engineering, geotechnical engineering, thermodynamics, and fluid mechanics, among others. The employed technique involves partitioning a continuous system into discrete and finite elements. Subsequently, the discretized model can be solved for nodal degrees of freedom by prescribing node displacements or stresses at the boundary nodes, commonly referred to as boundary conditions (Nordal, 2020).

2.7.1 PLAXIS 2D

PLAXIS 2D is a software application that employs finite element methodology to analyze deformation, stability, and groundwater flow in geotechnical engineering. The software facilitates the simulation of soil behavior. The precision of the model is contingent upon the user's expertise and familiarity with the problem's modeling, comprehension of soil model constraints, and model parameters, and ability to evaluate the resulting output (Bentley, 2022).

The summation of finite triangular elements can represent the complete structural system's behavior. The deformations of an element are defined by the deformations in a specific set of nodal points when said element undergoes deformation (Nordal, 2020). PLAXIS employs six or fifteen nodal point triangular elements, as illustrated in Figure 2.13.

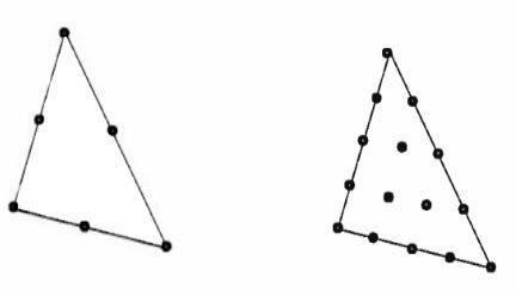

Figure 2- 18 Triangular element with 6 and 15 node points (Nordal, 2020)

2.7.2 Challenges in FEM

2.7.2.1 Boundary conditions

The boundary problem poses a significant challenge when modeling a dynamic problem using the finite element method (FEM). Utilizing soil deposits over bedrock is a prevalent practice; however, it results in a surge in the number of nodes and significant computational duration. Consequently, smaller models are favored. As stated in section 2.2.2, the reflection of waves occurs when they encounter the vertical boundaries of a model that represents a continuous soil media, resulting in energy trapping that would have otherwise dissipated. Potential solutions exist to address this matter, including the utilization of adequately sized models to facilitate wave energy dissipation, albeit at the expense of increased computation time. Alternatively, implementing viscous boundaries may be introduced to absorb these wave energies. These boundaries exhibit superior performance when subjected to waves that approach perpendicularly but produce additional undesirable boundary effects. These boundaries perform excellently when subjected to perpendicular waves but also create different unwanted boundary effects (Brandt, 2014).

2.7.2.2 Time stepping

Numerical integration techniques, such as the Newmark Method, are employed in Finite Element Method (FEM) for dynamic analyses. The process of numerical integration involves solving a global set of equations for a specific time, then applying a time step, and then repeating the process of equation solving.

The Finite Element Method (FEM) employs explicit and implicit time integration formulations. Explicit methods are numerical techniques that compute the subsequent step solely based on the present step, whereas implicit methods involve solving the equation utilizing both the current and the following time step. Explicit methods are comparatively simpler to develop but highly sensitive to time stepping. On the other hand, implicit methods are more challenging to handle but offer greater precision, making them more appropriate for dynamic analyses. It is imperative to ensure that the time step is set below the critical value, representing the duration required for the wave to propagate to the subsequent element.

Conversely, larger time steps should be circumvented as they may result in the omission of elements, yielding a solution of low accuracy and numerical instability. PLAXIS guarantees automatic compliance with the requirement that each wave traverses a single element per time

step. The calculation of the critical time step is determined based on the element's size and the material's stiffness. The time step adjustment is carried out based on the input data points, as stated by Laera and Brinkgreve in 2015.

$$\delta_t = \frac{\Delta t}{m \cdot n} \tag{2.44}$$

Where, δ_t Is the time-step calculated from dynamic time interval Δt, m is the maximum number of steps, and n is the number of sub-steps.

2.8 Pile Foundations

Pile foundations are typically deemed essential for augmenting the bearing capacity and mitigating differential settlement in soil comparatively softer or more susceptible to compression. During seismic activity, the lateral seismic load causes ground deformation, altering the forces acting on pile foundations. The primary cause of pile foundation failures in recent years is soil liquefaction. Consequently, there has been limited research on damage in non-liquefiable soil, as noted (Martin & Lam, 1995).

Numerous scholars have researched the patterns of damage and mechanisms involved in pile foundations subjected to seismic loading. Several methodologies have been developed to integrate the computation of altered forces resulting from seismic activity. Figure 2-16, as presented by (Teguh et al., 2006), provides a summary of the damage incurred by pile foundations during earthquakes based on the research conducted by Hamada (1991) and Mizuno (1987). Ground motion exceeding certain thresholds can induce failure during an earthquake. The various phenomena that can occur in a pile foundation system include deformation, high shear force, bending moment along the pile, and excessive shear force at the interface of the pile and pile cap, among others (Teguh et al., 2006).

Numerous investigations have assessed the sectional forces exerted on piles during seismic events. In 2015, Hamada J. conducted a series of tests involving shake table and lateral load on piles within a centrifuge. The present investigation proposes a methodology for the computation of bending moments under dynamic conditions. This is achieved by computing the difference between the bending moment estimated from static loading and the bending moment obtained from shaking table tests. In this scenario, determining the bending moment involves utilizing the relationship between the bending moment and shear force, expressed as $\alpha = M/Q$, where α represents a constant factor. The measurement of the bending moment is

derived from the shear force at the pile head. Thus, a similar technique is employed to evaluate the shear force under dynamic circumstances.

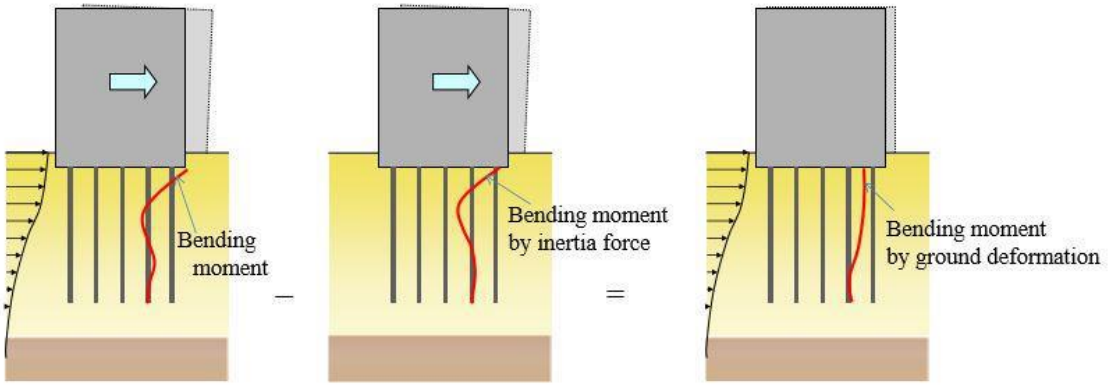

Figure 2- 19 Bending moment in piles due to ground deformation (Hamada J. , 2015)

2.8.1 Modeling pile in PLAXIS 2D

Piles are three-dimensional structural components that can pose a challenge when attempting

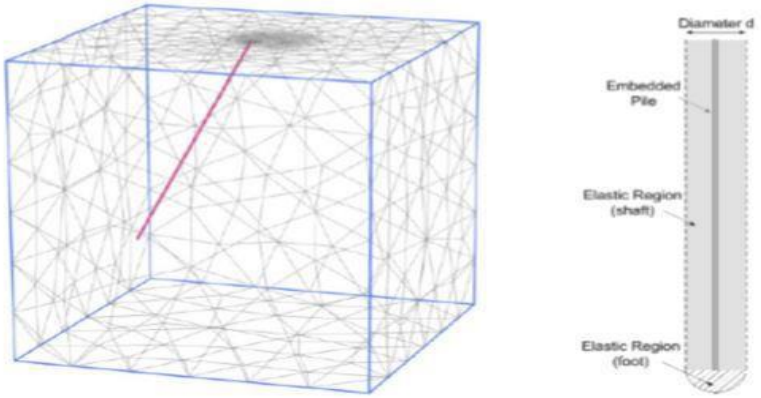

Figure 2- 20 Embedded beam shown in 3D mesh and elastic region around beam (Kwaak, 2015)

to represent them in a two-dimensional plain strain model, although such an approach may be required in certain circumstances. The existing FEM modeling techniques in PLAXIS 2D are imited in number. Historically, modeling was conducted in two dimensions using either plate elements or node-to-node anchors. These methodologies possess both advantages and constraints. Incorporating the embedded beam row element in PLAXIS is a recent development aimed at simulating piles in the out-of-plane direction. This approach has been shown to yield more accurate outcomes and address the shortcomings of alternative 2D techniques, as noted by (Sluis et al., Modelling of a pile row in a 2D plane strain FE-analysis, 2014).

Embedded beam row pertains to the capacity to simulate a two-dimensional pile configuration with a specific spacing in the direction perpendicular to the plane. In a two-dimensional plane, they apply a feature that creates a beam with reduced volume. An elastic zone of equivalent size is generated around the shaft after specifying the diameter. This is done to simulate the behavior of the pile as a volume element (Dao, 2011). How soil interacts with its surrounding environment is determined by a distinct interface. Line-to-volume interface elements represent the interaction between soil and pile shaft, whereas point-to-volume interface elements describe the interaction between soil and pile tip. The bearing capacity of a pile is considered an input rather than a resultant in the context of an embedded beam element. When designing an embedded beam row element, it is necessary to input both skin and tip resistance in both the axial and lateral directions. The 2D plain strain model depicted in Figure 2-22 illustrates the concept of an embedded beam row. The 2D plain strain model represents a 1-meter element slice intended to be extended in the out-of-plane direction. The embedded beam is segregated in the out-of-plane order through "pile spacing." This phenomenon results in the movement of soil particles around the pile, creating a cohesive mesh structure. A series of piles arranged in a repeating pattern with a specified distance between them is formed in a direction perpendicular to the plane.

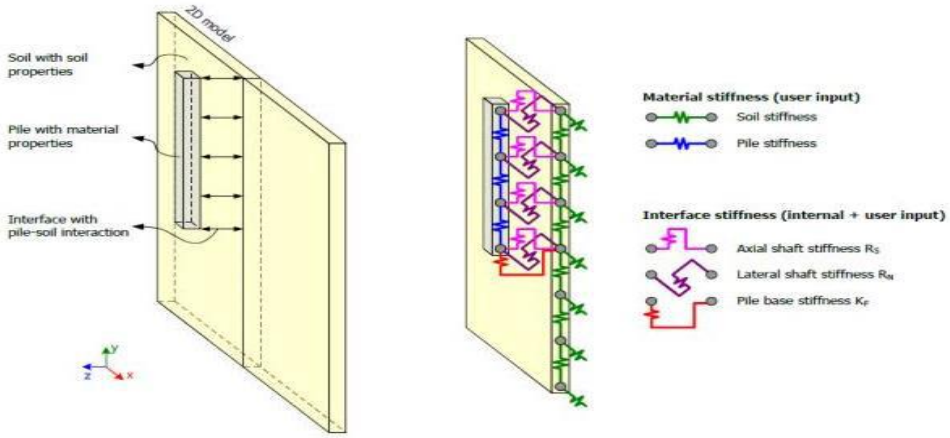

Figure 2- 21 Soil structure interaction using special interface elements, which is the concept of embedded beams (Sluis, Validation of embedded pile row in PLAXIS 2D, 2012)

Sluis (2012) expounded upon the soil structure interaction by utilizing specialized interface elements that establish a connection between piles and soil elements, as illustrated in Figures 2-22 and 2-23. The pile shaft interaction is characterized by a line-to-area interface and modeled using axial and lateral stiffness springs. The spring force is constrained by a maximum force in both directions. The maximum axial and lateral skin capacity ($T_{S;\,max}$ and $T_{N;\,max}$)

represents a significant force that must be pre-calculated and inputted as a parameter. The interface located at the base is a point-to-area interface. The fundamental interface is a point-to-area interface characterized by a spring with a numerical stiffness value (K_F) and a slide. The maximum base resistance force (Fmax) is computed as an input parameter. The determination of interface stiffness values, namely RS, RN, and KF, can be achieved by utilizing the formulae established by Sluis (2012). The mathematical expressions are derived from the soil's shear modulus, denoted as G_{soil}, the out-of-plane spacing, represented by $L_{spacing}$, and the corresponding interface stiffness factors.

$$R_s = ISF_{RS}\left(\frac{G_{soil}}{L_{spacing}}\right) \tag{2.45}$$

$$R_N = ISF_{RN}\left(\frac{G_{soil}}{L_{spacing}}\right) \tag{2.46}$$

$$K_F = ISF_{KF}\left(\frac{G_{soil}\ X\ R_{eq}}{L_{spacing}}\right) \tag{2.47}$$

The interface factors are calculated automatically by PLAXIS, and other literature is also available that confirms that the values from PLAXIS are reliable. Sluis (2012) compared the outcomes obtained from PLAXIS 2D, 3D, and Eurocode displacement curves. The study revealed that an embedded beam pile yields highly satisfactory results in 3D scenarios. The study has concluded that the usability of an embedded beam row is contingent upon the center-to-center lateral spacing to diameter ratio ($L_{spacing}/D$) in a two-dimensional context. When the ratio of $L_{spacing}$ to D is less than 2, plate elements exhibit unrealistic outcomes similar to those of the embedded element. When the value of $L_{spacing}/D$ exceeds 8, the group's collective behavior is no longer observed; instead, the system behaves as a singular entity in two dimensions.

Thus, it can be deduced from this study that using an embedded beam row component yields accurate outcomes in cases where the ratio of $L_{spacing}$ to D falls between 2 and 8.

2.8.2 Calculation of Axial, Lateral, and Base Resistance

As previously mentioned, the efficacy of the embedded beam row component is influenced by the input axial, lateral, and base resistances. Hence, it is crucial to compute them prior to their application in embedded beams accurately. Engineers commonly employ various techniques

to calculate axial, lateral, and base resistance.

2.8.2.1 Lateral resistance

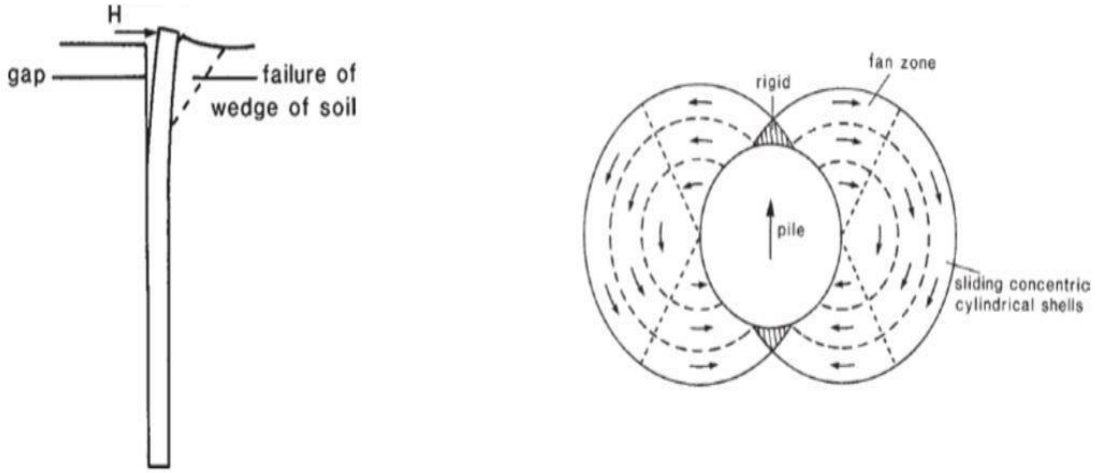

Figure 2- 22 Pile Deformation and soil failure around a pile under lateral load (Fleming et al., 2008)

The calculation of lateral resistance can be performed by utilizing the equations proposed by Brooms in 1964. The equation denoted as (2.38) pertains to a soil lacking cohesion.

$$Pu = 3 \times k_p \times \sigma'_v \times D \qquad (2.48)$$

Here, $k_p = \frac{1+\sin\phi'}{1-\sin\phi'}$

Pu = Lateral resistance of a pile

D = diameter of the pile

σ'_v = Effective vertical stress

For cohesive soil, the equation is dependent on the shear strength of the soil and varies with depth for non-uniform clay soil.

$$P_u = (2+7 \times \frac{z}{3D}) \times c_u \times D,\ z < 3D \qquad (2.49)$$

$$Pu = 9 \times c_u \times D,\ z \geq 3D \qquad (2.50)$$

2.8.2.2 Axial Resistance

Skir

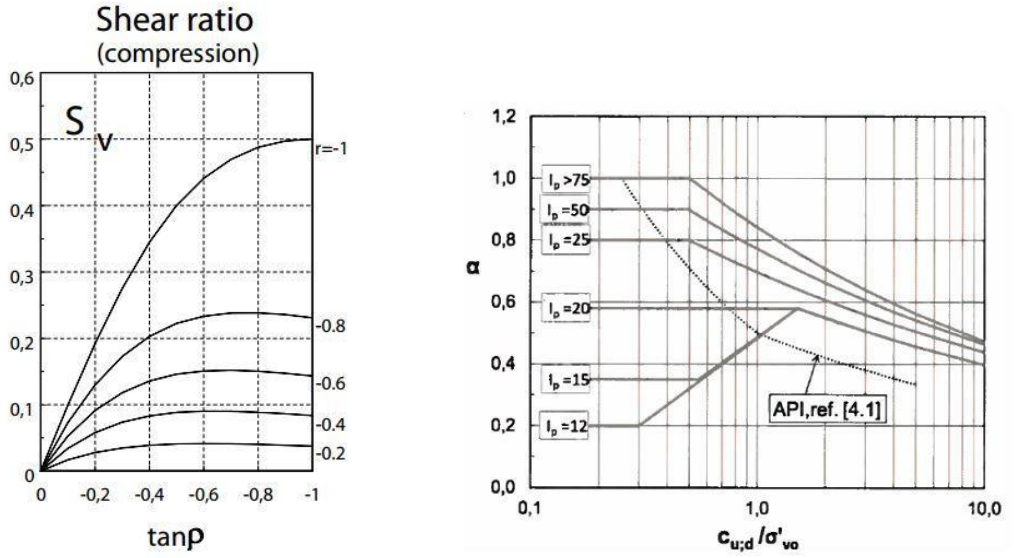

Figure 2- 23 Shear ratio for piles in compression in effective stress analysis and curve for normalized side friction (α-method)

$$\tau_s = r\, tan\, \phi'\, K_A(\sigma_v' + a) = S_v(\sigma_v' + a) \qquad (2.51)$$

Where r = mobilized roughness ratio along the pile

$tan\, \phi'$ = soil friction

KA = active earth pressure coefficient

Sv = Shear ratio

a = attraction

Thus, over the length of the pile, axial loading is given by:

$$Q_s = \int_0^z \tau_s A_s \, dz \qquad (2.52)$$

And τ_s is shear stress along the pile at a depth z = $\alpha\, c_u$ and as is the circumference of the pile.

2.8.2.3 Base resistance

Base resistance can be calculated as,

$$Q_p = A_p\, \sigma_{pn} \text{ and} \qquad (2.53)$$

For a floating pile, base resistance is given by,

σ_{pn} = Nc τ_c, where Nc = bearing capacity factor = 9 (for cohesive soil with deep foundations)

2.9 Eurocode 8

The European Standard EN 1998, also known as Eurocode 8, offers guidance for the design of earthquake-resistant structures. The design of various structures is divided into six parts (EN 1998-1 to EN 1998-6), with EN-1998-1:2004 (Eurocode 8: Design of structures for earthquake resistance – Part 1: General rules, seismic actions and rules for buildings) being the applicable standard for building design. These are the most pertinent sections for the present investigation. According to CEN (2004), a national annex is necessary due to the diverse seismic characteristics of member nations, despite the availability of alternative procedures and values in EN 1998-1:2004. Consequently, the Norwegian Annex serves as a point of reference for seismic characterization within the scope of this investigation.

This study draws pertinent information from "National Annex, NA." The document NS-EN 19981:2004+A1:2013+NA:2021 is used as a reference document. Determining the ground type and its corresponding design spectrum is carried out per the instructions outlined in Section 3. The determination of the shear force at the foundation of a structure is conducted through the utilization of the lateral force approach for analysis, as outlined in section 4 (NA. 4.3.3.2). This section provides a summary of significant factors, definitions, and equations that are pertinent to the topic at hand. Specific descriptions have been extracted from the English rendition of the European Standard, EN 1998-1:2004, to facilitate comprehension.

2.9.1 Ground Type Identification

As per the guidelines outlined in Eurocode 8, the categorization of soil types comprises seven distinct classifications, denoted as A, B, C, D, E, S1, and S2. A thorough investigation must be conducted to accurately ascertain the soil type at the site in question, as this information is necessary for precise calculations. The national annex provides information on soil types and their respective parameters for identification, as outlined in Table NA3.1 of Appendix A1. It is recommended that the categorization be based on the mean shear wave velocity of the initial 30-meter stratum, provided that the relevant data is obtainable. The average shear wave velocity for the uppermost 30 meters of soil layer (Vs, 30) is calculated using the equation provided by CEN in 2004, specifically designed for small strain levels.

$$v_{S,30} = \frac{30}{\sum \frac{h_i}{v_i}} \tag{2.54}$$

The given equation involves the variables hi and vi, representing the thickness of each layer and the corresponding shear wave velocity.

The national authority determines the seismic zones for each country based on the national hazard level, dividing the territory into multiple zones. The peak ground acceleration for various regions is associated with a reference return period, TNCR, of the seismic activity or the reference probability of surpassing a given threshold within a 50-year timeframe, PNCR. A reference return period is assigned an importance factor γ_I of 1.0. According to CEN (2004), the design ground acceleration on type A ground a_g can be determined for return periods other than the reference by multiplying a_{gR} with the importance factor γ_I.

$$a_y = \gamma_I a_{gR} \tag{2.55}$$

The important factors for structures are different depending on their usage. The importance classes and their corresponding γ_I values are given in the following table. For the return period mentioned above, the value of γ_I will be 1. Appendix 1 offers seismic zones of Norway (NS-EN 1998-1:2004+NA:2008).

2.9.2 Seismic Representation

The elastic response spectrum in figure 2-27 of EN 1998-1: 2004 depicts the earthquake motion at a specific location on the surface. The generalized form of EC-8 presents an elastic response spectrum that exhibits a similar shape for two different levels of earthquake magnitudes. In the Norwegian Annex, a single elastic response spectrum exists that describes variations in earthquake motion across different soil types. If the site is impacted by earthquakes originating from various sources, it is essential to consider multiple spectral shapes for designing seismic action. The magnitude of the input seismic action, a_g, will vary depending on the specific spectrum and earthquake type.

The European standard EC-8 describes four distinct types of elastic response spectrum.

2.9.2.1 Horizontal elastic response spectrum

The parameter denoted as Se (T) is interesting regarding the horizontal components of the seismic action. The concept of shape is characterized by a set of equations defined by the CEN (2004).

$$0 \le T \le T_B: S_e(T) = a_g S \left[1 + \frac{T}{T_B}(2 \cdot 5\eta - 1)\right] \quad (2.56)$$

$$T_B \le T \le T_C: S_e(T) = a_g S\ 2 \cdot 5\eta \quad (2.57)$$

$$T_C \le T \le T_D: S_e(T) = a_g S\ 2 \cdot 5\eta\ \left[\frac{T_C}{T}\right] \quad (2.58)$$

$$T_D \le T \le 4s: S_e(T) = a_g S\ 2 \cdot 5\eta\ \left[\frac{T_C T_D}{T^2}\right] \quad (2.59)$$

Here,

T = Natural vibration period of a linear SDOF system

ag= Design ground acceleration on type A ground ($a_g = \gamma_I . a_{gR}$)

TB = Lower limit of the period of the constant spectral acceleration branch

TC = Upper limit of the period of the constant spectral acceleration branch

TD =the value defining the beginning of the constant displacement response range of the spectrum.

S =Soil factor

η = Damping correction factor with a reference value of η = 1 for 5% viscous damping

Se(T) = The horizontal component elastic response spectrum

Table 2- 1 Various parameters of horizontal elastic response spectrum for different soil types as per Eurocode 8-1

Soil Type	S	T_B (s)	T_C (s)	T_D (s)
A	1	0.10	0.25	1.7
B	1.30	0.10	0.30	1.5
C	1.40	0.15	0.30	1.5
D	1.55	0.15	0.40	1.6
E	1.65	0.10	0.30	1.4

Eurocode 8-1 does not provide any recommended values for ground types S1 and S2, but the NA.3.2.2.2 of Norwegian Nation Annex in Table 3.3 has provided recommended values for

ground types S_1 and S_2, shown in Table 2- 2.

Table 2- 2 Various parameter of horizontal elastic response spectrum for soil type S1 and S2 as per Norwegian National Annex

Depth to rock	S	T_B (s)	T_C (s)	T_D (s)
6-20 m	2.0	0.10	0.40	1.4
20-35 m	1.9	0.15	0.50	1.5
35-60 m	1.8	0.20	0.60	1.6

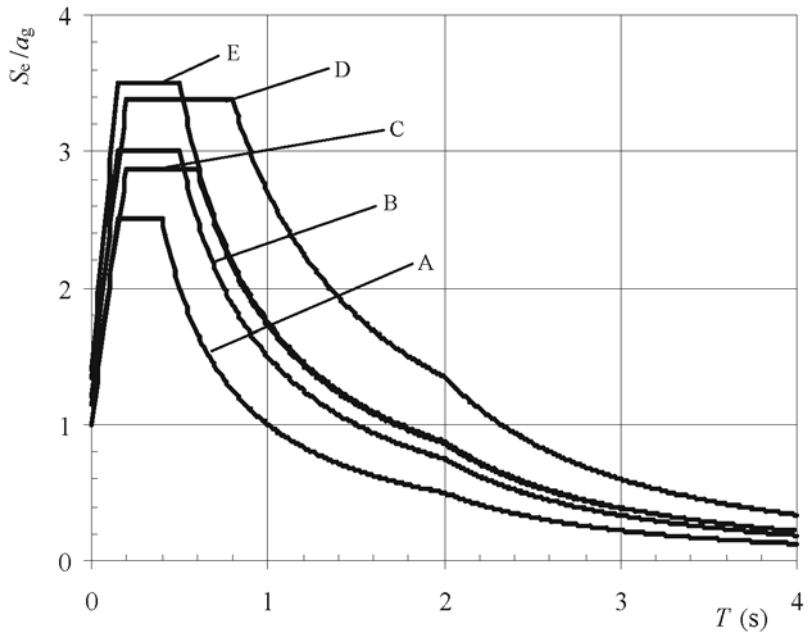

Figure 2- 24 Type 2 elastic response spectra for ground types A to E (5% damping), also recommended by Norwegian National Annex (CEN, 2004)

2.9.2.2 Elastic displacement response spectrum

The elastic displacement spectrum is derived by directly transforming the elastic response spectra for acceleration, denoted as Se(T), using the expression provided by the European Committee for Standardization (CEN, 2004).

$$S_{De}(T) = S_e(T)\left[\frac{T}{2\pi}\right]^2 \tag{2.60}$$

Then, to determine the design ground displacement, dg as per the corresponding acceleration is given by:

$$d_g = 0.025\ a_g\ S\ T_C\ T_D \tag{2.61}$$

2.9.2.3Elastic design spectrum

The values of the design spectrum utilized in elastic analysis are contingent upon various factors, including the specific characteristics of the local ground condition, the type of structure being considered, and the seismic input being applied. The spectrum's shape can be determined by utilizing the equations provided by CEN (2004).

$$0 \leq T \leq T_B: S_d(T) = a_g S \left[\frac{2}{3} + \frac{T}{T_B}\left(\frac{2.5}{q} - \frac{2}{3}\right)\right] \tag{2.62}$$

$$T_B \leq T \leq T_C: a_g S \, \frac{2.5}{q} \tag{2.63}$$

$$T_C \leq T \leq T_D: S_d(T) = \begin{cases} a_g S \frac{2.5}{q}\left[\frac{T_C}{T}\right] \\ \geq \beta a_g \end{cases} \tag{2.64}$$

$$T_D \leq T \leq 4s: S_d(T) = \begin{cases} a_g S \, \frac{2.5}{q} \left[\frac{T_C T_D}{T^2}\right] \\ \geq \beta a_g \end{cases} \tag{2.65}$$

In this context, q represents the behavior factor of the structure, while β denotes the lower bound element for the horizontal design spectrum, which can be obtained from the national annex. The Eurocode 8 describes the design of elastic response spectra, primarily influenced by a parameter known as the "behavior factor, q." This particular factor is responsible for determining the ductility of a structure, which can be understood as the structure's ability to dissipate energy effectively. The range of values for this parameter varies across different sections of Eurocode 8, depending on the ductility classes (low/medium/high) assigned to the structure (see Appendix A3).

The ability of structural systems to withstand seismic forces or dissipate energy in a non-linear manner is greater than that of a system operating within the elastic range. The inclusion of the behavior factor is employed as an approximation to account for the decrease in seismic forces exerted on the structure when conducting an elastic analysis, thereby circumventing the need for more complex inelastic analysis. In Norway, the utilization of low or medium ductility levels is authorized. In typical practice, most structures are designed by incorporating a value of q ≤ 1.5, per the Ductility Class Low (DCL). According to Rønnquist et al. (2012), the analysis of structures in Norway suggests that they are considered non-dissipative.

2.9.3 Base Shear Force

The base shear is determined using the lateral force method of analysis. The method of analysis is provided in section 4.3.3.2 of the European Standard EN 1998-1:2004, as referenced by the European Committee for Standardization (CEN) in 2004.

To utilize this method, the structure must meet the following condition:

$$T_1 \leq \{^{4T_C}_{2.0} \tag{2.66}$$

Then the shear force can be generated at the base using the equation:

$$F_b = S_d(T_1)\, m\, \lambda \tag{2.67}$$

Here,

$T_1 =$ natural period of vibration of the building for a given motion in the direction considered.

$S_d(T_1)$ = Design spectrum for T1

m = total mass of the building above the foundation or rigid basement

λ = correction factor, λ = 0.85 for T1 < 2 TC and for building with more than two stories or else λ = 1

The parameter λ is utilized to explain the observation that in structures consisting of a minimum of three levels and possessing translational degrees of freedom in both horizontal directions, the effective modal mass of the first (fundamental) mode is typically 15% lower than the overall mass of the building.

Following sections 4.3.3.2.2(3) of EN 1998-1:2004 (CEN, 2004), determining the fundamental period of vibration T1 for a building can be achieved by employing expressions derived from structural dynamics methods, such as the Rayleigh method. The approximation for the value of T_1 (in seconds) for buildings with heights up to 40 m can be expressed as follows:

$$T_1 = C_t\, H^{3/4} \tag{2.68}$$

C_t is 0.085 for moment-resistant steel space frames, 0.075 for moment-resistant space concrete frames and eccentrically braced steel frames, and 0.050 for all other structures, and H is the height of the structures in meters from the foundation or top of the rigid basement.

3 METHODOLOGIES

This section deals with model geometry, selection of soil parameters, dynamic analysis methods in PLAXIS 2D and DEEPSOIL, and use of horizontal elastic spectra from Eurocode 8. The models are then exposed to three different input motions generated by SeismoMatch 2023 to match the recommended elastic response spectra.

3.1 Models

There are three different models for analysis:

Model 1: Soil Column for Site Response Analysis

Model 2: Six stories, including a basement floor with a shallow foundation

Model 3: Six stories, including a basement floor with a piled raft

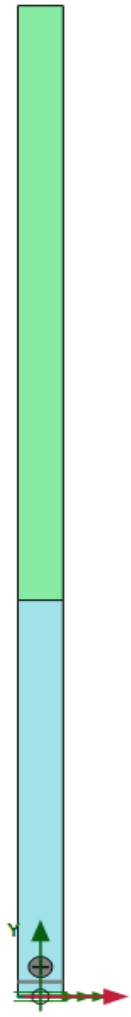

Figure 3- 1 Soil Column for Site Response Analysis

3.1.1 Model 1

The initial model, called Model 1, addresses the analysis of wave propagation in two-layered soil with three distinct input motions. The model considers a soil layer of stiff clay which is 10m, and above this lies 15m of soft clay, and the model is of dimension 1m x 25m. The stiffness parameters for these clay layers are provided in Table 3- 1. The geometry and parameters align with Ground Type S_1 as specified in Eurocode 8. This study aims to examine the response of the soil layers and the amplification factor and to establish their correlation with the DEEPSOIL and the theoretical framework presented in chapter vii. Please refer to Figure 3- 1 for the depiction of the geometric properties.

3.1.2 Model 2

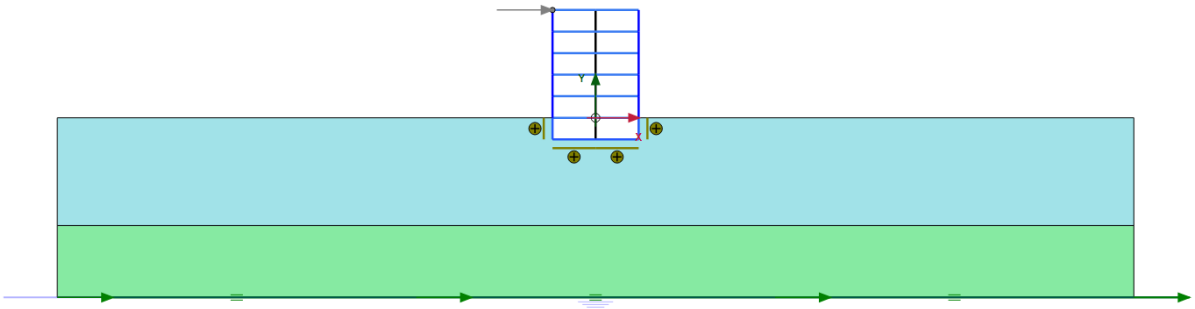

Figure 3- 2 Model 2 with shallow foundation

Model 2, as depicted in Figure 3- 2, exhibits a rectangular soil profile characterized by its inhomogeneity. It is worth noting that this model is of a different geometry than Model 1, a soil column mostly used for site response analysis. The stiffness parameters for the two distinct soil layers are provided in Table 3- 1. The uppermost layer extends from a vertical position of z = 0m to -15m and is classified as soft clay, and from position, z = -15m to -25 m is stiff clay. It incorporates a concrete structure with an excavation to depth of z = -3m, holding a basement. The structure is directly founded on the top layer of ground, and if the soil can hold this structure, a commercial building of 5 floors with a basement is modeled. The construction has a width of 12m and a height of 15m with a floor height of 3m, with material properties as referred to in Table 3- 2, Table 3- 3, and Table 3- 4. The structure bracing is mimicked using a node-to-node anchor that provides axial stiffness. The purpose of the model is to examine the structure's natural frequency when subjected to free vibration and seismic excitations and find out the base shear forces that arise due to the excitation and its verification with Eurocode 8.

3.1.3 Model 3

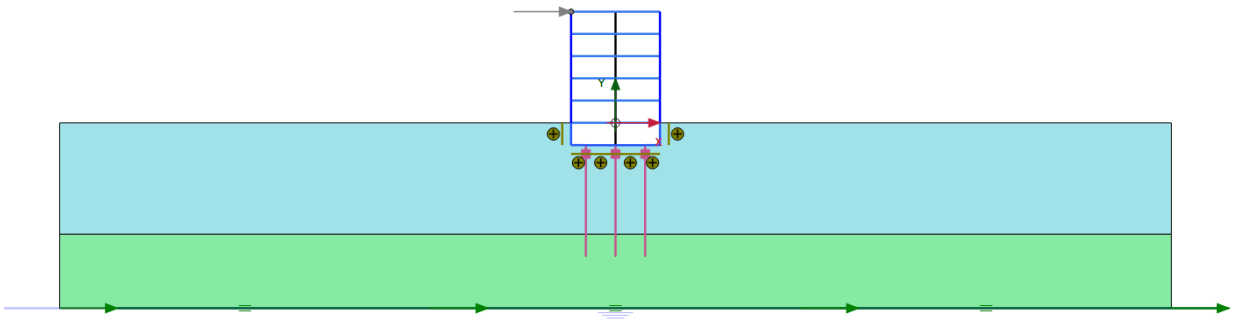

Figure 3- 3 Model 3 with piled-raft foundation

Model 2, as depicted in Figure 3- 3, exhibits a rectangular soil profile characterized by its inhomogeneity. It is worth noting that this model has the same geometry as Model 2, apart from the foundation system. All the information regarding this model is similar to model 2 apart from the foundation system, which is a piled raft foundation. The purpose of the model is to examine the structure's natural frequency when subjected to free vibration and seismic excitations and find out the base shear forces that arise due to the excitation and its verification with Eurocode 8.

3.2 Material Parameters

3.2.1 Soil Parameters

The Hardening Soil Model with Small Strain Stiffness was chosen for numerical analyses using PLAXIS 2D. The parameters for this soil model are presented in Table 3- 1, as per the conditions mentioned in section 2.6.1. The parameters are chosen carefully as it is essential to capture far-field seismic effects using the HSSmall model, which requires precise values of soil parameters. For simulating seismic effects, undrained loading is preferred, and the thesis will use Undrained (A) as it has better accuracy than Undrained (B), and Undrained (A) utilizes effective stress parameters. Undrained shear strength (cu) is also calculated using the effective stress parameters, as it is an input parameter is many of the calculations in this thesis. The modulus reduction curve and damping curves of the HSSmall model are defined by Hardin and Drnevich (1972) and Vucetic and Dobry (1991) for a plasticity index of 50%.

Table 3- 1 Parameter for soft and stiff clay

Parameters	**Soft clay – Upper Layer**	**Stiff Clay – Lower Layer**
Loading Condition	Undrained A	Undrained A
Saturated soil unit weight, γ_{sat}	17 kN/m^3	20 kN/m^3
Unsaturated soil unit weight, γ_{unsat}	17 kN/m^3	20 kN/m^3
Secant stiffness in standard drained triaxial test, E_{50}^{ref}	2000 kPa	20000 kPa
Tangential stiffness in primary oedometer loading, E_{oed}^{ref}	1000 kPa	25000 kPa
Unloading/Reloading stiffness, E_{ur}^{ref}	1000 kPa	95000 kPa
Stress-level dependency power, m	1.0	0.5
Cohesion, c'	5 kPa	10 kPa
Internal Friction, φ	25˚	25˚
Dilatancy angle, Ψ	0˚	0˚
Shear modulus at very small strain, G_0^{ref}	6392 kPa	60000 kPa
Small strain, $\gamma_{0.7}$	0.0001	0.00015
Poisson's ratioν_{ur}	0.2	0.2
K_0- for normally consolidated soil, K_0^{NC}	0.5774	0.5774
Reference stress, P_{ref}	100 kPa	100 kPa
Shear wave velocity, v_s	61.3 m/s	173.2 m/s

According to the PLAXIS reference manual, utilizing an interface factor of less than one is recommended to accurately represent the relative weakness and flexibility of the soil-structure interface compared to the surrounding soil. Hence, the interface between the structure and clay is provided with identical material properties as the clay, except for a manual interface factor R_{inter} of 0.7.

Table 3- 2,Table 3- 3 and Table 3- 4 indicate the material properties of structural elements. All structures' material properties are identical except for the unit weight.

Table 3- 2 Parameters for walls, slabs, and basement

Parameter	Values
Material Type	Elastic Isotropic
Axial Stiffness, EA	12 x 10^6 kN/m
Inertial Stiffness, EI	16 x 10^4 kNm^2/m
Rayleigh Damping, α	0.232
Rayleigh Damping, β	8 x 10^{-3}

Table 3- 3 Unit weights

Parts of Structures	Unit Weight
Walls	5 kN/m/m
Slabs and floors	10 kN/m/m
Basement	20 kN/m/m

Table 3- 4 Parameters for columns (node-to-node anchor)

Parameters	Values
Material Type	Elastic
Axial Stiffness, EA	2.5 x 10^6 kN
Spacing, $L_{spacing}$	3.0 m

3.2.2 Soil Type

To determine the soil type according to Eurocode 8, obtaining the average shear wave velocity of the uppermost layer extending up to a depth of 30 meters is necessary. Subsequently, it is postulated that the soil type can be classified as either bedrock or A-type to infer that the soil located at a depth of 25 meters possesses a shear velocity reaching up to 1000 m/s. Hence, the mean shear wave velocity within the uppermost 30 meters can be expressed as

$$v_{s,30} = \frac{30}{\sum_{1}^{n} \frac{h_i}{v_i}} = \frac{30}{\frac{15}{61.3} + \frac{10}{172.3} + \frac{5}{1000}} = 97.5 \text{ m/s}$$

From Appendix 1, the soil type corresponding to this shear wave velocity is ground type S_1. This is further confirmed by the fact that the ground consists of a 15m thick deposit of soft clay.

3.2.3 Damping parameters

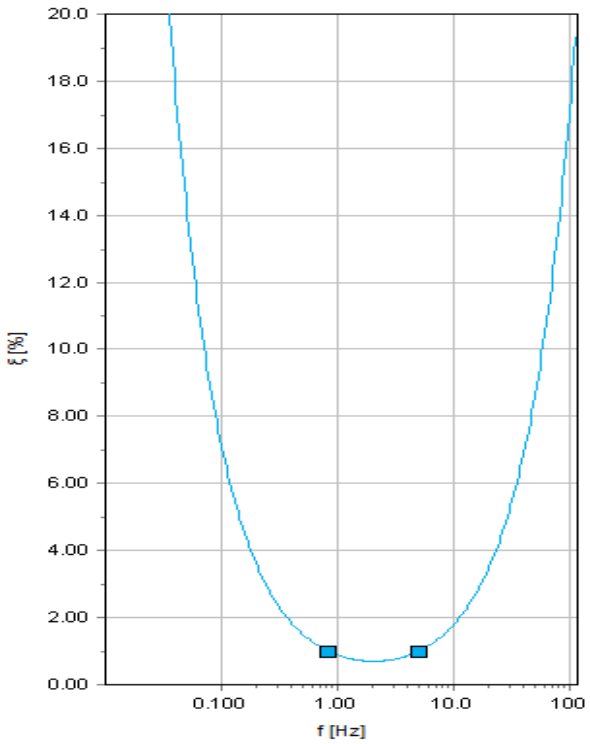

Figure 3- 4 Rayleigh parameter as calculated by PLAXIS 2D for Imperial Valley

The determination of Rayleigh parameters for the model is based on the comprehensive analysis presented in section 2.1.3.1. The initial target frequency refers to the mean inherent frequency of the soil deposit, while the second target frequency pertains to the proportion between the input motion's fundamental frequency and the soil's natural frequency.

The average shear wave velocity of 25 thick soil deposits is,

$$v_{s,25} = \frac{25}{\sum_{1}^{n} \frac{h_i}{v_i}} = \frac{25}{\frac{15}{61.3} + \frac{10}{172.3}} = 82.58 \text{ m/s}$$

And the fundamental frequency of the soil deposit, $f1 = \frac{v_{s,25}}{4H} = 0.83$ Hz

Three different input motions are used for the analysis: Imperial Valley, Friuli, and Nahanni. Since all these motions are naturally occurring, they have varying frequencies and different predominant periods. The input motions Imperial Valley, Friuli, and Nahanni have predominant periods of 0.32s, 0.22s, and 0.36s, which corresponds to 3.125Hz, 4.54Hz, and 2.78 Hz,

respectively. This means that f_2 will be 5 Hz, 7 Hz, and 5 Hz when Imperial Valley, Friuli, and Nahanni are used as input motions, respectively, with a target damping ratio of 1%. Using these parameters, Rayleigh parameters are calculated by PLAXIS 2D.

Figures 3- 5 and 3- 6 depict the damping curve for the stiff and soft clay layers, respectively. The curves displayed are automatically generated by PLAXIS 2D using specifically selected values of G_0^{ref} and $\gamma_{0.7}$.

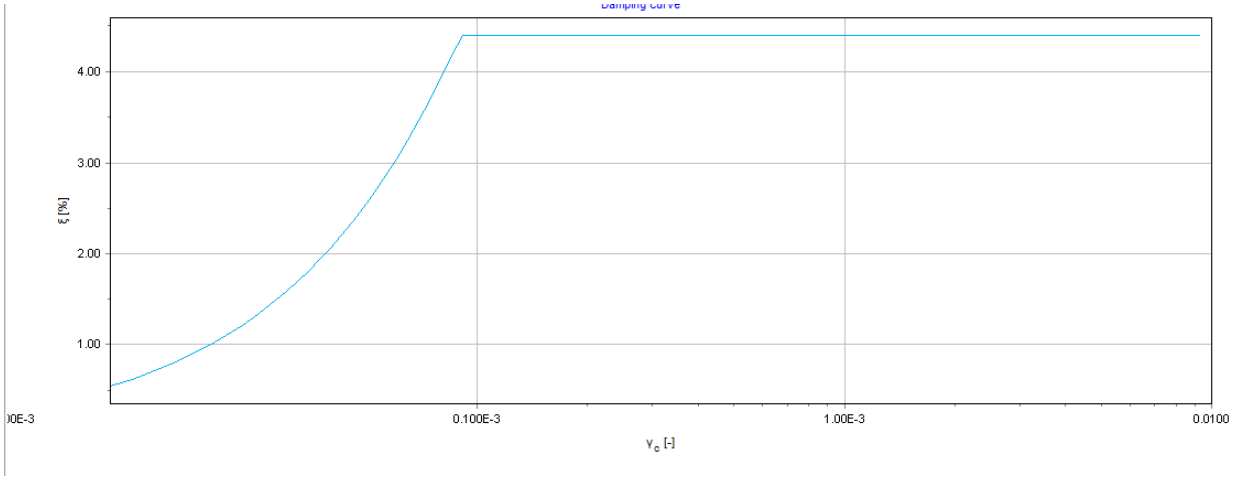

Figure 3- 5 Damping curve for stiff clay generated by PLAXIS 2D

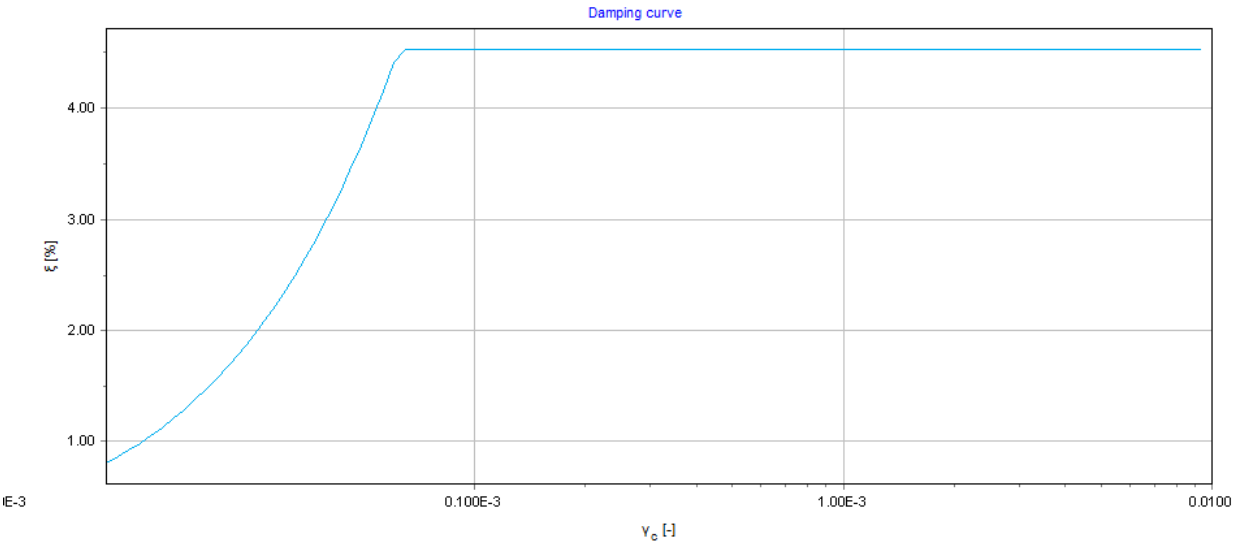

Figure 3- 6 Damping curve for soft clay generated by PLAXIS 2D

3.2.4 Shear Modulus

Figure 3- 7 and Figure 3- 8 depict the reduction curves for the shear modulus, G, for the stiff and soft clay layers. G_t and G_s represent the tangent and secant shear moduli, respectively. The

curves displayed are automatically generated by PLAXIS 2D using selected values of G, with reference values of G_0^{ref} and $\gamma_{0.7}$.

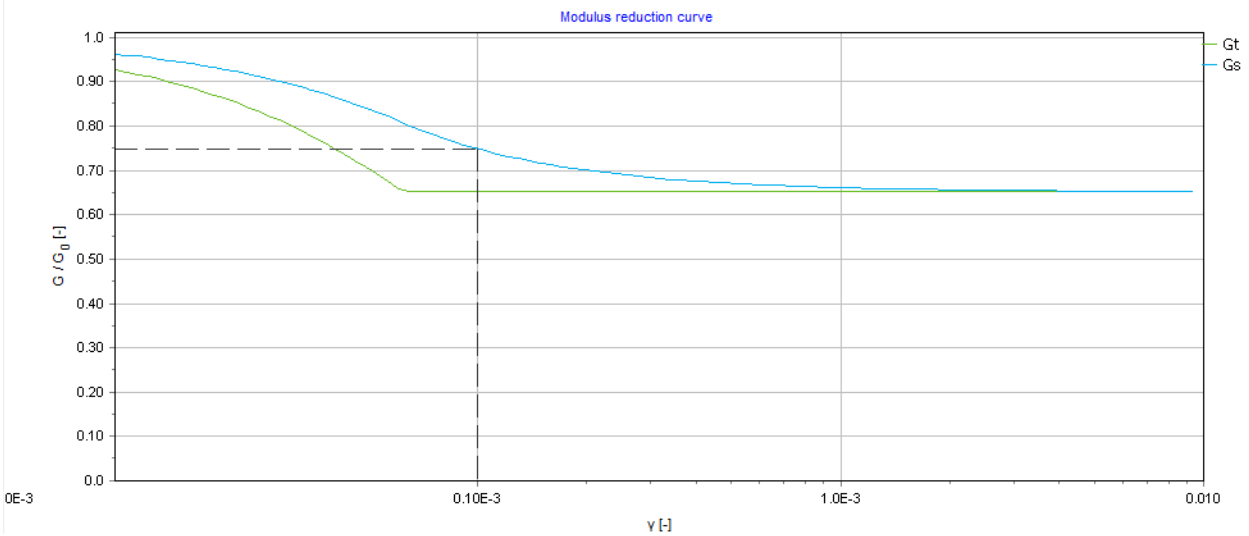

Figure 3- 7 Modulus Reduction curve for Soft Clay generated in PLAXIS 2D

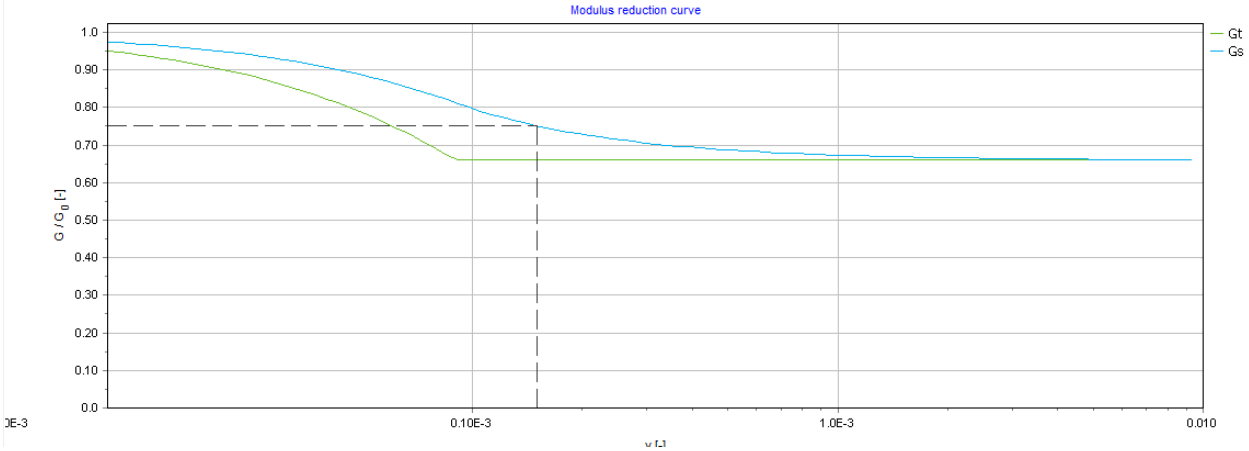

Figure 3- 8 Modulus Reduction curve for Stiff Clay generated in PLAXIS 2D

3.2.5 Modeling of Pile as Embedded Beam Row

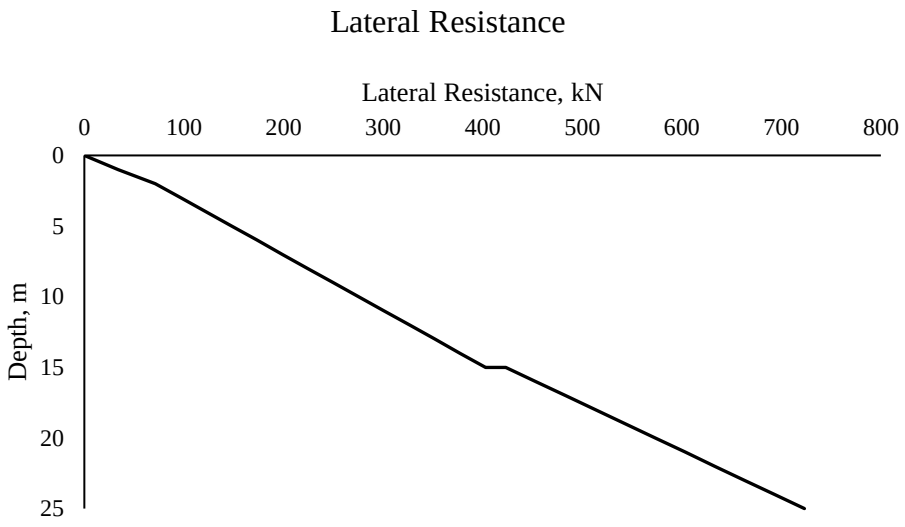

Figure 3- 9 Lateral resistance of pile over the depth

The construction and use of the pile as an embedded beam row are carried out following the principles outlined in section 2.8.2. The input influences the sensitivity of the performance of an embedded beam. Hence, the initial step involves the computation of the axial, lateral, and base resistances. The Appendix contains a comprehensive calculation of these input parameters, and they are entered in PLAXIS 2D as muti-linear data. The center-to-center spacing between piles in the plane is 4m for the structure.

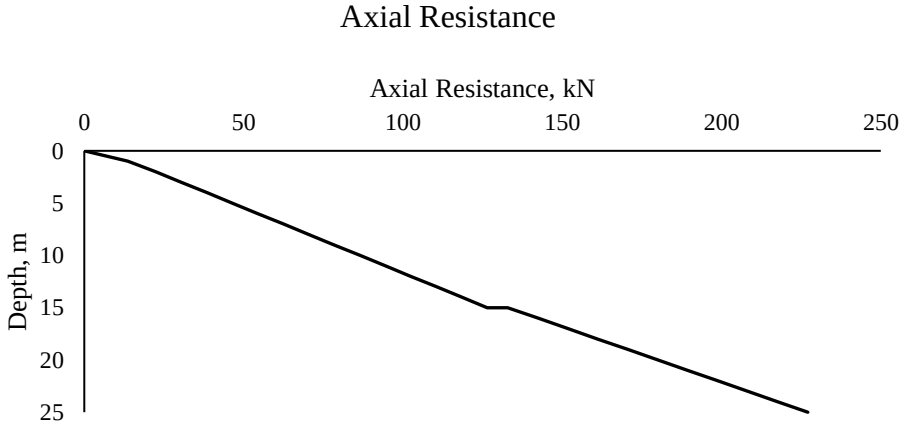

Figure 3- 10 Axial resistance of the pile over the depth

Table 3- 5 Parameters for pile modeled as embedded beam row element.

Parameter	Values
Material Model	Elastic
Young's Modulus, E	30 x 10^6 kN/m^2
Unit Weight, γ	25 kN/m3
Pile Type	Predefined circular pile
Diameter, D	0.5m
Out of plane c/c spacing, $L_{spacing}$	4m
Base Resistance,	
Interface Stiffness Factor	Generated by PLAXIS 2D
Axial Stiffness Factor, ISF_{Rs}	0.5256
Lateral Stiffness Factor, ISF_{Rn}	0.5256
Base Stiffness Factor, ISF_{Kf}	5.356

3.3 Earthquake Input Motions

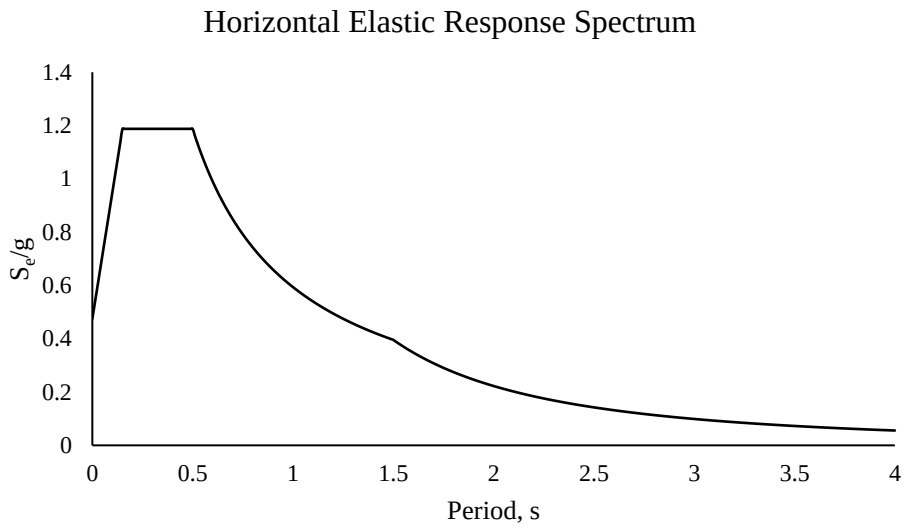

Figure 3- 11 Horizontal elastic response spectra when bedrock is between 20-35m.

As previously stated, each model is exposed to three different seismic events: Imperial Valley, Friuli, and Nahanni as per the recommendations in report by Bungum H. et al. (1998). The program SeismoMatch does a spectral matching of an input motion with a desired target spectrum, in this case, as mentioned in section 2.9.2.1 and national annex of NS-EN 1998-1 for soil type S1 recommended values when the bedrock is between 20-35m are chosen. Thus, using S = 1.9, T_B = 0.15, T_C = 0.50, T_D = 1.5, and choosing Trondheim as our site location, and as per Appendix 1, a_{gR} is given as 0.25g. Finally, an elastic response spectra, as shown in Figure 3- 11, is established per Eurocode 8.

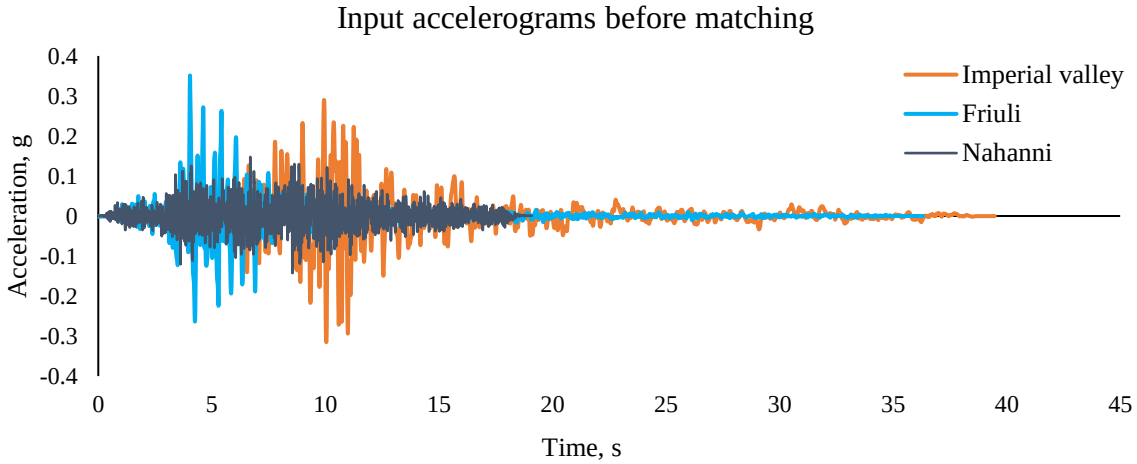

Figure 3- 12 Input accelerograms before spectral matching

This is the recommended horizontal elastic spectrum with which the three different earthquake motions were matched, and input motions for our thesis study were created.

The input motion before spectral matching is shown in Figure 3- 12, where all of them are overlayed over each other, with varying peak ground acceleration and period. Table 3- 6 presents the characteristics of the chosen accelerograms.

Table 3- 6 Characteristics of input motions before spectral matching

Accelerogram	Friuli	Imperial Valley	Nahanni
Max Acceleration (g)	0.35	0.32	0.15
Max Velocity (cm/sec)	22.02	31.50	6.08
Max Displacement (cm)	4.07	14.13	3.08
Arias Intensity	0.78	1.26	0.28
Predominant Period (sec)	0.26	0.14	0.12

The accelerogram, upon spectral matching, produced matched accelerogram and spectrum as shown in Figure 3- 13, where it can be seen that the PSA of all the input motions has matched around the target spectra and the resulting accelerograms are made accordingly as seen in Figure 3-4, and Table 3- 7 Characteristics of input motions after spectral matching shows the properties of the matched accelerograms.

Table 3- 7 Characteristics of input motions after spectral matching

Accelerogram	Friuli	Imperial Valley	Nahanni
Max Acceleration (g)	0.60	0.53	0.45
Max Velocity (cm/sec)	55.60	47.25	40.17
Max Displacement (cm)	10.67	31.90	9.49
Arias Intensity	2.64	4.53	3.66
Predominant Period (sec)	0.22	0.32	0.36

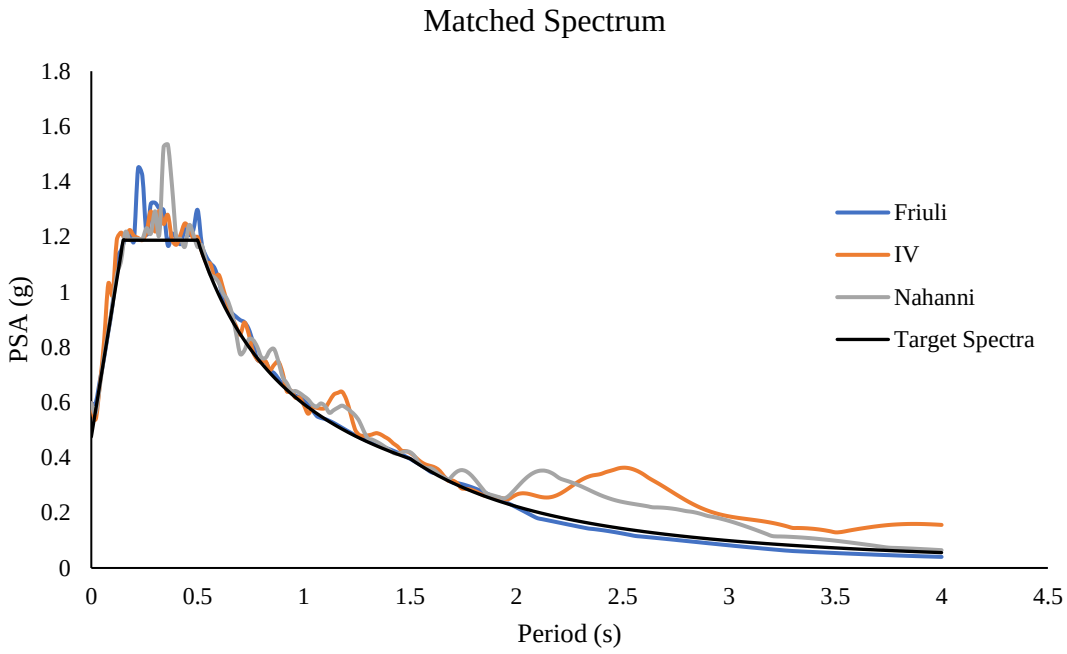

Figure 3- 13 PSA spectrum of the input motions after spectral matching

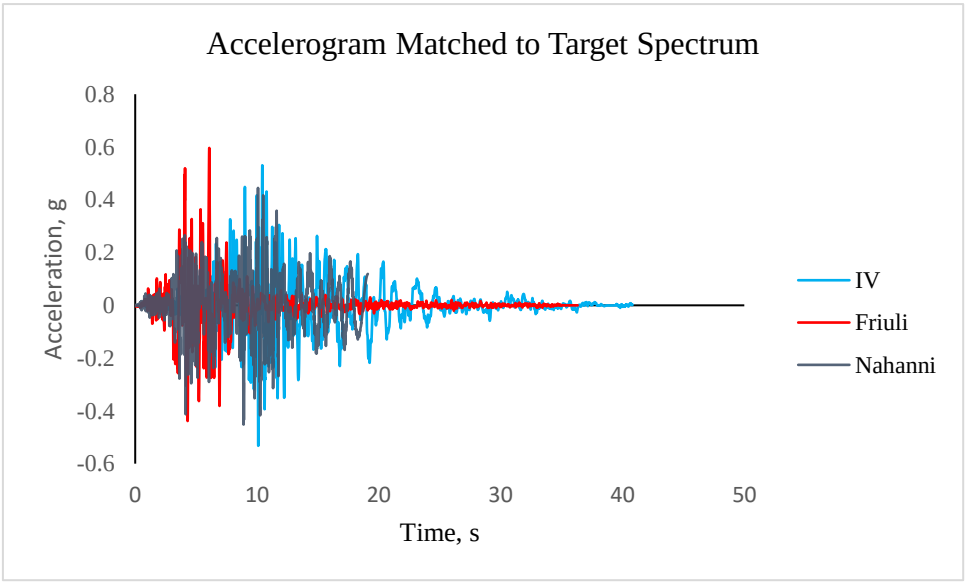

Figure 3- 14 Final input accelerograms after spectral matching

3.4 Dynamic Analysis in PLAXIS 2D

The PLAXIS 2D model is built using a 15-node triangular element under plain strain conditions, where the out-of-plane strain is constrained and, therefore, equal to zero. Before commencing analysis, it is necessary to incorporate loading and appropriate boundary

conditions into the models, following the soil and structural geometry modeling and the application of material properties. The following are the enumerated steps of dynamic analysis.

3.4.1 Boundary Condition and Time Stepping

The dynamic line displacement is applied as ground motion at the lower boundary. The x-component of the line displacement of the lower boundary is determined by a constant value of 1.0m, while the y-component remains fixed. The input motion has a duration of 40.82s, 36.32s, and 19.09 for Imperial valley, Friuli, and Nahanni accelerograms with a time interval of 0.01 seconds except for Nahanni, for which the time interval is 0.005, and the manual time step determination yields a maximum number of steps equal to 4082, 3632 and 1909 respectively. The sub-steps while analyzing the Nahanni accelerogram is set to 2 as per numerical requirements.

As previously mentioned, the vertical boundaries on both sides are adequately spaced to minimize the boundary condition's impact due to the seismic wave's reflection. It is a widely accepted convention to provide a depth of three times the soil profile (3H) on each side. In the present study, each model is allocated a width of 75 meters on both sides, resulting in a total width of 150 meters. The depth of the models is set at 25 meters. The selection of the most viable boundary condition for dynamic analysis is determined through a review of previous studies conducted by various authors, including Brandt(2014), (Chadha (2015), and Magar (2016).

Consequently, the lateral boundaries on both sides are given tied degrees of freedom, while the top and bottom boundaries are constrained with standard fixities (none). Prior research and expert suggestions determine the selection of boundary conditions. The evaluation of performance boundary conditions and the assessment of their applicability are crucial tasks; for this thesis study, using all three accelerograms in the established model 1, the input motion for Imperial valley was compared to the motion registered at the base of the model 1 and the result for is shown in Figure 3- 15. The figure concludes that the selected boundary conditions provide good performance and can also be used in all upcoming analyses.

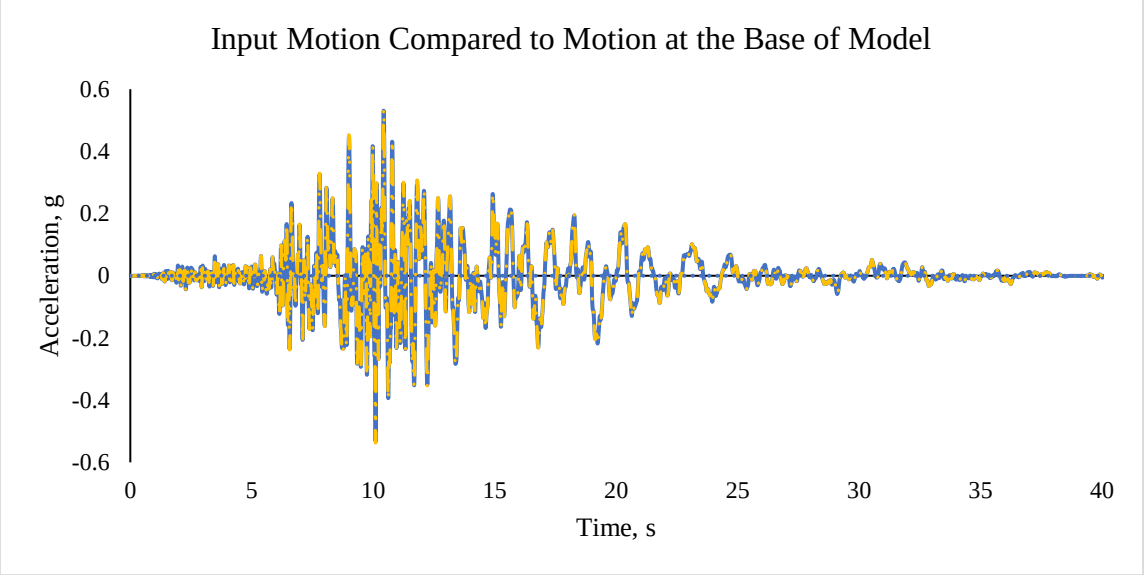

Figure 3- 15 Input motion compared to the motion registered at the base of the PLAXIS soil model

3.4.2 Stage Construction

Table 3- 8 and Table 3- 9shows the model without structural components is constructed in 3 steps, and models with structural elements are built with five phases, respectively.

Table 3- 8 Phases for site response analysis

Phase	Calculation Type	Description
Initial Phase	K0-Procedure	
Phase-1	Plastic	
Phase-2	Dynamic	Site Response Analysis, Dynamic time interval as per accelerogram used

Table 3- 9 Phases for seismic analysis of buildings

Phase	Calculation Type	Description
Initial Phase	K0-Procedure	Structures Deactivated
Phase-1	Plastic	Activated Structure, excavation to -3m
Phase-2	Plastic	Horizontal load activated; displacement reset to zero
Phase-3	Dynamic	Dynamic time interval 5s
Phase-4	Dynamic	Displacement and time set to zero, dynamic time interval as per accelerogram used

4 RESULTS

The preceding chapter describes constructing a Finite Element Method (FEM) model in PLAXIS 2D. The constructed models are subjected to analysis to evaluate their performance concerning the input motion provided.

Initially, a site response analysis is performed to ascertain the behavior of soil material in its unaltered state, devoid of any structural modifications. The soil response is subsequently compared to a one-dimensional DEEPSOIL analysis to validate the findings. Later, the structures are built and subjected to free vibration analysis to determine the natural frequencies associated with each model. A comprehensive dynamic analysis is conducted on both models, incorporating structural considerations. The shear force calculation at the base is derived from the PLAXIS 2D analysis, and the soil-structure interaction is analyzed. The determination of the natural period of the structure and the shear force at the base is performed as per the guidelines outlined in Eurocode 8. The results obtained are subsequently subjected to comparison.

4.1 Site response analysis

Site Response Analysis's purpose is to evaluate a soil deposit's behavior in response to an earthquake motion. This statement elucidates how shear wave motion is distributed from the underlying bedrock to the uppermost layer of soil. Additionally, it assesses the amplification of the input acceleration as it propagates through the soil stratum. The comprehension of site amplification is crucial to ascertain the intensity of the seismic wave that a structure will encounter and anticipate the structure's critical natural frequency in response to said seismic motion.

In this study, the site response analysis is crucial to understand the local site effects and the capacity of the soil layers to dampen or amplify the seismic waves. The models built in PLAXIS 2D produce results that are verified with the results from DEEPSOIL. If the models are constructed accurately, the results should demonstrate a reasonable level of similarity. It is anticipated that there will be variations in the results of these two analyses due to differences in analysis methodology and underlying assumptions. The findings of these two analyses are presented about:

a. Acceleration (g) vs Time (s)

b. Response spectra: PSA (g) vs. Period (s)

The correlation between the peak horizontal acceleration and the dynamic forces exerted on a structure by earthquake motion is significant, yet it alone does not comprehensively describe the earthquake characteristics.

Apart from the accelerogram and response spectra, the generated accelerogram is often transformed to the frequency domain, and a Fast Fourier Transform is obtained. This gives information about how the amplitude of the ground motion is distributed among various frequencies, and this information is much helpful since a structure's dynamic response depends on both the amplitude of loads applied and the frequency range in which the seismic wave is concentrated. Likewise, the relative displacement response spectrum is also evaluated as this provides the maximum displacement that can occur in a structure which is essential for visualizing the impending hazard.

4.1.1 PLAXIS 2D

A non-linear dissipative model is constructed in PLAXIS 2D using the HS small model to account for the hysteresis phenomenon exhibited by the soil under seismic conditions. The soil parameters are utilized per section 3.2. Two nodes are chosen from the generated mesh to observe the outcome. One node is selected at the bedrock level, while the other is determined at the surface.

Table 4- 1 Coordinated of selected nodes

Nodes	Coordinate	Location
TOP	(0, 25)	Surface Level
BOTTOM	(0, 0)	At the bottom of the soil layer

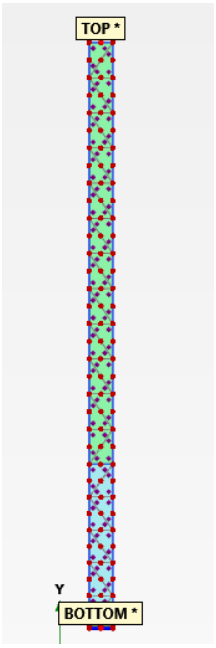

Figure 4- 1 Soil column: Model 1

4.1.1.1 Friuli

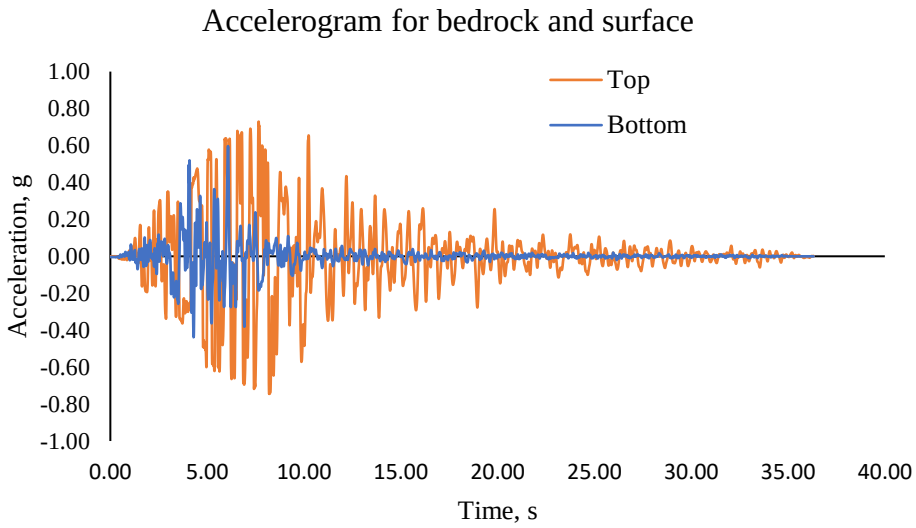

Figure 4- 2 Accelerogram registered at the base and surface of soil column for Friuli obtained from PLAXIS

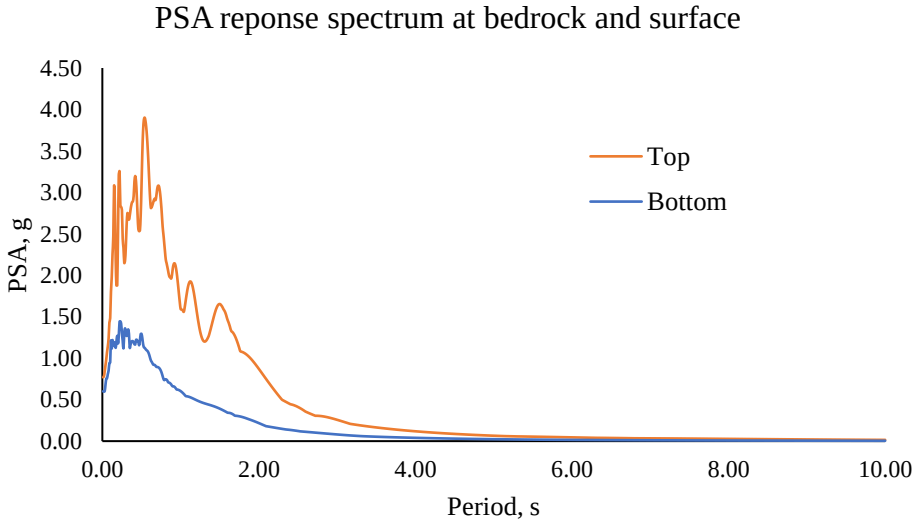

Figure 4- 3 PSA response spectrum at bedrock and surface for Friuli obtained from PLAXIS

4.1.1.2 Imperial Valley

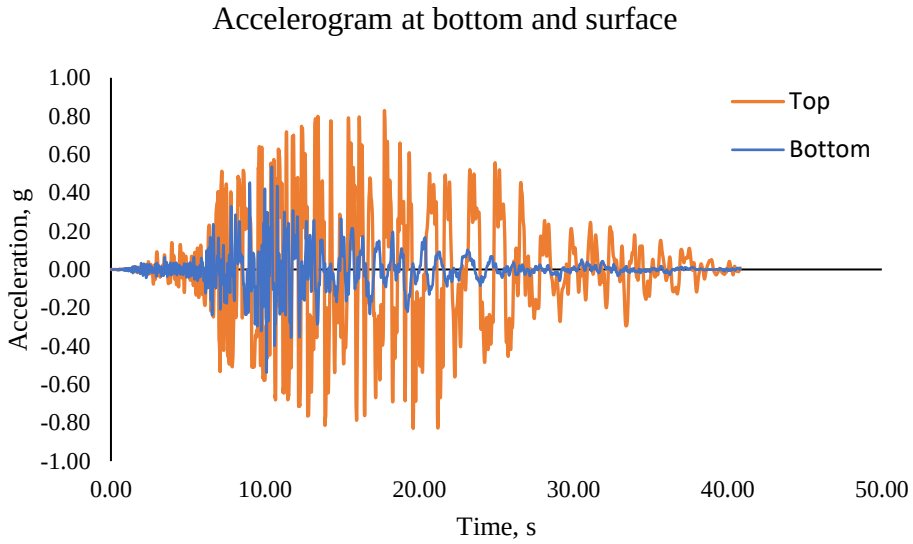

Figure 4- 4 Accelerogram registered at the base and surface of soil column for Imperial Valley obtained from PLAXIS.

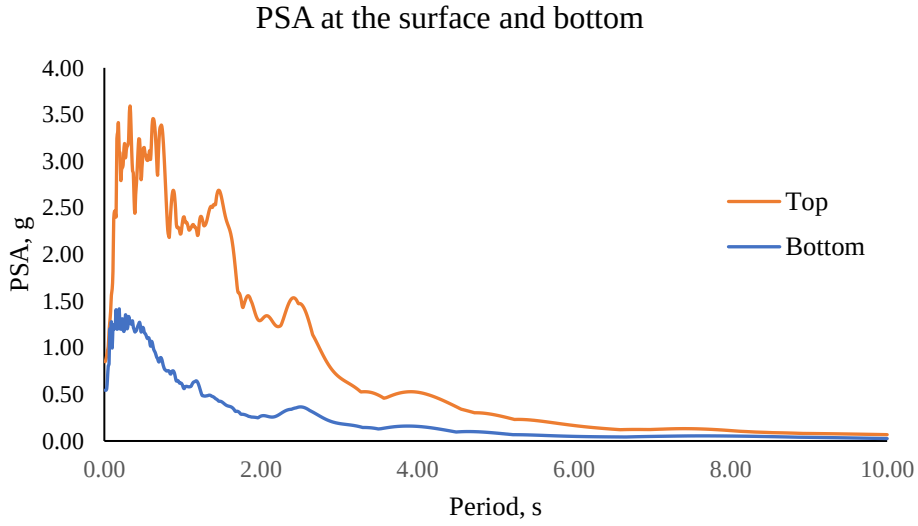

Figure 4- 5 PSA response spectrum at bedrock and surface for Imperial Valley obtained from PLAXIS.

4.1.1.3 Nahanni

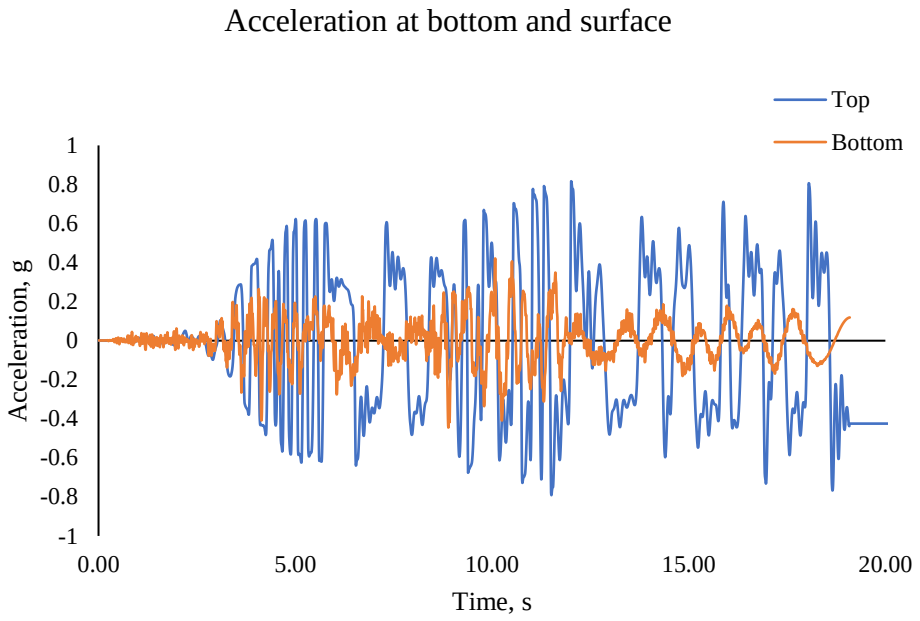

Figure 4- 6 Accelerogram registered at the base and surface of soil column for Nahanni obtained from PLAXIS

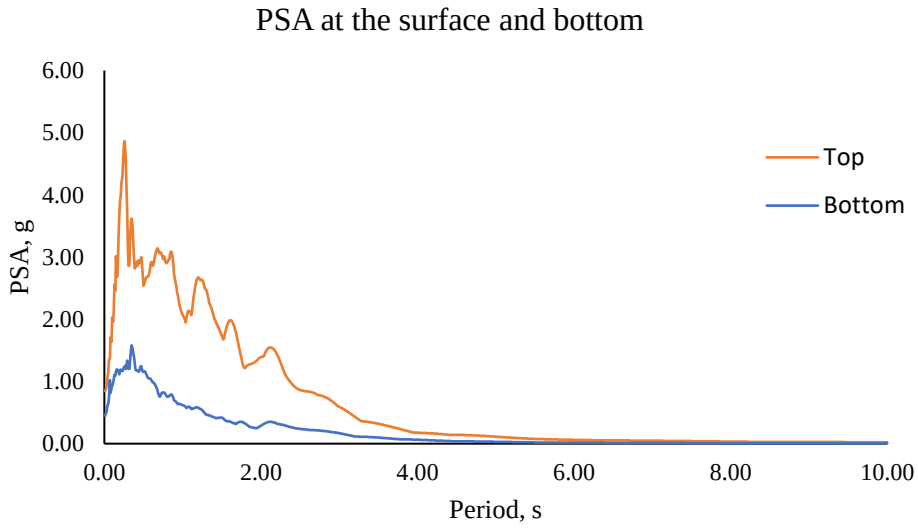

Figure 4- 7 PSA response spectrum at bedrock and surface for Nahanni obtained from PLAXIS

4.1.2 DeepSoil

One-dimensional non-linear and equivalent linear ground response analysis has been conducted utilizing the specialized software DEEPSOIL. The study is performed utilizing a total stress method within the time domain. The classification of soil layers is determined based on the unit weight and average shear wave velocity, as used in the PLAXIS 2D software. The material model utilized in this program offers the flexibility to select from a predefined dataset, such as the Vucetic and Dobry (1991) model specifically designed for clay. In this study, the modulus reduction curve defined by Hardin and Drnevich (1972) is chosen, and the damping ratio curve is based on Vucetic and Dobry's (1991) approach, specifically at a plasticity index of 50%. This selection is made to align it with the HSsmall model, as detailed in. It is possible to choose bedrock properties in elastic half-space. The shear wave velocity of the bedrock is assumed to be 1000 m/s, unit weight 35 KN/m, and default damping ratio of 2%. The number of iterations is 15, and the effective shear strain ratio is 0.65.

The input motion described in section 3.3 is also utilized in the DEEPSOIL software. Once all the necessary steps have been completed, the model is examined to obtain the ground response at the top layer.

The obtained accelerograms demonstrate an increase in peak acceleration on the top layer. The site amplification factor is determined to be 1.6, and the peak acceleration is observed at different periods of these selected natural time-history, as shown in Figure 4- 8 to Figure 4-13. The response spectra for peak acceleration are calculated assuming a damping ratio of 5%.

4.1.2.1 Friuli

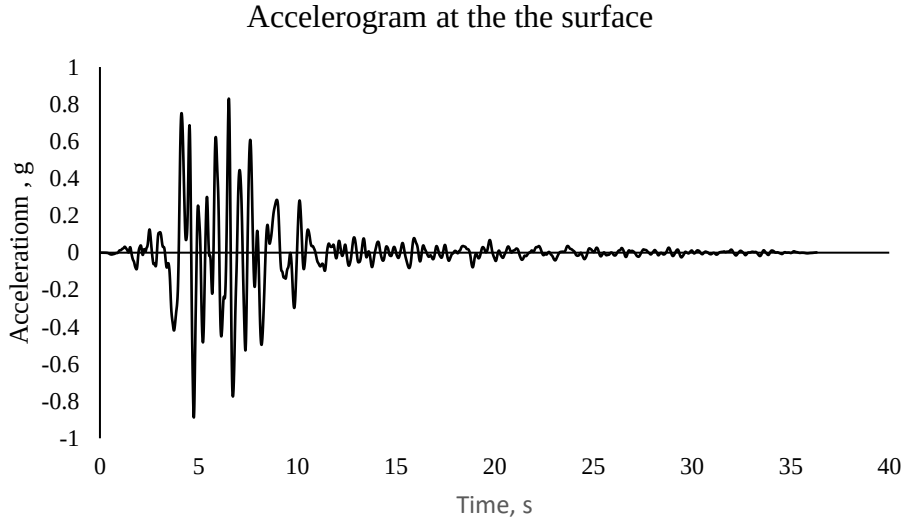

Figure 4- 8 Accelerogram registered at the base and surface of soil column for Friuli obtained from PLAXIS

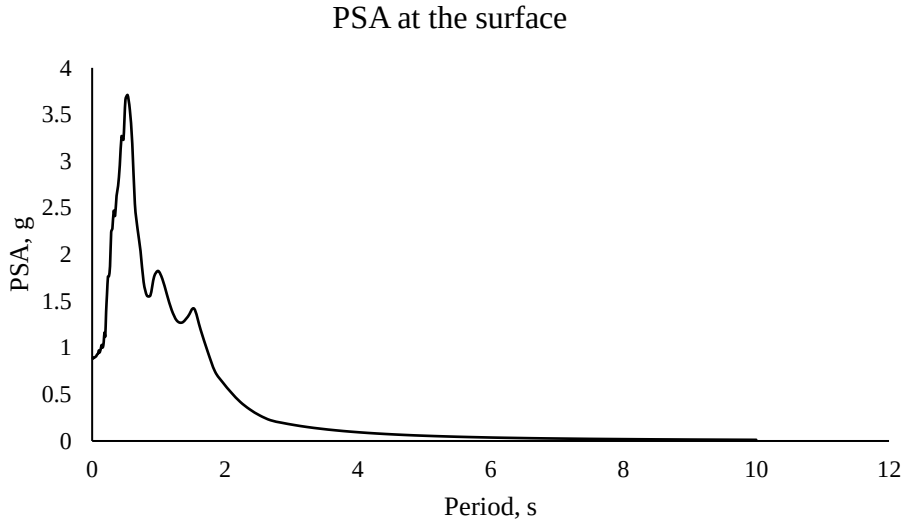

Figure 4- 9 PSA response spectrum at bedrock and surface for Friuli obtained from PLAXIS

4.1.2.2 Imperial Valley

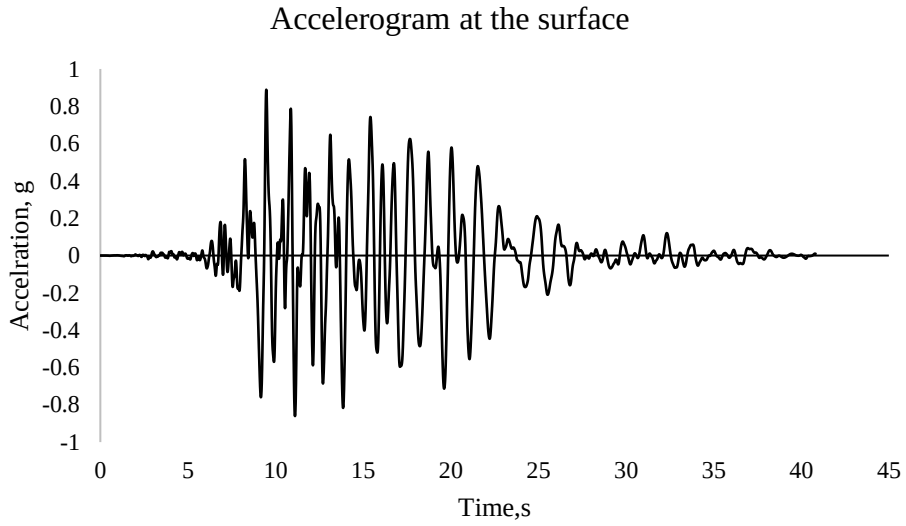

Figure 4- 10 Accelerogram registered at the base and surface of soil column for Imperial Valley obtained from PLAXIS.

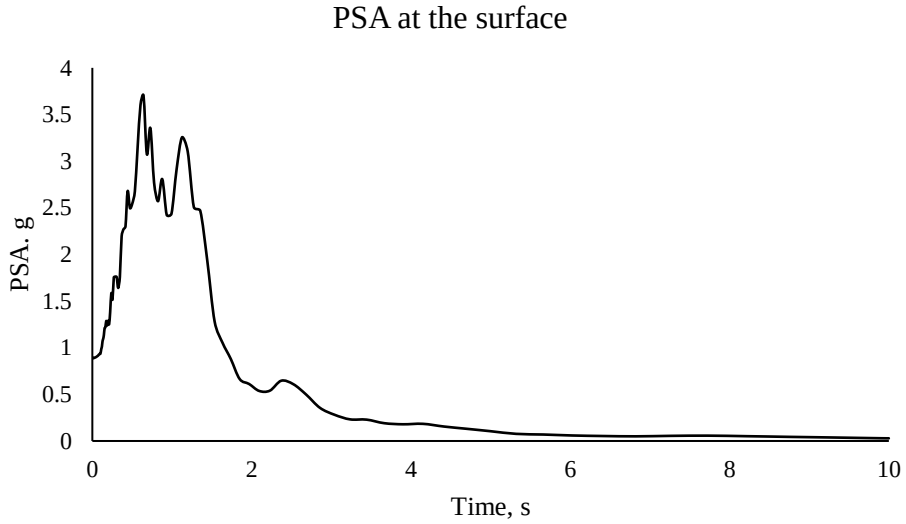

Figure 4- 11 PSA response spectrum at bedrock and surface for Friuli obtained from PLAXIS

4.1.2.3 Nahanni

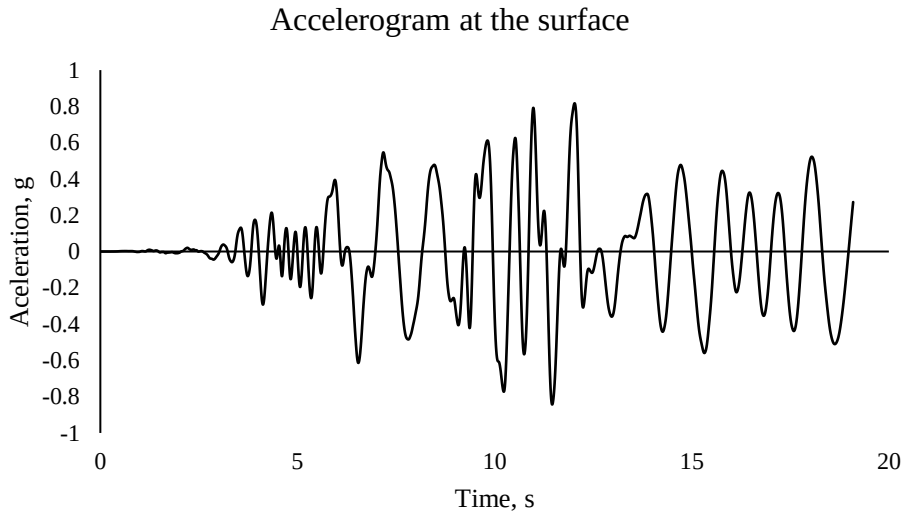

Figure 4- 12 Accelerogram registered at the base and surface of soil column for Imperial Valley obtained from PLAXIS

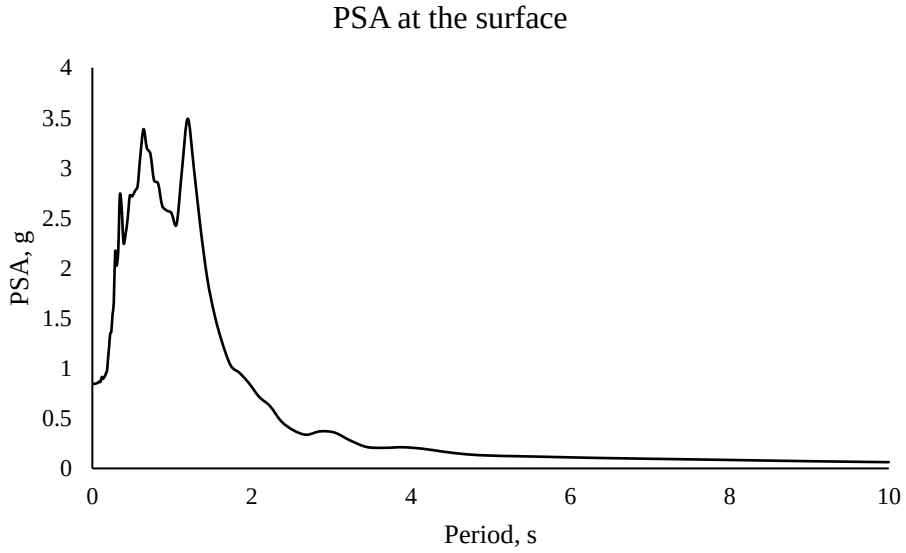

Figure 4- 13 PSA response spectrum at bedrock and surface for Friuli obtained from PLAXIS

4.1.3 Summary and Discussion

Figure 4- 14, Figure 4- 15, and Figure 4- 16 show the results from PLAXIS and DEEPSOIL regarding the PSA response spectrum and the accelerogram at the surface, respectively. The result displays sufficient commonalities as the peak acceleration is between 3.5 and 4.7 when the base layer is subjected to input motions matched to the same target elastic spectrum. In all situations, when the accelerograms presented in section 4.1.1 are compared to the one from DEEPSOIL at the surface level, they offer great similarities and peaks at the same period with similar peak ground acceleration.

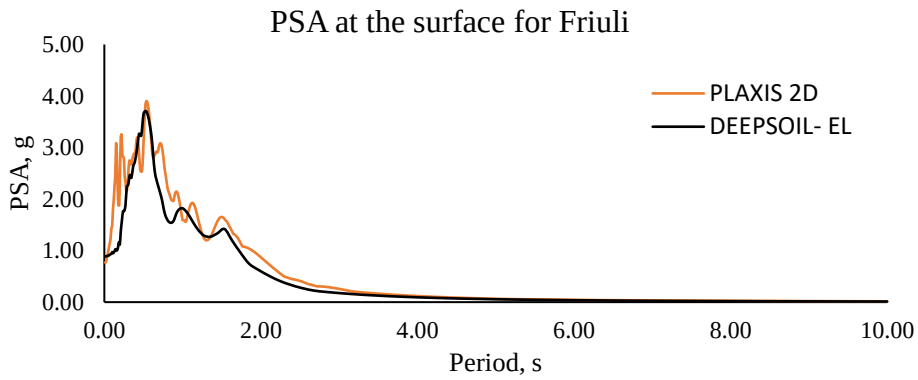

Figure 4- 14 Comparison PSA spectrum for Friuli

Since all the input motions peak at different periods, this provides realistic ideas of how the natural structure period would interact with varying input motions. Thus, it is recommended to perform a site response analysis with multiple input motions so that structure design can be proceeded based on the response of soil and averaging out all results. The input motions chosen are based on a study performed for the Norwegian coastline. Hence, avoiding the periods where peak accelerations occur while building construction will be helpful to prevent resonance. A structure's natural period can be determined in a variety of ways. It is determined analytically using the stiffness and damping ratio. In a later section of this study, structures' natural frequencies are estimated using PLAXIS, logarithmic decrement, and Eurocode 8. The

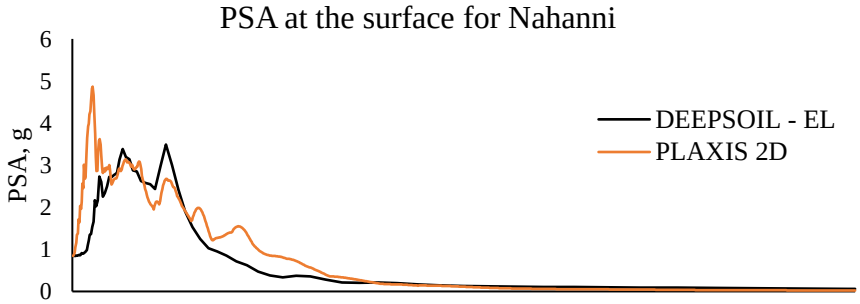

Figure 4- 15 Comparison PSA spectrum for Nahanni

response spectra's y-axis in Figure 4- 15 shows the range of possible acceleration for the SDOF system and when these accelerations are likely to occur when 5% damping is considered.

While DEEPSOIL is characterized by the General Quadratic/Hyperbolic model and input shear wave velocity and unit weight, the soil model in PLAXIS 2D is distinguished by HSsmall, which also integrates the non-linear dissipative behavior and appropriate stiffness qualities according to the input value. The stiffness properties of these two programs are difficult to match, and the manual computation is not calibrated for one another. Boundary circumstances might potentially impact the results. DEEPSOIL specified the bedrock properties with a certain shear wave velocity and unit weight. It was only established in PLAXIS with a tied boundary in the y direction and a predetermined displacement in the x direction. As a result, a periodic vibration with a significant amplitude is produced in PLAXIS because the deposit's bottom border is configured to be entirely reflecting.

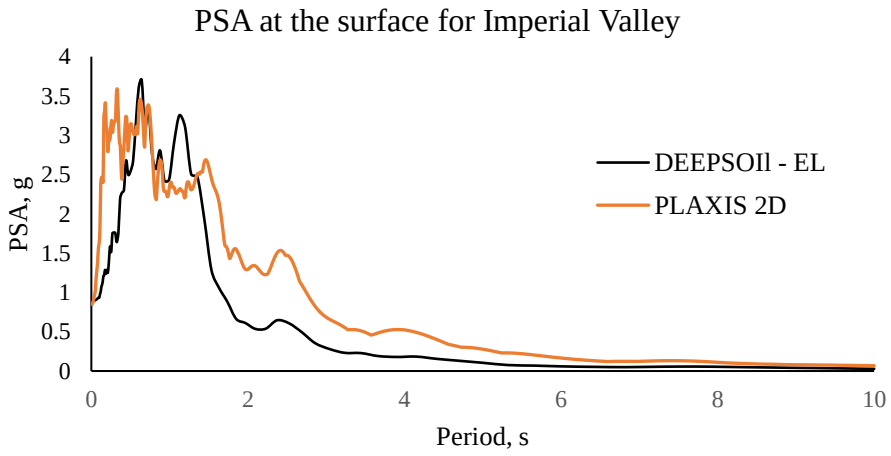

Figure 4- 16 Comparison PSA spectrum for Imperial Valley

Assumptions for one-dimensional non-linear and equivalent linear analysis are also based on iteratively updating the tangent shear modulus and secant shear modulus, and damping ratio until they align with the degree of strain in each layer. At the same time, the PLAXIS analysis is based on the soil's nonlinear hysteresis characteristic.

However, the final results reveal the soil behavior and the equivalent linear analysis performed in DEEPSOIL and nonlinear analysis in PLAXIS 2D are in general agreement, as seen in the above three response spectra. Although, it should be noted that the non-linear analysis performed in DEEPSOIL predicted the peak ground acceleration and PSA at different frequencies much lower than previous models predicted. The results have been attached to Appendix 4 as additional information, and it has been evaluated that even though similar

material parameters were utilized, the non-linear analysis in DEEPSOIL undervalued the extended linear behavior of extremely soft clay that has been used. The model could have overvalued the soft clay's non-linear behavior, which generally does not happen in reality. Thus, the thesis has decided to use the equivalent linear results from DEEPSOIl to verify results from PLAXIS 2D.

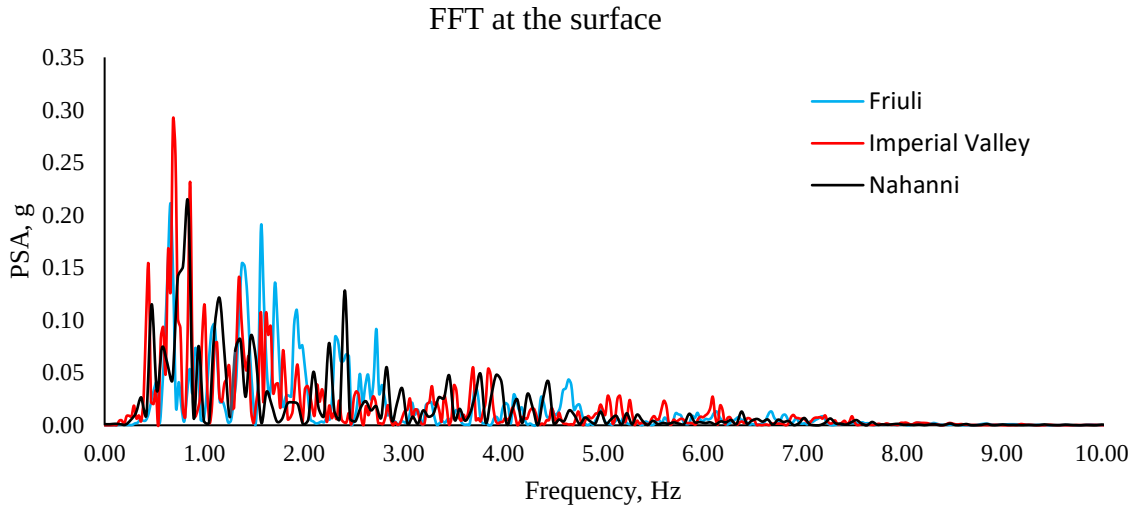

Figure 4- 17 FFTs registered at the surface as per PLAXIS

According to Figure 4- 17, 1 Hz corresponds to the greatest acceleration at the ground level. The frequency range where the main energy content is dispersed is 0.5 Hz–2 Hz. On the other hand, between 2 Hz and 3 Hz, the energy content of input acceleration is relatively equally distributed. This indicates that the energy content was affected by the filter action of the soil deposit and was focused on a narrower range.

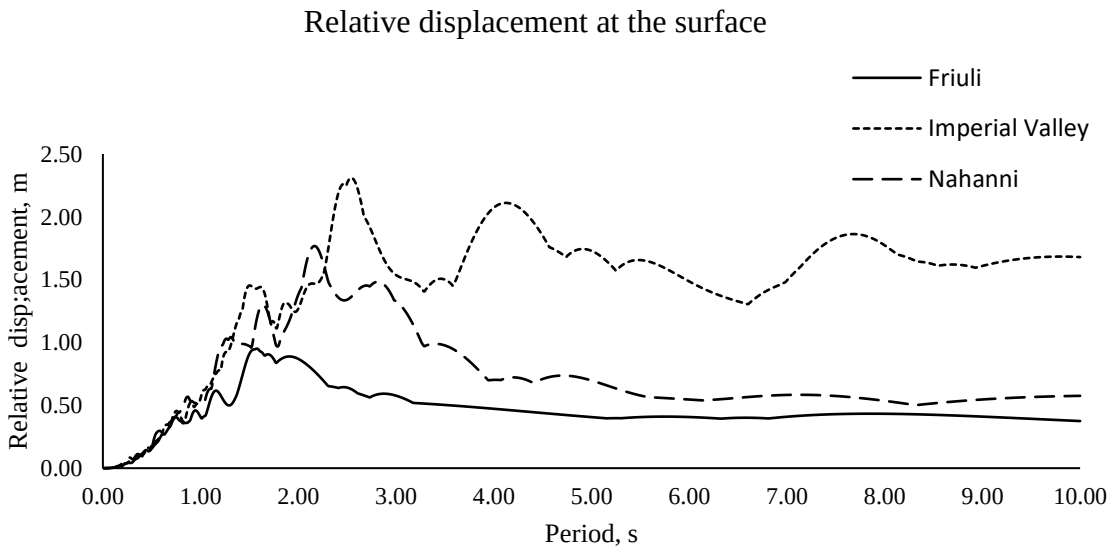

Figure 4- 18 Relative displacement at the surface as per PLAXIS

The relative displacement response spectrum shows the maximum displacement of a structure possible for the given period. Maximum static force may be estimated from this maximum displacement by multiplying it by the structure's stiffness. Figure 4- 18 shows that the displacement is relatively small for structures with higher natural periods and gets larger as the natural period is short, especially between 2 and 3m, yet it can be noticed that the Imperial Valley motion creates very high displacements for the structure situated in the ground type considered for the this. These kinds of anomalies are the reason for probabilistic study before building any structure on the proposed site, and multiple motions can be regarded as suitable for given site conditions and time and cost constraints.

4.2 Free Vibration Analysis

Once the site response analysis provides an in-depth idea of the site conditions, the structure is

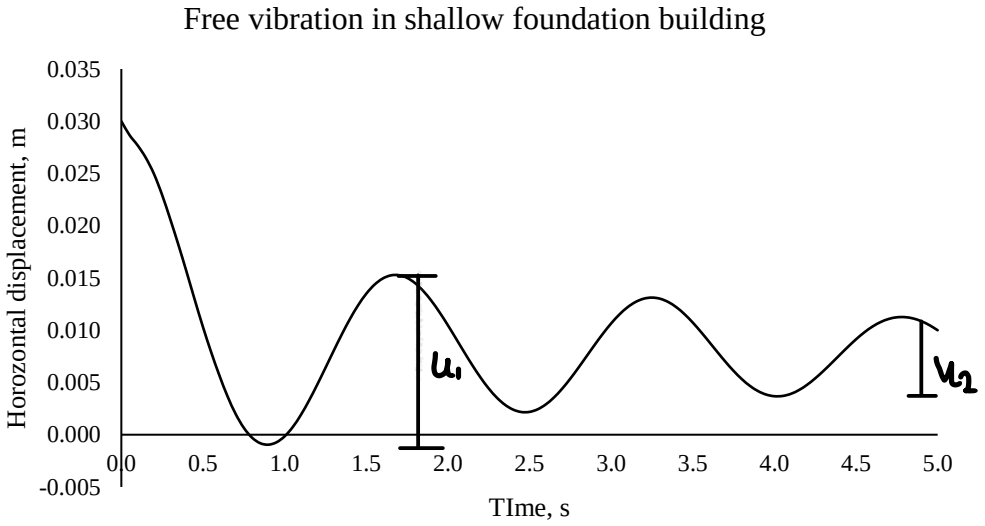

Figure 4- 19 Free vibration in shallow foundation building

built into the model to facilitate the free vibration analysis. Free vibration analysis is conducted to ascertain the structure's natural frequency. A load of 10 kN/m is applied to the upper left corner of the building. The earthquake motion is used for five seconds, and the structure can undergo free vibration. Hence, the natural period of the structure is determined.

The natural frequency derived from the PLAXIS 2D can be compared to the frequency computed using the logarithmic decrement method, as outlined in section 2.1.3.2. The logarithmic decrement δ is calculated initially for the five-storey structure with a shallow

foundation, as shown in Figure 4- 19. The equation below is employed to analyze the structural behavior of a five-storey building.:

$$\delta = \frac{1}{n}\ln\frac{u_1}{u_{n+1}} \cong \frac{1}{2}\ln\frac{0.0163}{0.0076} = 0.4$$

$$\xi = \frac{1}{\sqrt{1+\left(\frac{2\pi}{\delta}\right)^2}} = 0.0635$$

From Figure 4- 19, TD = $\frac{1}{2}$ (4.85-1.75) = 1.55s

Then, the natural period of vibration, Tn = $T_D\sqrt{1-\xi^2}$ = 1.55s, and for a five-storey building with a piled raft natural vibration period, Tn was 1.37s.

Table 4- 2 Natural period of vibration of the buildings

Natural Period	**5-storey building with a shallow foundation**	**5-storey building with a piled raft**
PLAXIS	1.6	1.4
Logarithmic decrement	1.55	1.37

It can be summarized that the calculations for both cases are in tandem with PLAXIS 2D

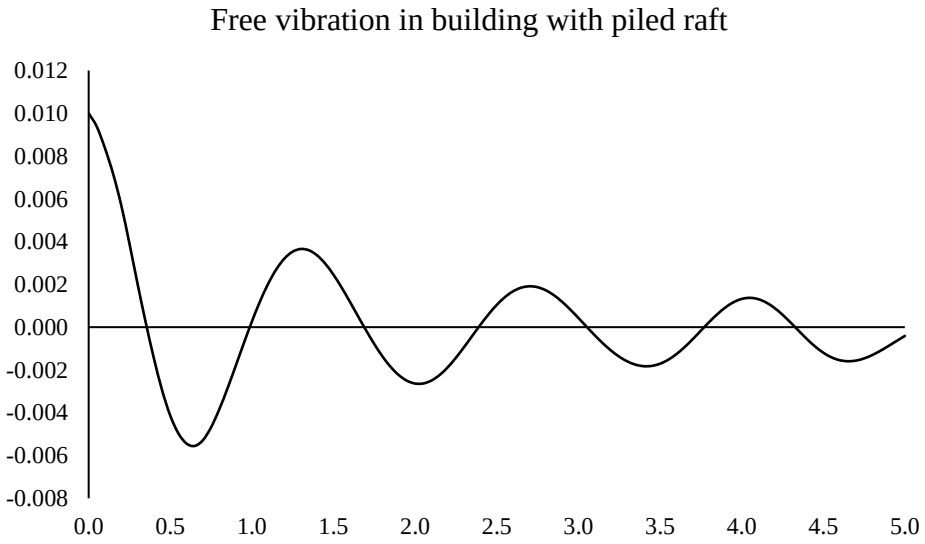

Figure 4- 20 Free vibration in building with piled raft

outputs.

4.3 Soil Structure Interaction in PLAXIS 2D

Once the natural frequency has been calculated, the input motion is applied for the entire duration of the dynamic time, which are 40.82s, 36.32s, and 19.09s for Imperial Valley, Friuli, and Nahanni, respectively. Both models experience deformation because of seismic activity. The response and interaction of the structure are determined based on the data obtained from the result charts. The PLAXIS output provides information on acceleration and horizontal displacement during dynamic time.

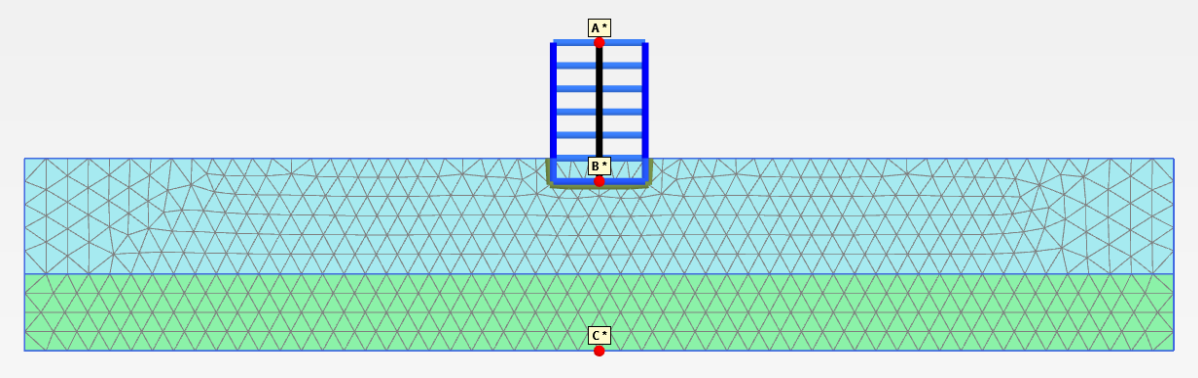

Figure 4- 21 5 storey building with shallow foundation showing three selected nodes A, B and C

Three nodes have been chosen to obtain the structural response at the base and slab levels.

Table 4- 3 Coordinates of the selected nodes

Nodes	Co-ordinate	Location
A	(0, -25)	At the bottom of the soil layer
B	(0, -3)	At the midpoint of the basement
C	(0, 15)	Top of the 5-storey building

4.3.1 Five Storey Structure with a Shallow Foundation

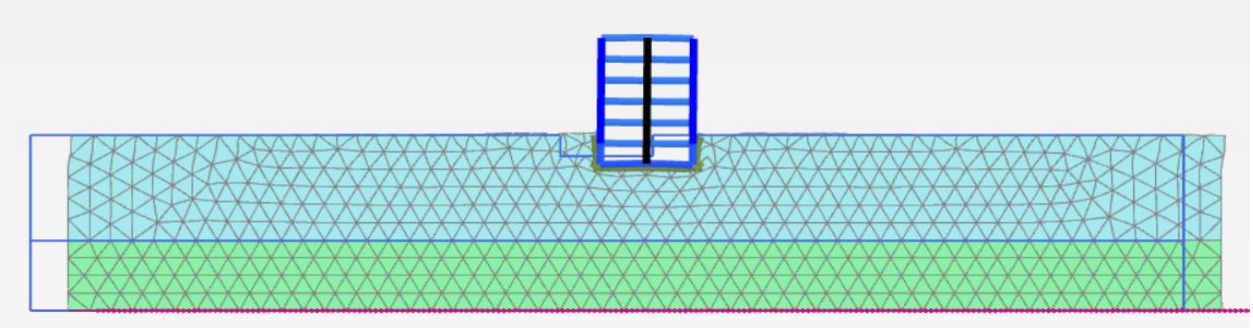

Figure 4- 22 Deformed mesh with the structure after dynamic analysis

Figure 4- 22 shows the distorted mesh at the slab's maximum acceleration at a dynamic time of 14.5 s. The output is enlarged and representative of three different input motions. The acceleration at the top of the structure is not significantly higher than the ground acceleration, as seen by the accelerogram in , and this can be verified from previous sections depicting input motion and comparison of motions at the base of the soil layer, basement and top of building that has been attached to Appendix 5. The maximum input amplitude at point A reaches a peak value of 0.53g at point C due to Nahanni input motion. The greatest horizontal displacement of the structure's roof, measured from the time displacement curve in Figure 4- 24, is 1.69m due to Nahanni, which happens at t=15.57s.

It can be noticed that despite the maximum acceleration at the building top not being much higher than the input motion, the horizontal displacement of the structure is much higher, implying that despite the low amplification in acceleration by the building, high displacements can be observed in ground type S_1.

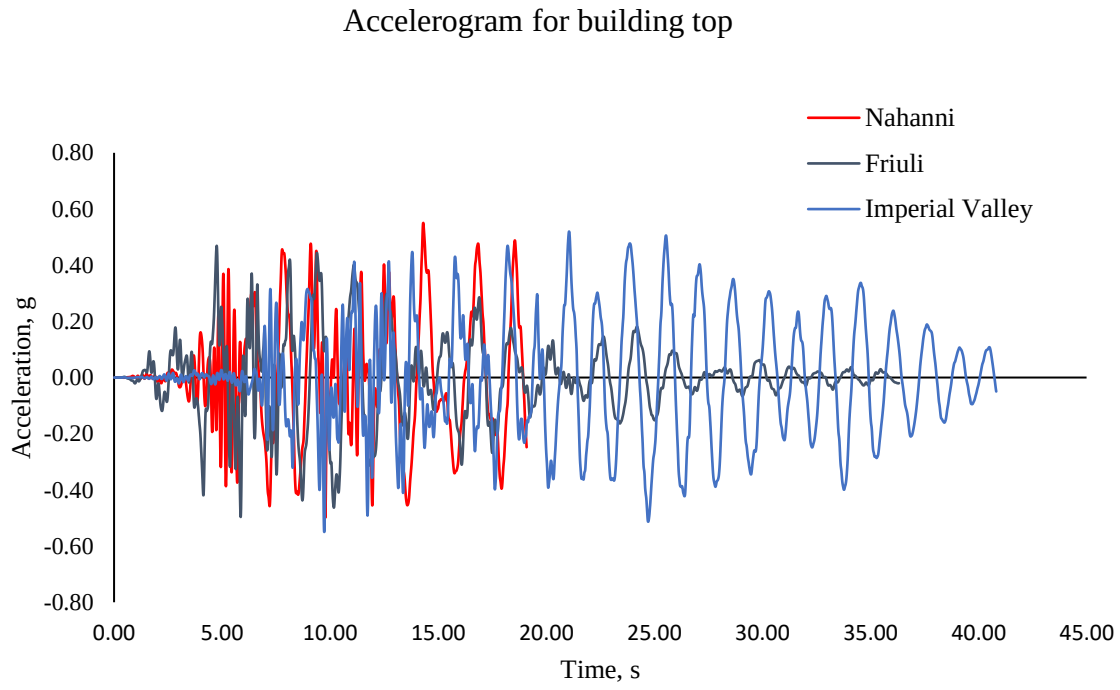

Figure 4- 23 Accelerogram for building a top for different input motions for shallow foundation

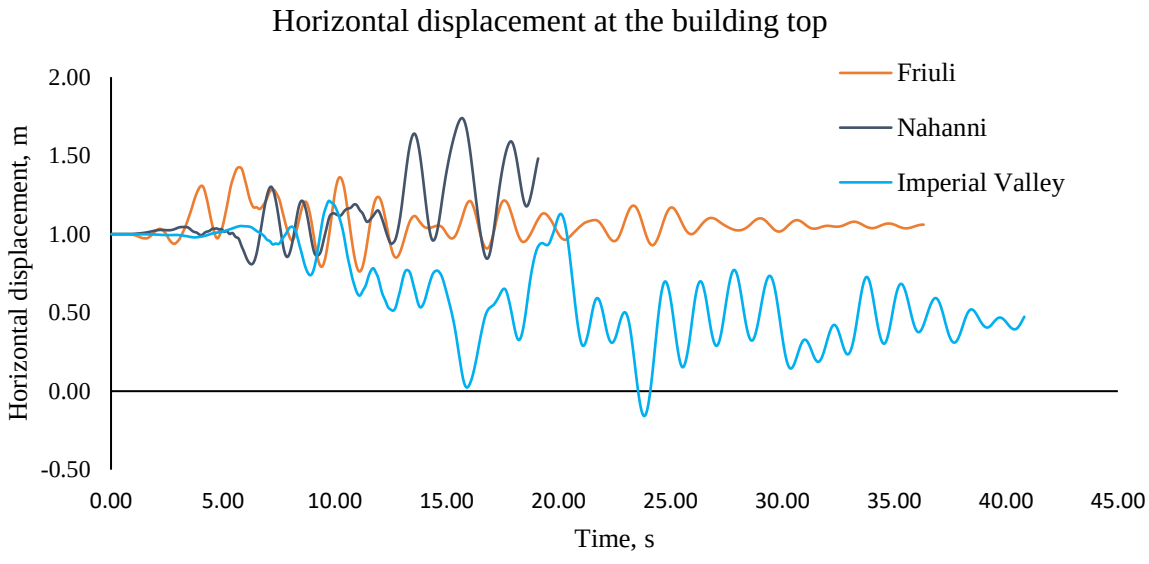

Figure 4- 24 Horizontal displacement at the surface for different earthquakes for shallow foundation

4.3.2 Five-storey Structure with Piled Raft

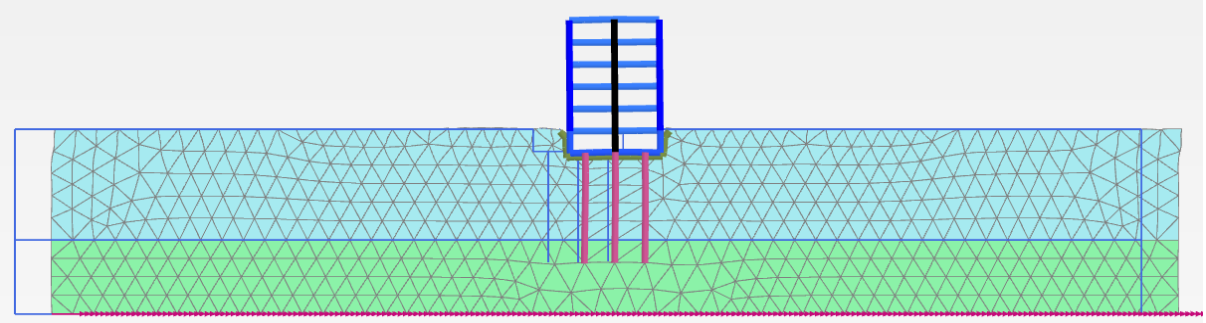

Figure 4- 25 Deformed mesh obtained on dynamic analysis of building with piled raft.

Figure 4- 25 shows the distorted mesh at the slab's maximum acceleration at a dynamic time of 14.2 s. The output is enlarged and representative of three different input motions. The acceleration at the top of the structure is higher than the ground acceleration, as seen by the accelerogram in Figure 2-26, and this can be verified from previous sections depicting input motion and comparison of motions at the base of the soil layer, basement and top of the building that has been attached to Appendix 6. The maximum amplitude at point A reaches a peak of 0.81g due to the Imperial Valley motion. The greatest horizontal displacement of the structure's roof, measured from the time displacement curve in Figure 4- 27, is 1.47m due to Imperial Valley motion, which happens at t= 9.54s.

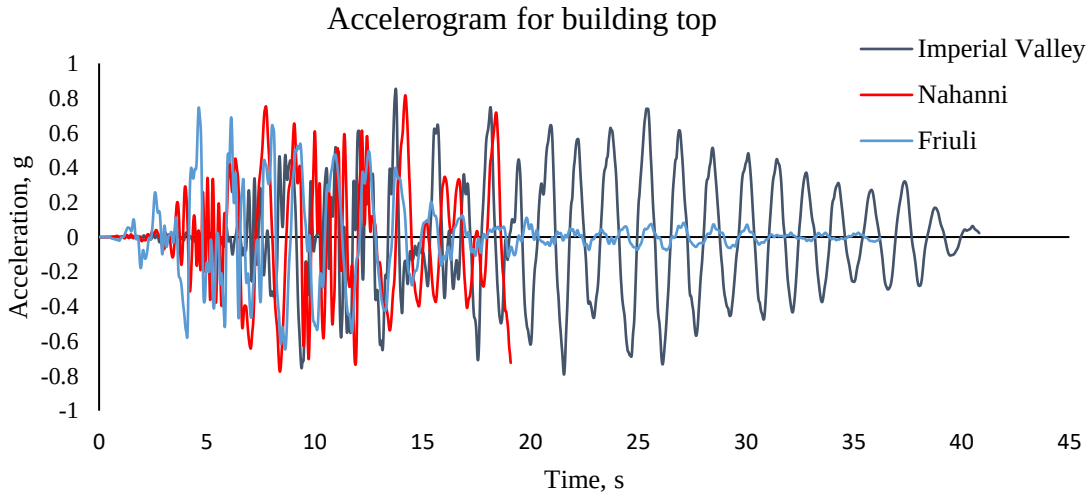

Figure 4- 26 Accelerogram for building top for different input motions for shallow foundation

It can be noticed that despite the maximum acceleration at the building being 1.6 times higher than the input motion, the horizontal displacement of the structure is much higher, implying that despite the low amplification in acceleration by the building, high displacements can be observed in ground type S_1. Also, the graph denotes that upon application of piles, when encountering motions such as Nahanni, the displacement is much lower than the other two motions presented in Figure 4-27.

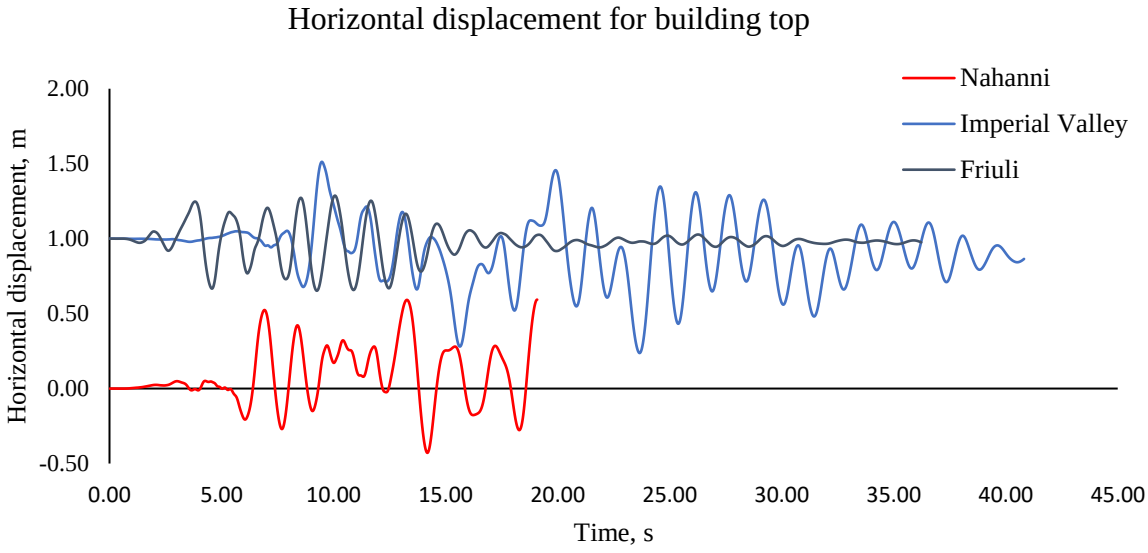

Figure 4- 27 Horizontal displacement at the surface for different earthquakes for shallow foundation

4.3.3 Summary and Discussion

The impact of foundation type may be determined by observing the seismic response of structures with two different types of foundation. The accelerograms demonstrate how the structure's reaction varies from input and free field motions for various types of foundations. When a structure is supported by a piled raft rather than a shallow base, it oscillates more rapidly. Since the shear force at the bottom also relies on the degree of acceleration, a significant change in it may be anticipated; thus, the base shear force will later be calculated to check this.

4.4 Calculation of base shear force

4.4.1 Eurocode 8

Based on the lateral force technique provided by Eurocode 8 and covered in section 2.3.3, the shear force at the rigid base is computed. The design spectrum S_d (T) horizontal component for the specified seismic activity is calculated to determine these shear forces. The formulas

provided in section 2.9.3 provide the foundation for the computation.

An appropriate value for the behavior factor "q" must be chosen for this. As stated in section 2.9, based on the ground acceleration of the site in question and the material type of the structure, Eurocode 8 offers values for three "Ductility Classes" (DCL/DCM/DCH, low/medium/high). The peak ground acceleration of type A ground in Trondheim is a_{gR}=0.25 m/s. The highest acceleration of the input motion in this investigation is 0.1g or 0.98m/s 2. Section 3.2.2 identifies the soil type as type "S_1" based on the Norwegian National Annex. For a structure with seismic class II, the soil factor S is 1.9 from table NA.3.3 when the depth to bedrock is between 20-35m, and the ground acceleration will be a_{gS} = 0.475g > 0.25g, which is higher than value recommended in Eurocode 8 for concrete structures. However, in Norway, it is quite common to use values of $q \leq 1.5$, and, as per section 4.4.2.6(2)P of Eurocode 8-1, foundation resistance for seismic design assumes an elastic behavior, i.e., q = 1. This will also correspond well to the modeling used in PLAXIS, where it is assumed that all the structures are completely elastic. Hence the comparison will be more suitable.

Table 4- 4 Parameters for the construction of horizontal design elastic spectrum

Parameters	**Values**
Peak ground acceleration, a_g	0.25g
Period of motion, T	0.5s
Soil factor, S	1.9
Seismic Class	II ($\gamma_I = 1.0$)
Behavior factor, q	1.0 (DCL)
T_B	0.15
T_C	0.50
T_D	1.5

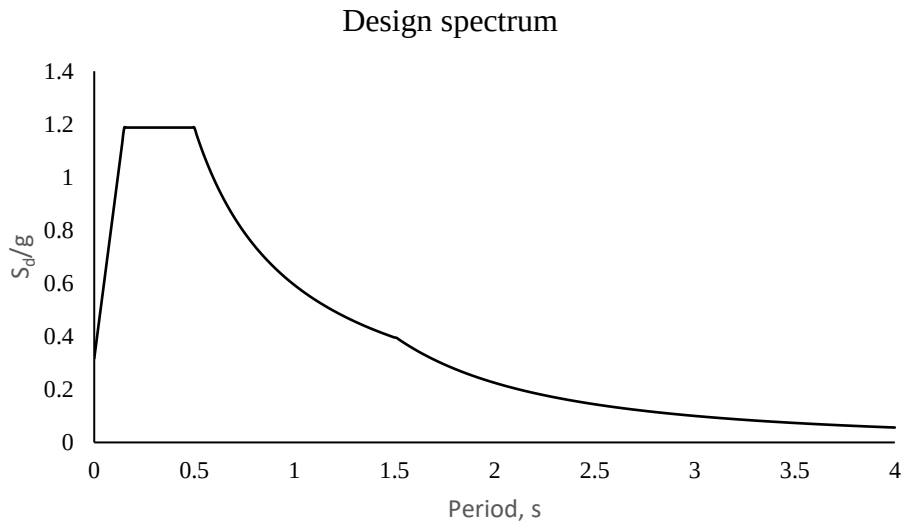

Figure 4- 28 Design the horizontal elastic spectrum.

Base shear of the five-storey structure

Height of the structure, H = 18m

$C_1 = 0.075$

$T_1 = 0.075 \times 183/4 = 0.65s$

Then, $4T_C = 2$, and thus the condition of: $T_1 \leq \begin{cases} 4T_C \\ 2.0 \end{cases}$ has been satisfied. Now, $T_D \leq T_1 \leq 4s$; thus, the component, S_d (T) for T_1, can now be calculated. The mass of the structure above the rigid foundation is:

m = 120 kN/m/m

For $T_1 \leq 4T_C$, correction factor $\lambda = 0.85$.

$S_d(T1) = S_d(0.65) = 0.91 \times 9.81 = 8.93$ m/s2

Thus, the shear force at the base of the structure is,

Fb = 8.93 x 120 x 0.85 = 911 kN/m

4.4.2 PLAXIS 2D

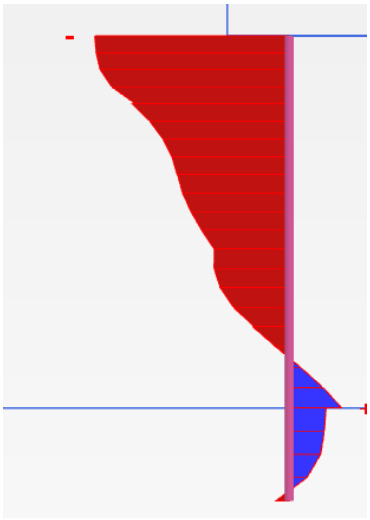

Figure 4- 29 Shear force registered along the length of the pile after a dynamic analysis with Friuli input motion

The maximum shear forces in the basement and the pile can be obtained from PLAXIS using the feature to calculate structural forces in the plates. Using this, features all the absolute maximum shear forces have been tabulated in the table:

Table 4- 5 Base shear forces obtained at the rigid base of the building with a shallow foundation

Input Motion	**Base shear forces**
Imperial valley	390.5 kN/m
Friuli	373.3 kN/m
Nahanni	478.3 kN/m

Table 4- 6 Shear forces obtained at the rigid base and piles of the building with a piled raft

Input Motion	**Shear forces at the basement**	**Left pile**	**Middle pile**	**Right Pile**
Imperial valley	368.3 kN/m	58.86 kN	28.54 kN	93.18 kN
Friuli	370.6 kN/m	78 kN	38.93 kN	85.66 kN
Nahanni	753.4 kN/m	268.5 kN	330.3 kN	102.3kN

4.4.3 Summary and Discussion

It has been demonstrated by the results above that how the pile's presence significantly increases the base shear force. With the addition of piles, the shear force for both buildings increases by almost a factor of two total of the shear forces when Friuli motion is considered. It suggests that even while piles are necessary or perform well in bearing capacity or vertical displacement, they are ineffective in an earthquake. Therefore, proper consideration for any anticipated seismic activity should be considered while building the structure using piled raft foundations or pile groups. The structure may sustain significant damage and cracks in the event of very high base shear, including damage to the pile-raft basement and cracks in the walls. It should be emphasized that the assumption of "behavior factor, q" significantly impacts the fundamental depiction of seismic action in Eurocode 8. It is allowable to assume $q \leq 1.5$ for DCL material, and the behavior factor 1.5 would likely reduce base shear by a much higher degree. Thus, carefully selecting the q is essential for the correct and safe structure design.

The findings also point to the need for a detailed design basis for shear analysis rather than a simplified study to prevent overestimation, as seen in the case of the shallow foundation when the base shear forces registered are less than one-third of the estimation as per Eurocode 8. The shear force predicted using Eurocode 8 was anticipated to be significantly larger than the shear force derived from PLAXIS 2D analysis. The calculations recommended by Eurocode 8 are based on basic assumptions and ought to be sufficient for all types of constructions on a certain soil envelope.

The Norwegian National Annex has recommended an overdesign for soil type S1 to prevent any catastrophic failure in case of any seismic event, although this could be much less economically feasible. However, when the design scenario is changed to a building with the piled-raft system, the estimates from the Eurocode and National Annex make much more sense, which could be the reason for such recommendations.

Eurocode 8 proposes formulas for the lateral force approach and elastic response spectrum analysis based on a linear, single-degree-of-freedom (SDOF) system on a fixed foundation. The structures are MDOF systems, which might impact the estimate. The first basic structure is simulated in this work to represent an SDOF system. However, the structure's rocking motion provides an additional degree of freedom. Even though the study's conclusions were derived from Eurocode under the premise that each structure represented an SDOF system, none of the structures did behave as an SDOF system when PLAXIS analysis was done.

102.4 Parametric Study

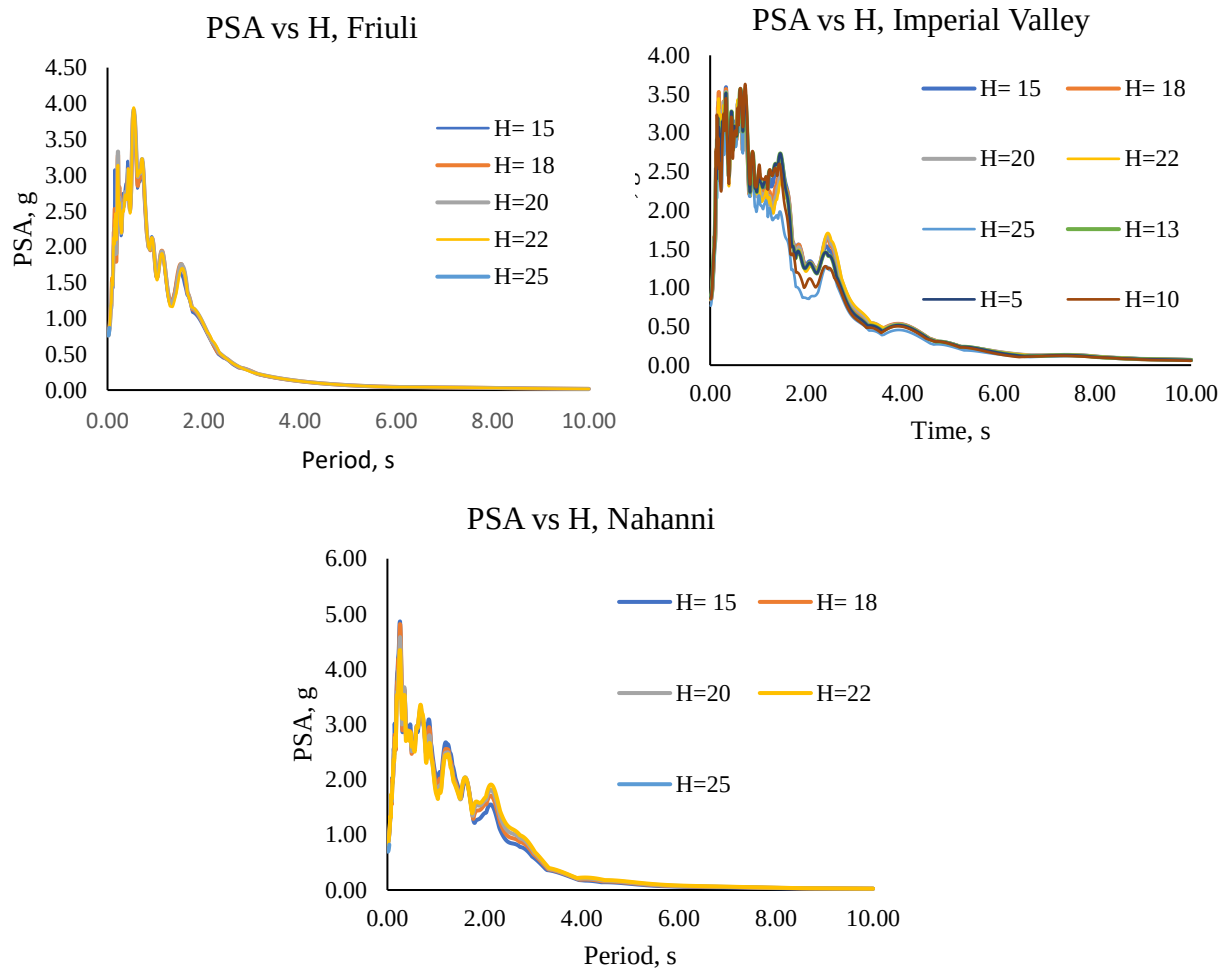

Figure 4- 30 PSA spectrum variation with respect to the thickness of soft clay layer for different input motions

As per the suggestion in Eurocode 8-1, several models were built with varying depths of the soft clay layer such that the average velocity of the upper 30m of the ground would still lead to a ground-type S_1. After that, multiple models with varying soft clay depth were analyzed with three chosen inputs and peak ground motion registered, as shown in Figure 4-30. However, it was confirmed by these graphs that the increase or decrease in depth of soft clay made no difference in the response pattern on the ground. The depth of soft clay was reduced as far as 5m, and Imperial Valley motion was used for analysis to validate the claim.

Along with that, several analyses with increased and decreased stiffness of the stiff clay layer were also run, and few earlier models showed that this led to no change in the response of the ground until and unless the thickness of clay was as low as 5m in the ground such that the ground type would remain S_1. From the parametric study, it can be concluded that for the considered ground condition, the decrease or increase of soft clay depth and modulus of stiff clay play no role in the response of the soil system.

5 CONCLUSION AND DISCUSSION

5.1 Conclusion

Using three recommended input motions with a peak acceleration of 0.5 g spectrally matched with a horizontal elastic response spectrum recommended by Eurocode 8 and Norwegian National Annex and a ground type that has shear wave velocity within the range of soil type "S1," the seismic response of two different types of foundations (shallow foundation and piled raft) is tested. For these two types of foundations, numerical analysis is carried out in the finite element program PLAXIS 2D, and base shear forces in the raft and shallow foundations, along with shear details experienced by each pile, are obtained. The outcomes are also compared to a shear calculation made using Eurocode 8.

In PLAXIS 2D, a representative model of the soil and structure is built before analysis. The selection of the material parameters is based on an intensive literature review focused on imitating Norwegian ground condition and simplified by merging layers so that the final soil profile has two soil layers, namely soft and stiff clay. The average shear wave velocity of the ground is used to establish the soil type according to Eurocode 8. In PLAXIS 2D, the piles are modeled as an embedded beam row. The axial and lateral pile resistance are the input factors for the embedded piles. After supplying all required material characteristics, the ideal boundary conditions, time-stepping, and mesh configurations are selected for dynamic analysis. The lateral direction is provided with a tied degree of freedom for site response analysis with a dummy plate. The same configuration is continued for soil-structure interaction analysis for building with shallow and piled-raft foundations.

Dynamic boundary conditions are checked by verifying that the input motion was registered at the model's base. The test result was perfect, which suggests that the boundary condition selection is appropriate for the dynamic analysis. Finally, a complete dynamic analysis is performed utilizing the input motion created using SeismoMatch simulated at bedrock motion using a displacement boundary condition at the bottom of the soil profile.

In addition, the dynamic analysis performed in PLAXIS 2D, DEEPSOIl was used to verify the results from the site response analysis so that the results can be verified, and the model can be used for further research. A viscous boundary model was used to find the natural period of vibration of the structure considered in this thesis, and calculations, as recommended by Eurocode 8 for base shear forces, were done. Also, a parametric study was done to check the

role of the depth of soft clay and stiffness of stiff clay in response of the soil system to seismic waves.

5.2 Discussion

A site response analysis is performed on PLAXIS 2D and DEEPSOIL to assess soil behavior during seismic action. The goal of comparing the results between one-dimensional analysis in DEEPSOIL and PLAXIS 2D is to determine whether the soil reaction for a particular earthquake exhibits any degree of similarity. While DEEPSOIL performed a non-linear and equivalent linear analysis in time history, and the PLAXIS 2D performs a non-linear dissipative analysis in 2D. Similar site amplification and peak acceleration response spectra are provided by the findings of these two investigations, which agree with one another. The highest acceleration determined using PLAXIS and DEEPSOIL is 0.81g and 0.87g, both in the case of Imperial Valley input motion of 0.5g, respectively.

The maximum PSA for the soil layers occurs on an average between the period of 0.2s to 1.2s as per the three PSA curves obtained from PLAXIS and DEEPSOIL, meaning that any structure with a natural period of oscillation in this range will be in resonance with the subsoil and may sustain significant damage. Relative displacement spectra were also made and analyzed to comprehend soil behavior, along with frequency content, which provides the amplitude distribution over frequencies. These provide expected maximum displacement and amplitude that could be expected at certain frequencies of incoming seismic waves.

The examination of free vibrations yields the structures' natural frequency. Natural frequencies for buildings with shallow foundation is 1.6s, whereas, for piled-raft buildings, they are 1.4s. Theoretical values derived from the logarithmic decrement approach are compared with the natural periods of vibration as determined by PLAXIS analysis, and all these findings are in good accord with the natural period specified using Eurocode 8.

For the different earthquakes, seismic analyses of the models were performed. Graphs showing acceleration and displacement concerning time have been made that show the reaction of the top of the structure upon seismic excitation. It has been seen that piles accelerates the top of the structure more quickly compared to shallow foundations, and the acceleration at the top remains almost the same for shallow foundations and increases by 1.6 times for piled-raft buildings when compared to input motions. This verifies that the accelerogram does not provide entire picture of the soil-structure interaction, and other graphs, such as horizontal

displacement, give a more elaborate and visual idea of the seismic reaction, which is verified in results that show high displacement for the selected input motions of this thesis. The parametric study of the soil layers was done, and it can be concluded that for the ground condition, the decrease or increase of soft clay depth and modulus of stiff clay play no role in the response of the soil system until the depth of soft clay is as less as 5m.

Based on the lateral force technique provided by Eurocode 8, the shear force at the rigid basement is computed. The design spectrum $S_d(T)$ horizontal component is calculated to determine these shear forces per Eurocode 8. The first step in calculating the design spectrum's horizontal components for a particular seismic activity is to assume that the structures are entirely elastic (q = 1.0). The building's base shear is computed as 911 kN/m, and the structure's natural period is estimated and compared with previously acquired data from PLAXIS and theoretical solutions.

For both types of foundations, the PLAXIS output is used to determine the force at the interface of the rigid base. The obtained data demonstrates that in both situations, the pile increases base shear, which depends on the input motion used, but stays true for all cases. This reflects the significance of base shear design considerations when pile foundations are required in Norwegian ground conditions, or else the buildings may not operate as intended in the event of an earthquake. When the results are compared to Eurocode 8, the values for base shear show good agreement with pile foundation, which has a base shear of 753.4 kN/m in the rigid basement as per results from PLAXIS, however for shallow foundations; Eurocode 8 offers overestimated base shear values that would not be economically feasible.

The findings present a significant impact of piles on a structure's interaction with seismicity and surrounding soil. Although piles increase base shear, it is still lesser than predicted by Eurocode 8. However, the findings are consistent with the current design spectrum proposed in the design guideline and the assumptions made in this thesis. However, it could be noted that this highlights the need for a detailed design code for base shear design for seismic conditions in Norway.

6 RECOMMENDATIONS FOR FURTHER WORK

Analysis of several different other earthquakes, structures albeit more complex, and complex soil conditions might be necessary to comprehend the spectral behavior for various foundation systems in a more realistic way. This can offer a more cost-effective and less cautious seismic design option for different foundation types.

This thesis shows that it is possible to do additional analysis using a similar methodology for other popular foundation systems and ground types, for example, including a saturated ground conditions such that the ground water level is on the surface or considering a ground type S2 and performing a liquefaction analysis. Further earthquake analysis can be done on the partially founded structures, i.e., they rest on a rock outcrop.

A more realistic simulation of the three-dimensional behavior of the piles and shallow foundations that includes study of dynamic and static foundation stiffness can be achieved by calculations using experimental soil data and three-dimensional numerical models.

BIBLIOGRAPHY

Aki, K. (1972). Earthquake mechanism. *Tectonophysics, 13*(1-4), 423-446. https://doi.org/https://doi.org/10.1016/0040-1951(72)90032-7

Athanasiu, C., Bye, A., Tistel, J., Ribe, A., Arnesen, K., Feizikhanhandi, S., & Sørlie, E. R. (2015). Simplified earthquake analysis for wind turbines and subsea structures on closed caisson foundations. In *Frontiers in Offshore Geotechnics III.* https://doi.org/10.1201/b18442-14

Bentley. (2022). *General Information Manual.* Bentley.

Bentley. (2022a). *Material Models Manual.* Bentley.

Brandt, M. (2014). *Earthquake Analysis of Subsea Structure on Caisson Foundation using Finite Element Solution.* Norwegian University of Science and Technology, Department of Civil and Transport Engineering.

Bungum, H., Lindholm, C. D., Dahle, A., Hicks, E., Hogden, H., Nadim, F., . . . Harbitz, C. (1998). *Development of a seismic zonation for Norway. Report for Norwegian Council for Building Standardization (on behalf of a consortium of industrial partners).* Oslo: NORSAR and Norwegian Geotechnical Institute.

Bungum, H., Lindholm, C., & Faleide, J. I. (2005). Postglacial seismicity offshore mid-Norway with emphasis on spatio-temporal–magnitudal variations. *Marine and Petroleum Geology, 22*(1-2), 137-148. https://doi.org/https://doi.org/10.1016/j.marpetgeo.2004.10.007.

CEN. (2004). *Eurocode 8: Design of structures for earthquake resistance—Part 1: General rules, seismic actions and rules for buildings (EN 1998-1: 2004).* European Committee for Normalization, Brussels.

CENa. (2004). *Eurocode 8: Design of structures for earthquake resistance Part 5:Foundations, retaining structures and geotechnical aspects.* European Committee for Normalization, Brussels.

Chadha, K. (2015). *Jordskjelvberegning i henhold til Eurokode 8 og PLAXIS 2D - Masters thesis.* NTNU.

Chopra, A. K. (1995). *Dynamics of Structure Theory and Applications to Earthquake Engineering.* Prentice-Hall, Inc.

Chopra, A. K. (2007). *Dynamics of Structures: Theory and Application to Earthquake Engineering.* Prentice Hall.

Dao, T. (2011). *Validation of plaxis embedded piles for lateral loading: Masters Thesis.* Delft University.

Fleming, K., Weltman, A., Randolph, M., & Elson, K. (2008). *Piling engineering.* CRC press.

Gazetas, G. (1991). Foundation Vibrations. In *Foundation Engineering Handbook.* Springer US. https://doi.org/https://doi.org/10.1007/978-1-4615-3928-5_15

GEOFUTURE. (2013). *Earthquake Design Issues.*

Hamada , J. (2015). Bending moment of piles on piled raft foundation subjected to ground deformation during earthquake in centrifuge model test . *The 15th Asian Regional Conference on Soil Mechanics and Geotechnical Engineering.*

Hamada, M. (1991). Damage of Piles by LiquefactionInduced Ground Displacements. *e Third US Conference Lifeline Earthquake Engineering.* Los Angeles.

Hardin, B. O., & Drnevich, V. P. (1972). Shear modulus and damping in soils: Design Equations and Curves. *ASCE: Journal of the Soil Mechanics and Foundations. .*

Hudson, M., Idriss, I. M., & Beikae, M. (1994). *A computer program to evaluate the seismic response of soil structures using finite element procedures and incorporating a compiant base. Center for Geotechnical Modeling.* QUAD4M.

Imtiaz, A. B. (2009). *Seismic Microzonation of Cox's Bazar Municipal Area. (Thesis).* Bangladesh Univeristy of Engineering and Technology.

Joyner, W. B., & Chen, A. T. (1975). Calculation of nonlinear ground response in earthquakes. *Bulletin of the Seismological Society of America, 65*(5), 1315-1336. https://doi.org/https://doi.org/10.1785/BSSA0650051315

Kausel, E., Whitman, R. V., Morray, J. P., & Elsabee, F. (1978). The spring method for embedded foundations. *Nuclear Engineering and Design, 48*(2-3), 377-392. https://doi.org/https://doi.org/10.1016/0029-5493(78)90085-7.

Kramer, S. L. (1996). *Geotechnical Earthquake Engineering.* Prentice-Hall,Inc.

Kramer, S. L. (2014). *Geotechnical Earthquake Engineering.* Pearson Eductation Limited.

Kumar, S., Krishna, A. M., & Arindam, D. (2013). Parameters Influencing Dynamic Soil Properties: A Review Treatise. *National Conference on Recent Advances in Civil Engineering.* NERIST, Nirjuli.

Kwaak, V. D. (2015). *lling of dynamic pile behaviour during an earthquake using.* Delft University.

Laera, A., & Brinkgreve, R. B. (2015). *Ground Response Analysis in PLAXIS.*

Lunne, T. A., & Andersen, K. H. (2007). Soft Clay Shear Strength Parameters For Deepwater Geotechnical Design. *6th OSIG*, (pp. 151-176). London.

Magar, A. T. (2016). *Earthquake Response of Different Types of Retaining Walls - Masters thesis.* NTNU.

Martin, G. R., & Lam, I. P. (1995). Seismic Design of Pile Foundations: Structural and Geotechnical Issues. *Third International Conference on Recent Advancement in Geotechnical Earthquake Engineering and Soil Dynamics.* St. Louis, Missouri.

Mizuno, H. (1987). Pile Damage During Earthquake in Japan. *Geotechnical Engineering Division of the American Society of Civil Engineers in conjunction with the ASCE Convention.* Atlantic City, New Jersey.

Molina, S., & Lindholm, C. (2005). A logic tree extension of the capacity spectrum: Method developed to estimate seismic risk in Oslo, Norway. *Journal of Earthquake Engineering, 9*(6), 877-897. https://doi.org/10.1080/13632460509350570

Nordal , S. (2020). *Geotechnical Engineering Advanced Course.* NTNU, Geotechnical Division.

NTNU IBM. (2021). *Pile Handout.* NTNU.

Rønnquist , A., Remseth, S., & Lindholm, C. (2012). Earthquake engineering design practice in Norway: Implementation of Eurocode 8. Retrieved from https://www.iitk.ac.in/nicee/wcee/article/WCEE2012_2229.pdf

Rønnquist, A., Karlson, T., & Remseth, S. (2012a). Earthquake Design Practice of Traditional Norwegian Buildings According to Eurocode 8.

Seed, H. B., Idriss, I. M., Makdisi, F., & Banerjee, N. (1975). *Representation Of Irregular Stress Time Histories By Equivalent Uniform Stress Series In Liquefaction Analayses.* University of California, Berkeley.

Sluis, J. (2012). *Validation of embedded pile row in PLAXIS 2D.* Delft University.

Sluis, J., Besseling, F., & Stuurwold, P. (2014). *Modelling of a pile row in a 2D plane strain FE-analysis.*

Teguh, M., Duffield, C. F., Mendis, P. A., & Hutchinson, G. L. (2006). Seismic performance of pile-to-pile cap connections: An investigation of design issues. *Electronic Journal of ructural Engineering, 6*.

Vucetic, M., & Dobry, R. (1991). Effect of soil plasticity on cyclic response. *Journal of Gotechnical Engineering*.

Wolf, J. P. (1985). *Dynamic Soil-Structure Interaction.* Prentice-Hall, Inc.

Ziotopolou , A., & Gazetas, G. (2010). Are Current Design Spectra Sufficient for Soil-Structure Systems on Soft Soils? In E. Faradis, *Advances in performance-based earthquake engineering.* Springer.

APPENDICES

Appendix 1: Relevant Sections of Eurocode 8-1

(NS-EN 1998-1:2004+A1:2013+NA:2021)

Ground type

Tabell NA.3.1 – Grunntyper [1)]

Grunn-type	Beskrivelse av stratigrafisk profil	Parametere [2) 3)]		
		$v_{s,30}$ (m/s)	N_{SPT} (slag/30cm)	c_u (kPa)
A	Fjell eller fjell-liknende geologisk formasjon, medregnet høyst 5 m svakere materiale på overflaten.	> 800	–	–
B	Avleiringer av svært fast sand eller grus eller svært stiv leire, med en tykkelse på flere titalls meter, kjennetegnet ved en gradvis økning av mekaniske egenskaper med dybden.	360 – 800	> 50	> 250
C	Dype avleiringer av fast eller middels fast sand eller grus eller stiv leire med en tykkelse fra et titalls meter til flere hundre meter.	180 – 360	15 - 50	70 - 250
D	Avleiringer av løs til middels fast kohesjonsløs jord (med eller uten enkelte myke kohesjonslag) eller av hovedsakelig myk til fast kohesjonsjord.	120 – 180	10 – 15	30 – 70
E	Et grunnprofil som består av et alluviumlag i overflaten med v_s-verdier av type C eller D og en tykkelse som varierer mellom ca. 5 m og 20 m, over et stivere materiale med v_s > 800 m/s.			
S_1	Avleiringer som består av eller inneholder et lag med en tykkelse på minst 10 m av bløt leire/silt med høy plastisitetsindeks (PI > 40) og høyt vanninnhold.	< 100 (antydet)	–	10 - 20
S_2	Avleiringer av jord som kan gå over i flytefase (liquefaction), sensitive leirer eller annen grunnprofil som ikke er med i typene A – E eller S_1.			

[1)] Hvis minst 75 % av konstruksjonen står på fjell og resten på løsmasser, og konstruksjonen står på ett kontinuerlig fundament (platefundament), kan grunntype A benyttes.

[2)] Valget av grunntype kan være basert på enten $v_{s,30}$, N_{SPT} eller c_u. $v_{s,30}$ anses som den mest aktuelle parameteren å benytte.

[3)] Der det er tvil om hvilken jordtype som skal velges, velges den mest ugunstige.

Seismic zones in Norway

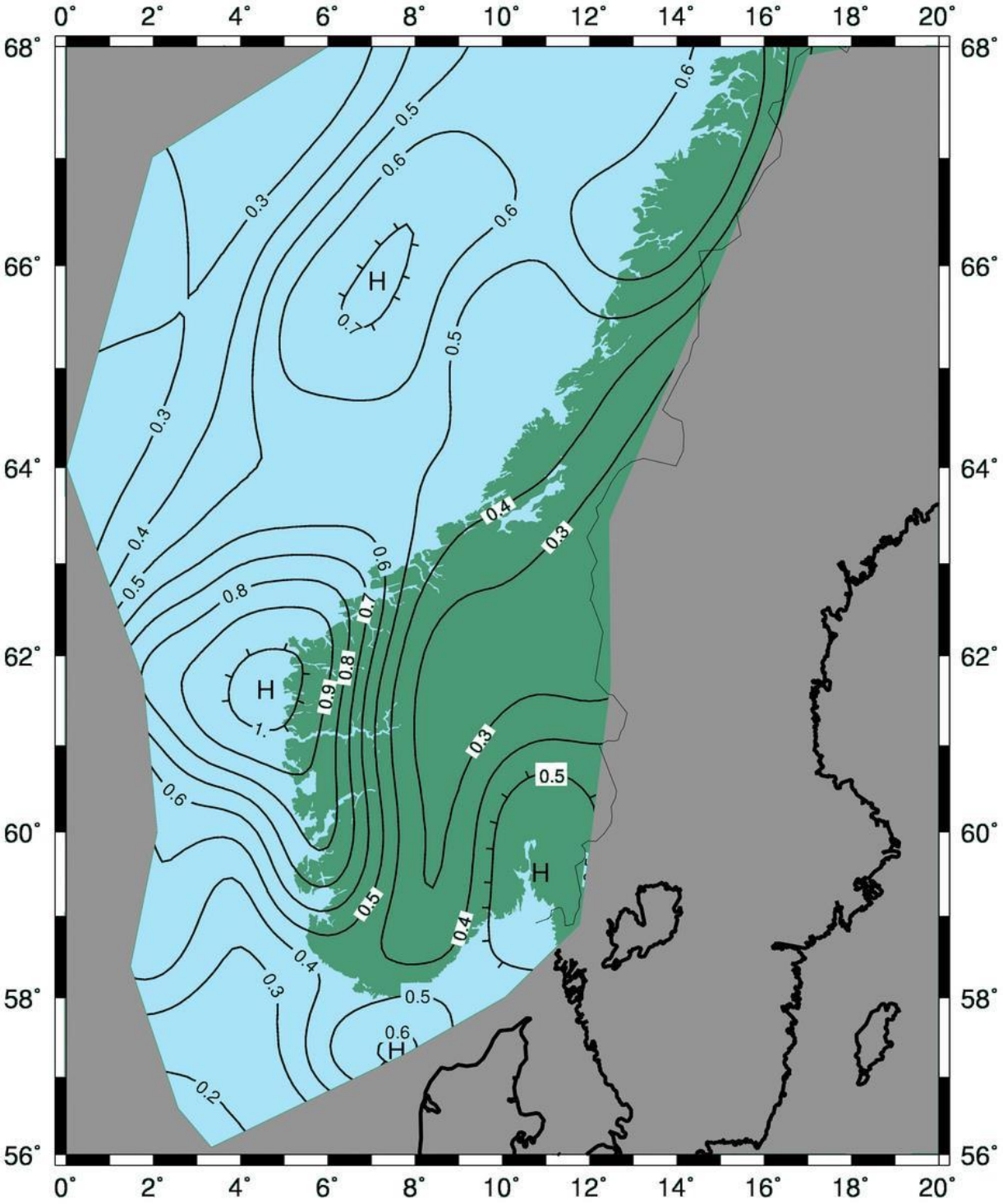

Seismic classes and Ductility classes

Tabell NA.4(902) – Veiledende tabell ved valg av seismisk klasse

Byggverk	I	II	III	IV
Byggverk der konsekvensene av sammenbrudd er særlig store				X [1)]
Viktig infrastruktur: sykehus, brannstasjoner, redningssentraler, kraftforsyning og lignende			(X)	X
Høye bygninger, mer enn 15 etasjer		(X)	X	
Jernbanebruer [2)]			X	(X)
Veg- og gangbruer [2)]		(X)	X	(X)
Byggverk med store ansamlinger av mennesker (tribuner, kinosaler, sportshaller, kjøpesentre, forsamlingslokaler osv.)		(X)	X	
Kaier og havneanlegg		X	(X)	
Landbaserte akvakulturanlegg for fisk		X	(X)	
Tårn, master, skorsteiner, siloer	(X)	X	(X)	
Industrianlegg		X	(X)	
Skoler og institusjonsbygg		(X)	X	
Kontorer, forretningsbygg og boligbygg		X	(X)	
Småhus, rekkehus, bygg i én etasje, mindre lagerhus osv.	X	(X)		
Støttemurer med høyde lavere enn 3 m langs veger i klasse II [3)]	X	(X)		
Kulverter	X	(X)	(X)	
Landbruksbygg	(X)			
Kaier og fortøyningsanlegg for sport og fritid	(X)			

[1)] For byggverk der konsekvensene av sammenbrudd er særlig store, for eksempel ved atomreaktorer og lagringsanlegg for radioaktivt avfall, store dammer og marine konstruksjoner bør jordskjelvrisikoen vurderes spesielt, eventuelt basert på en risikoanalyse.

Lagertanker for flytende gass og store hydrokarbonførende rørledninger over land er behandlet i NA til NS-EN 1998-4.

[2)] Se veiledende tabell for valg av seismisk klasse for bruer i NA til NS-EN 1998-2.

[3)] For støttemurer langs jernbane, støttemurer langs veger med høyde over 3 m og støttemurer langs viktige veier (klasse III) benyttes samme seismiske klasse som for vegen eller jernbanen

Tabell NA.6.1 – Dimensjoneringsprinsipper, duktilitetsklasser og øvre grense for referanseverdier for konstruksjonsfaktorer

Dimensjoneringsprinsipp	Konstruksjonens duktilitetsklasse	Område av referanseverdier for valg av konstruksjonsfaktor q
Prinsipp a) Konstruksjon med lite energiabsorpsjon	DCL (Lav)	$\leq 1{,}5$
Prinsipp b) Energiabsorberende konstruksjon	DCM (Middels)	≤ 4 Også begrenset av verdiene for DCM i tabell 6.2
	DCH (Høy)	Som for DCM

Appendix 2: Calculation Chart of Resistances of Pile

	z	σ_v'	$\sigma_H' = k_0\sigma_v'$	$\sigma_p' = 0.5\ (\sigma_v' + \sigma_H')$	c_U	c_U/σ_v'	α	τ_s	Total side friction, Q_s	Lateral Resistance, P_u	End Bearing
Soft Clay	0	0	0.00	0.00	4.53	-	-	-	0	-	-
	1	17	9.82	13.41	10.20	0.60	0.85	8.67	13.61	33.99	72.05
	2	34	19.63	26.82	15.86	0.47	0.9	14.28	22.42	71.39	112.08
	3	51	29.45	40.22	21.53	0.42	0.9	19.38	30.42	96.89	152.12
	4	68	39.26	53.63	27.20	0.40	0.9	24.48	38.43	122.39	192.15
	5	85	49.08	67.04	32.86	0.39	0.9	29.58	46.44	147.89	232.18
	6	102	58.89	80.45	38.53	0.38	0.9	34.68	54.44	173.39	272.21
	7	119	68.71	93.86	44.20	0.37	0.9	39.78	62.45	198.88	312.25
	8	136	78.53	107.26	49.86	0.37	0.9	44.88	70.46	224.38	352.28
	9	153	88.34	120.67	55.53	0.36	0.9	49.98	78.46	249.88	392.31
	10	170	98.16	134.08	61.20	0.36	0.9	55.08	86.47	275.38	432.35
	11	187	107.97	147.49	66.86	0.36	0.9	60.18	94.48	300.88	472.38
	12	204	117.79	160.89	72.53	0.36	0.9	65.28	102.48	326.38	512.41
	13	221	127.61	174.30	78.19	0.35	0.9	70.38	110.49	351.88	552.45
	14	238	137.42	187.71	83.86	0.35	0.9	75.48	118.50	377.38	592.48
	15	255	147.24	201.12	89.53	0.35	0.9	80.58	126.50	402.88	632.51
Stiff clay	15	255	147.24	201.12	94.06	0.37	0.9	84.65	132.91	423.27	664.53
	16	275	158.79	216.89	100.73	0.37	0.9	90.65	142.33	453.27	711.63
	17	295	170.33	232.67	107.39	0.36	0.9	96.65	151.75	483.26	758.73
	18	315	181.88	248.44	114.06	0.36	0.9	102.65	161.16	513.26	805.82
	19	335	193.43	264.21	120.72	0.36	0.9	108.65	170.58	543.26	852.92
	20	355	204.98	279.99	127.39	0.36	0.9	114.65	180.00	573.26	900.02
	21	375	216.53	295.76	134.06	0.36	0.9	120.65	189.42	603.26	947.1171
	22	395	228.07	311.54	140.72	0.36	0.9	126.65	198.84	633.26	994.2151
	23	415	239.62	327.31	147.39	0.36	0.9	132.65	208.26	663.26	1041.313
	24	435	251.17	343.08	154.06	0.35	0.9	138.65	217.68	693.26	1088.411
	25	455	262.72	358.86	160.72	0.35	0.9	144.65	227.10	723.25	1135.509

Appendix 3: SeismoMatch 2023

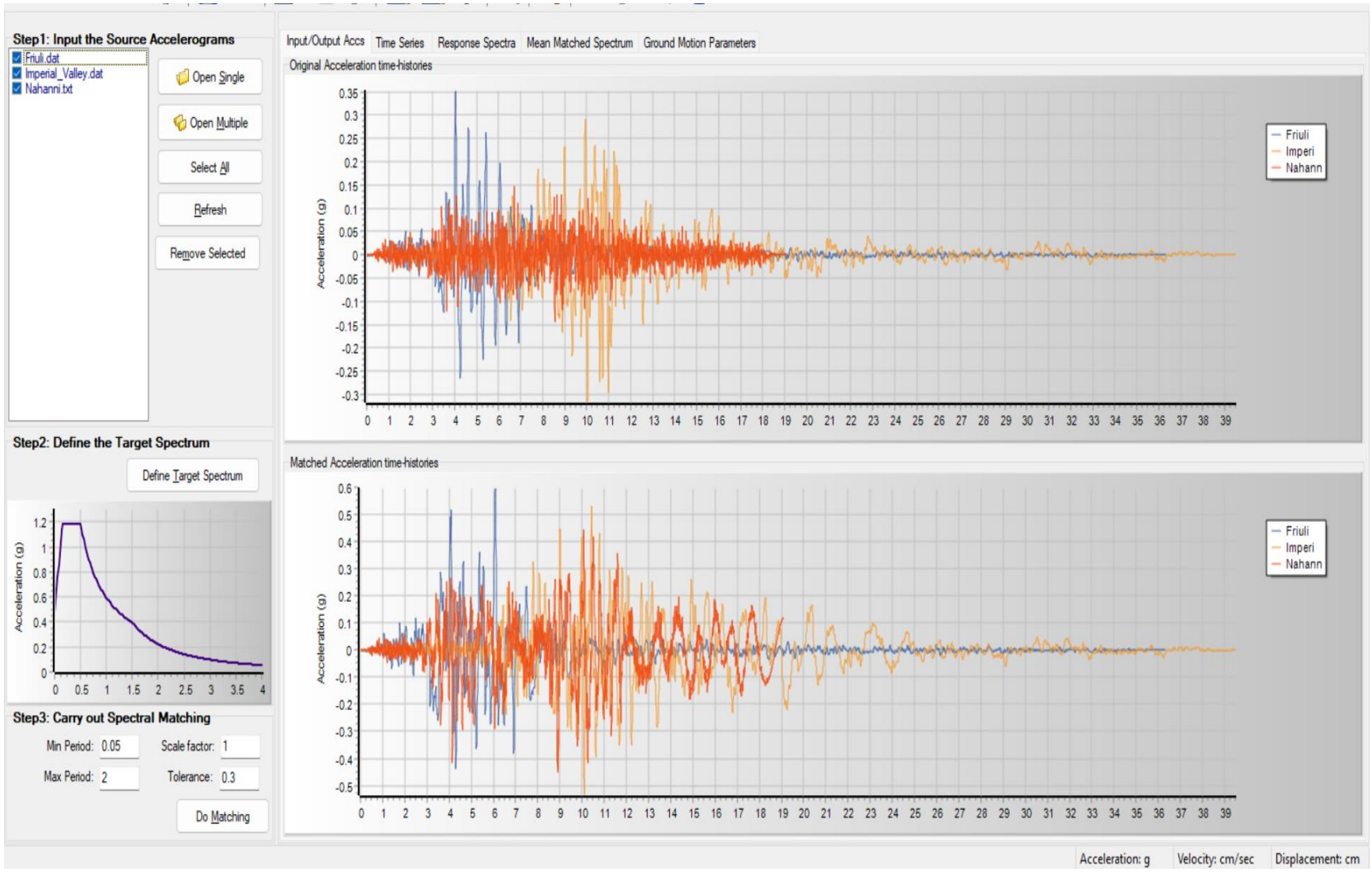

Appendix 4: Analysis of DEEPSOIL

The analysis in DEEPSOIL was performed in a non-linear method and by generating profiles such that the frequency does not exceed 50 Hz, as this is recommended for a proper analysis within DEEPSOIL. The rest of the process is shown in the pictures in complete detail:

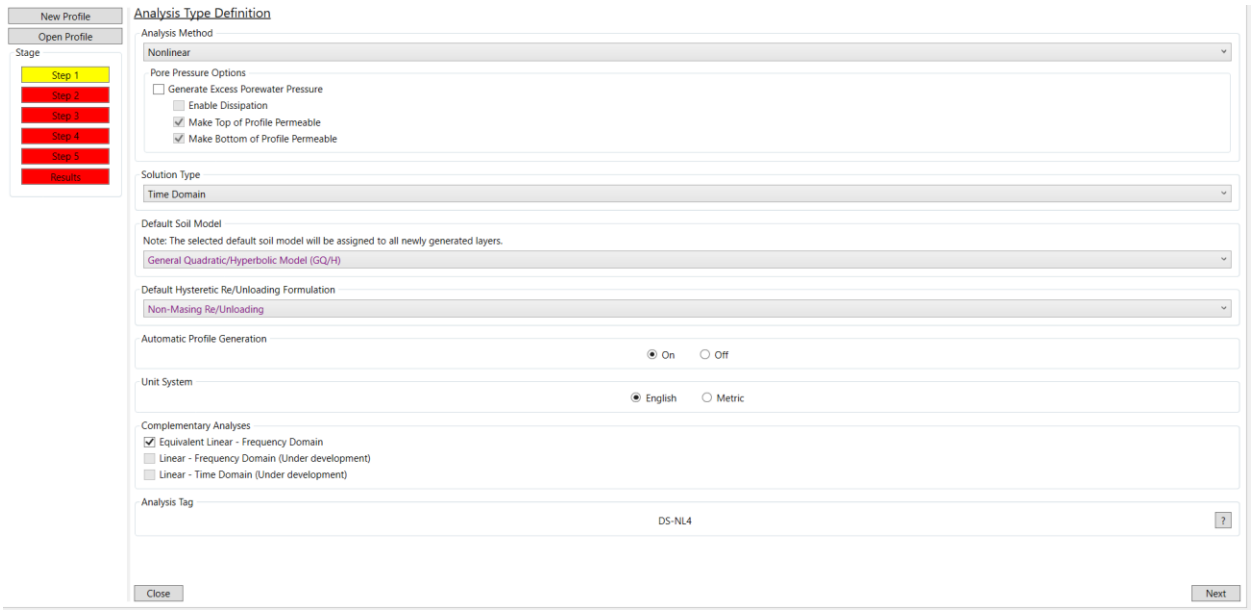

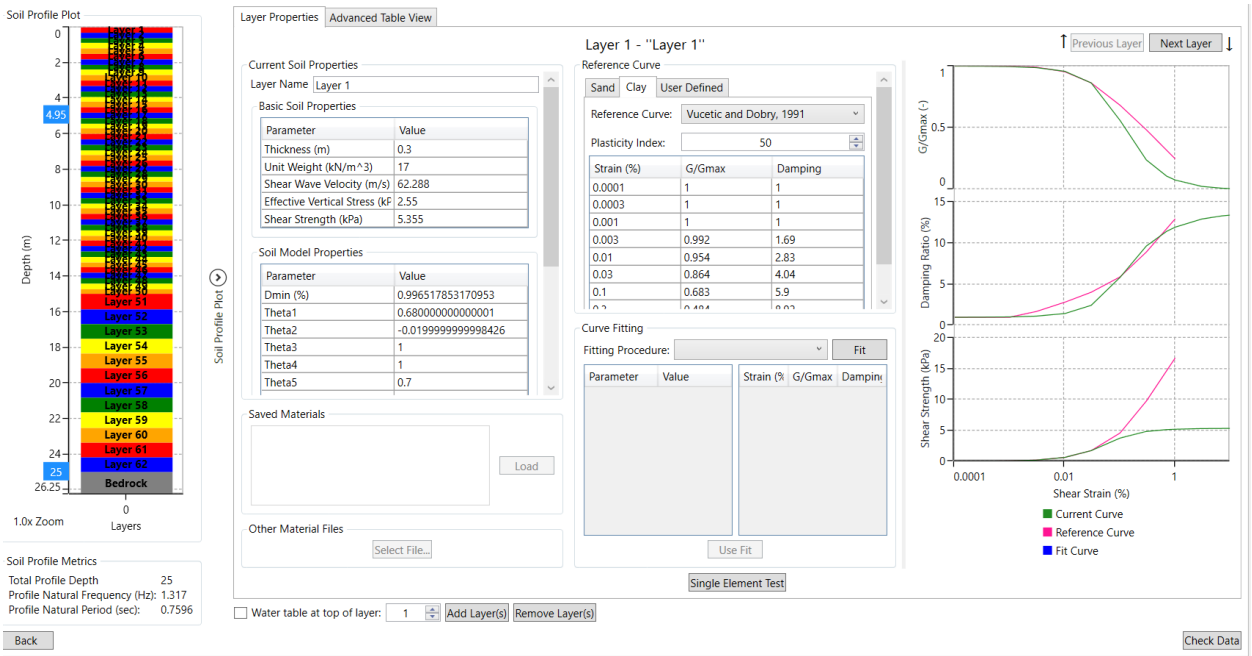

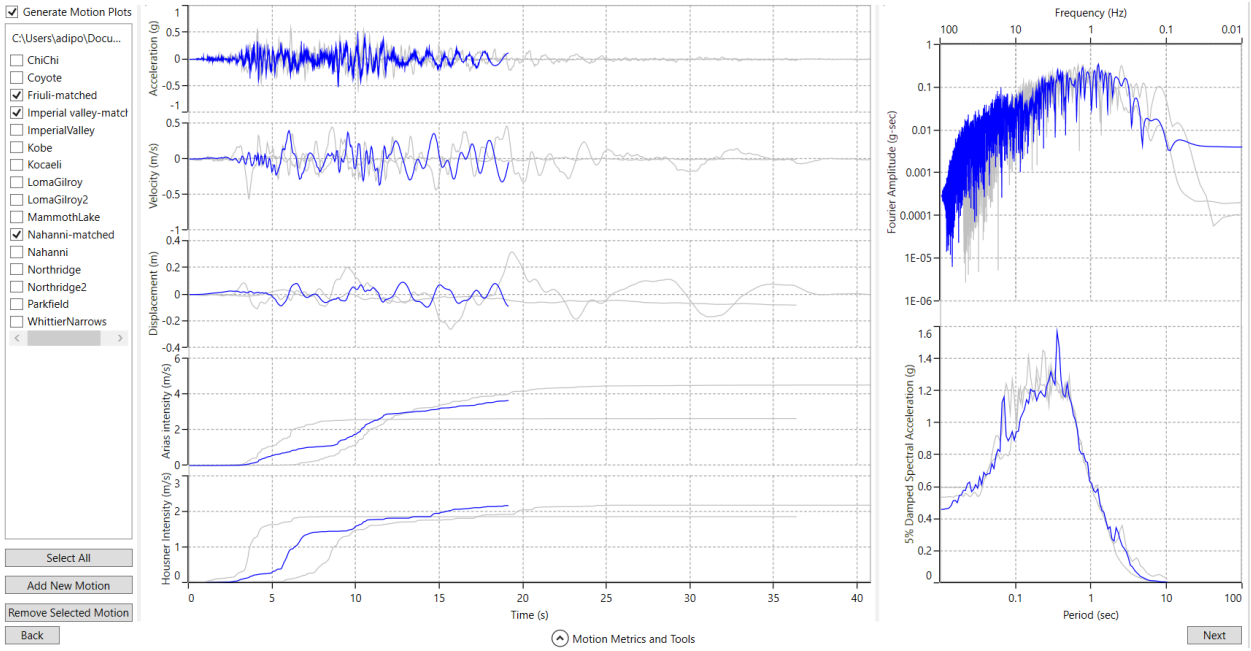
Generate Motion Plots
C:\Users\adipo\Docu...
ChiChi
Coyote
Friuli-matched
Imperial valley-matcl
ImperialValley
Kobe
Kocaeli
LomaGilroy
LomaGilroy2
MammothLake
Nahanni-matched
Nahanni
Northridge
Northridge2
Parkfield
WhittierNarrows
Select All
Add New Motion
Remove Selected Motion
Back
Acceleration (g)
Velocity (m/s)
Displacement (m)
Arias intensity (m/s)
Housner intensity (m/s)
Time (s)
Frequency (Hz)
Fourier Amplitude (g-sec)
5% Damped Spectral Acceleration (g)
Period (sec)
Motion Metrics and Tools
Next

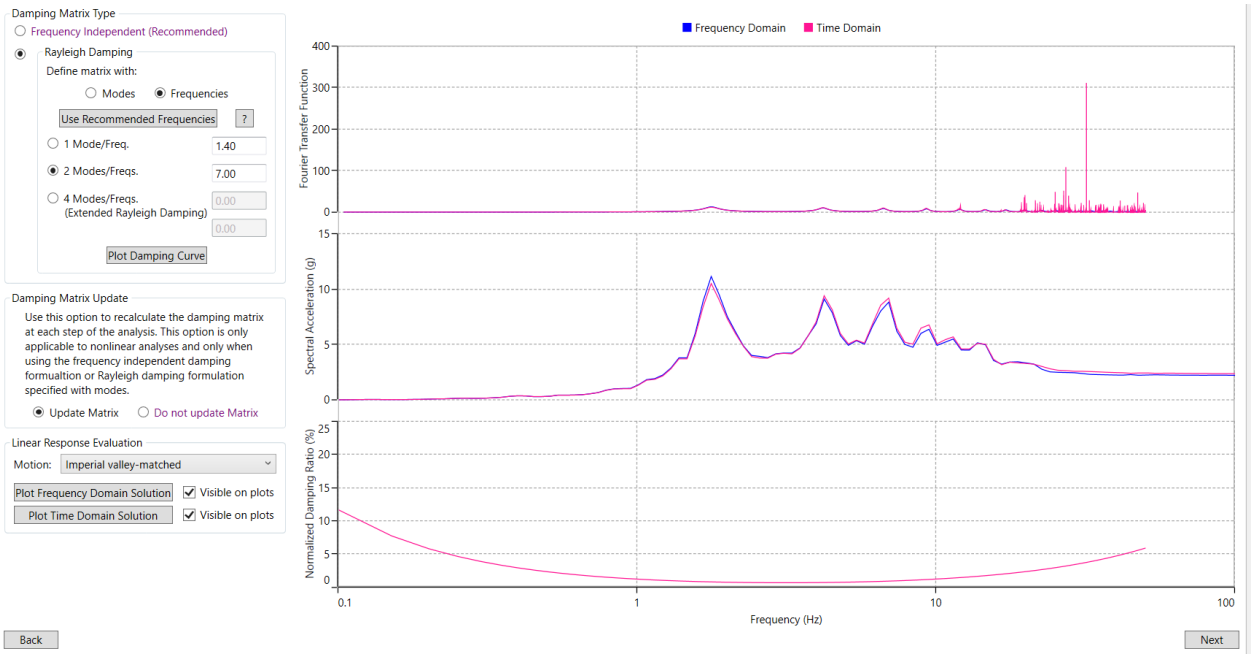
Damping Matrix Type
Frequency Independent (Recommended)
Rayleigh Damping
Define matrix with:
Modes
Frequencies
Use Recommended Frequencies
?
1 Mode/Freq.
1.40
2 Modes/Freqs.
7.00
4 Modes/Freqs.
(Extended Rayleigh Damping)
0.00
0.00
Plot Damping Curve
Damping Matrix Update
Use this option to recalculate the damping matrix at each step of the analysis. This option is only applicable to nonlinear analyses and only when using the frequency independent damping formualtion or Rayleigh damping formulation specified with modes.
Update Matrix
Do not update Matrix
Linear Response Evaluation
Motion:
Imperial valley-matched
Plot Frequency Domain Solution
Visible on plots
Plot Time Domain Solution
Visible on plots
Back
Frequency Domain
Time Domain
Fourier Transfer Function
Spectral Acceleration (g)
Normalized Damping Ratio (%)
Frequency (Hz)
Next

Analysis Control Definition

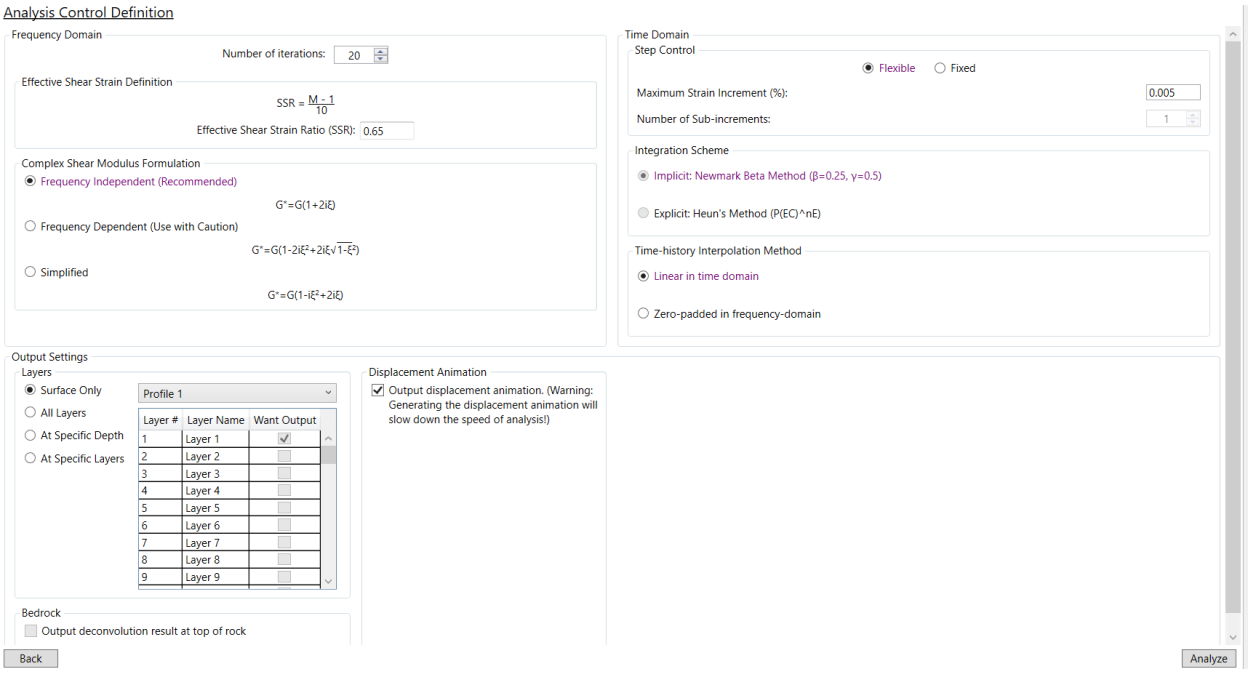

Appendix 5: Accelerograms and PSA Spectrum Obtained from Non-linear Analysis using DEEPSOIL

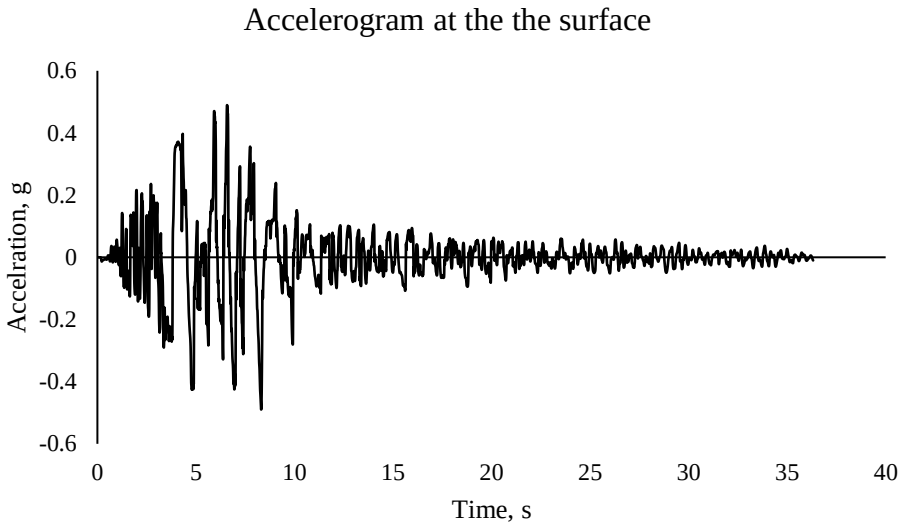

Appendix- 1 Accelerogram at the surface from non-linear analysis using DEEPSOIL with Friuli input motion

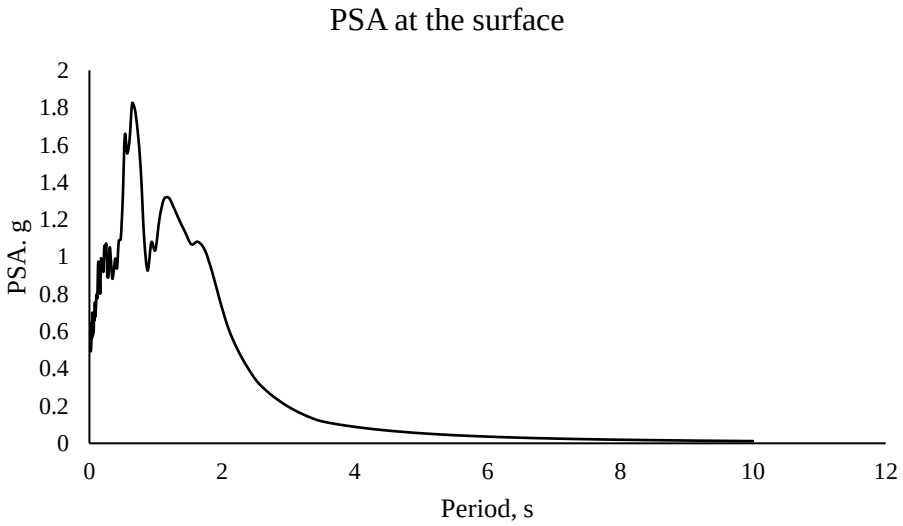

Appendix- 2 PSA at the surface from non-linear analysis using DEEPSOIL with Friuli input motion

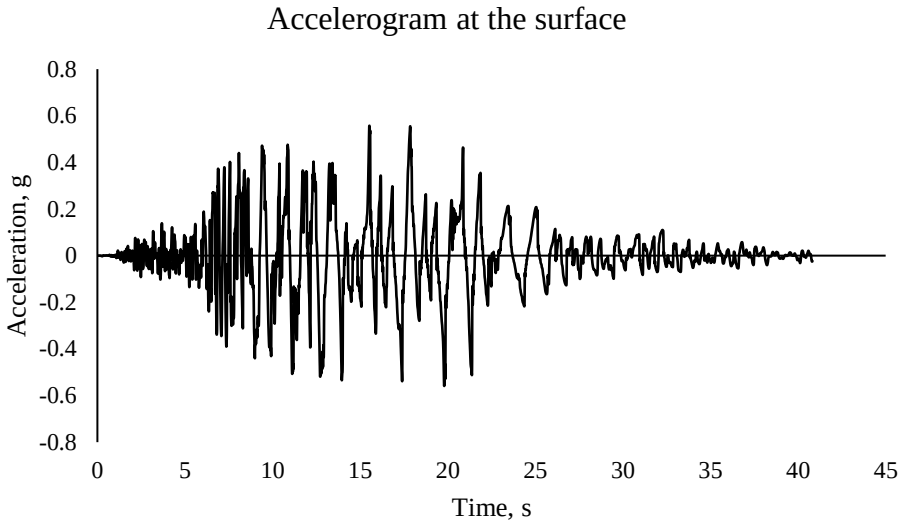

Appendix- 3 Accelerogram at the surface from non-linear analysis using DEEPSOIL with Imperial Valley input motion

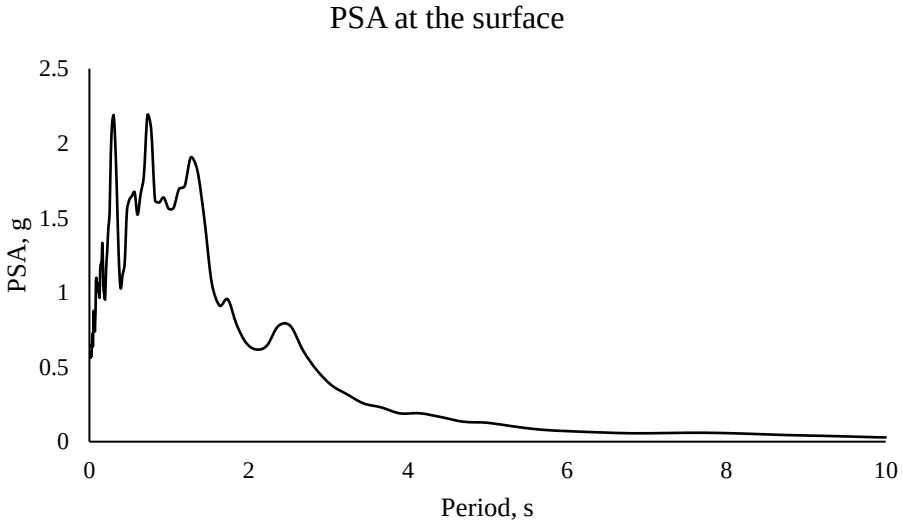

Appendix- 4 PSA at the surface from non-linear analysis using DEEPSOIL with Imperial Valley input motion

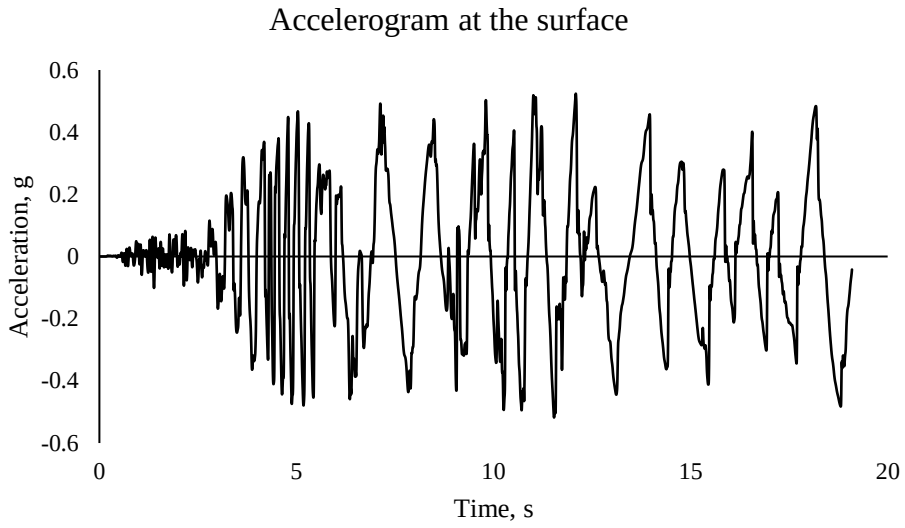

Appendix- 5 Accelerogram at the surface from non-linear analysis using DEEPSOIL with Nahanni input motion

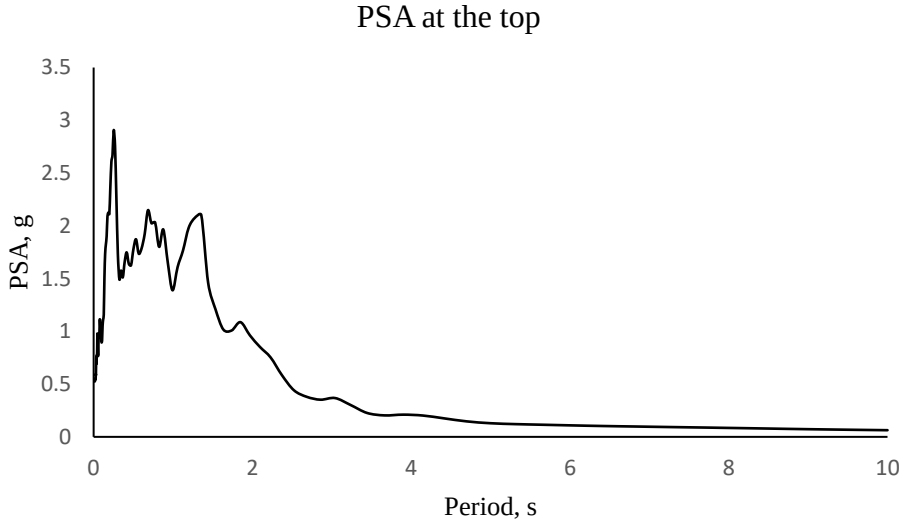

Appendix- 6 PSA at the surface from non-linear analysis using DEEPSOIL with Nahanni input motion

Appendix 6: Accelerograms and Horizontal Displacement Obtained from PLAXIS Analysis on a Shallow Foundation

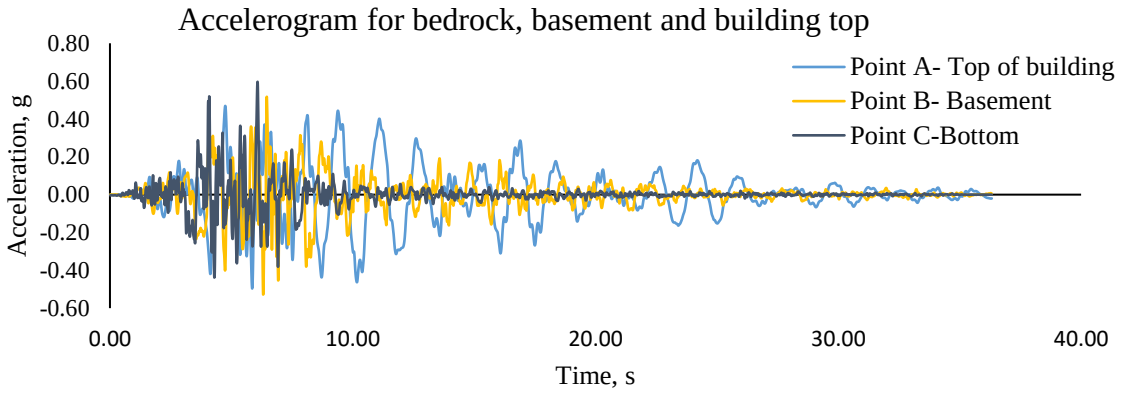

Appendix- 7 Accelerogram for bedrock, basement, and building top for Friuli input motion

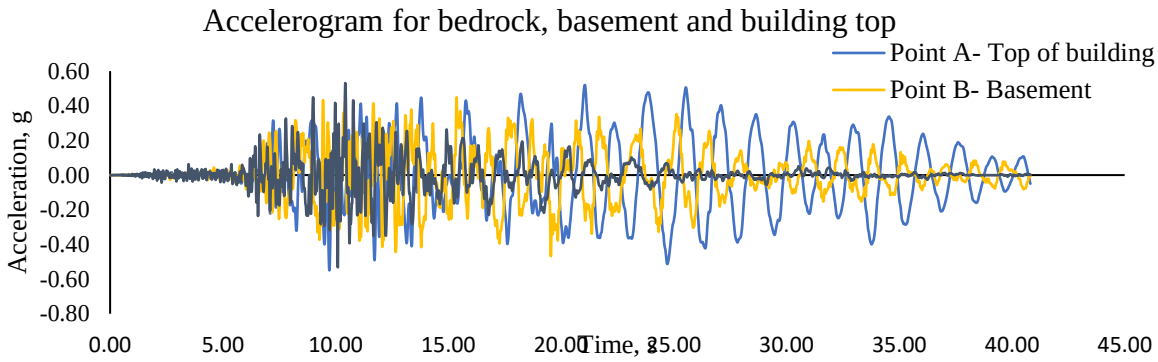

Appendix- 8 Accelerogram for bedrock, basement and building top for Imperial Valley input motion

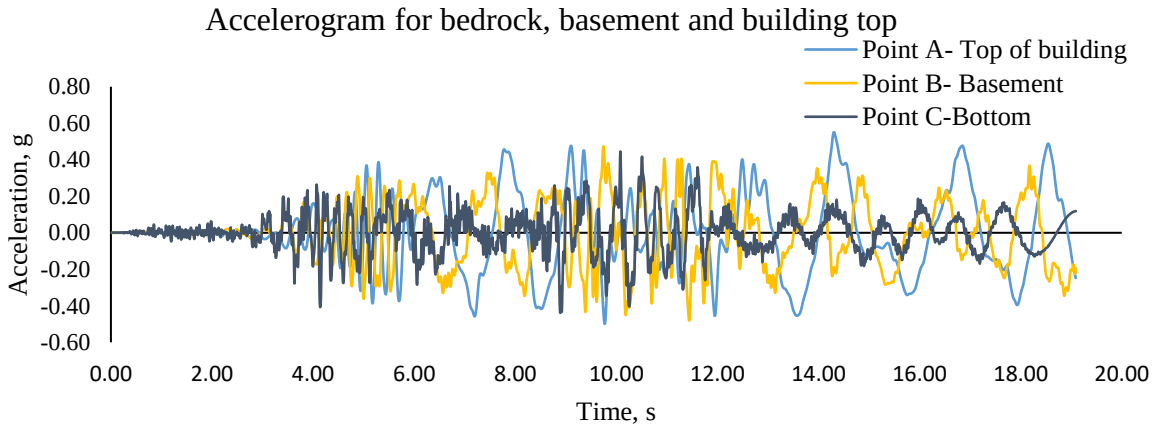

Appendix- 9 Accelerogram for bedrock, basement and building top for Nahanni input motion

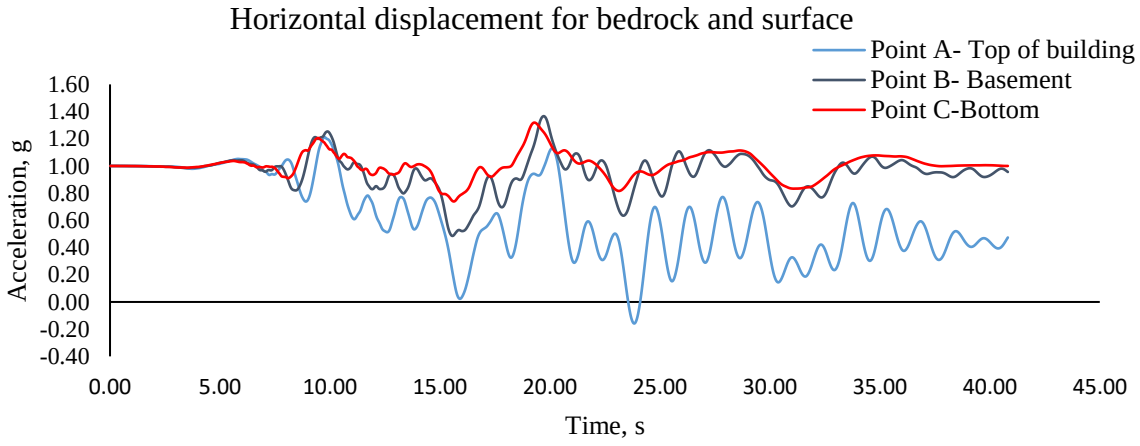

Appendix- 10 Horizontal displacement for bedrock, basement, and building top for Friuli input motion

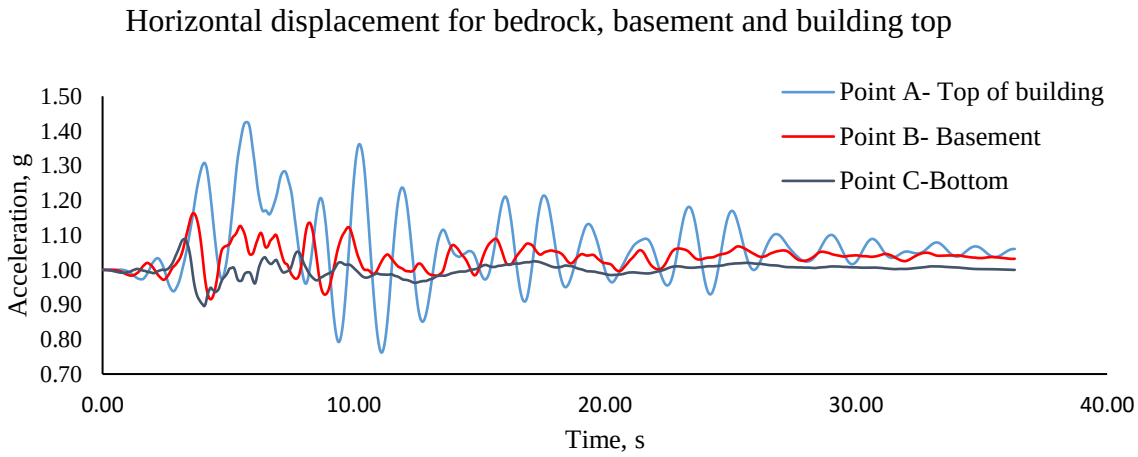

Appendix- 11 Horizontal displacement for bedrock, basement, and building top for Imperial Valley input motion

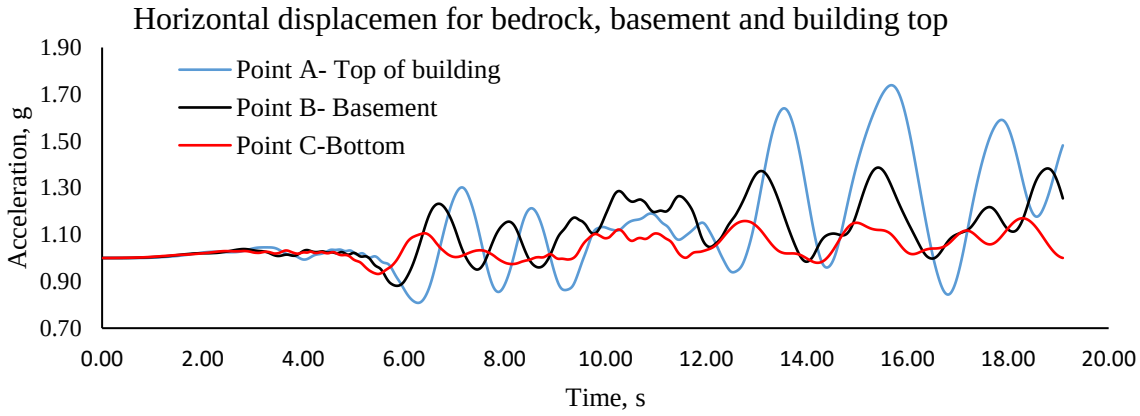

Appendix- 12 Horizontal displacement for bedrock, basement, and building top for Nahanni input motion

Appendix 7: Accelerograms and Horizontal Displacement Obtained from PLAXIS Analysis on a Shallow Foundation

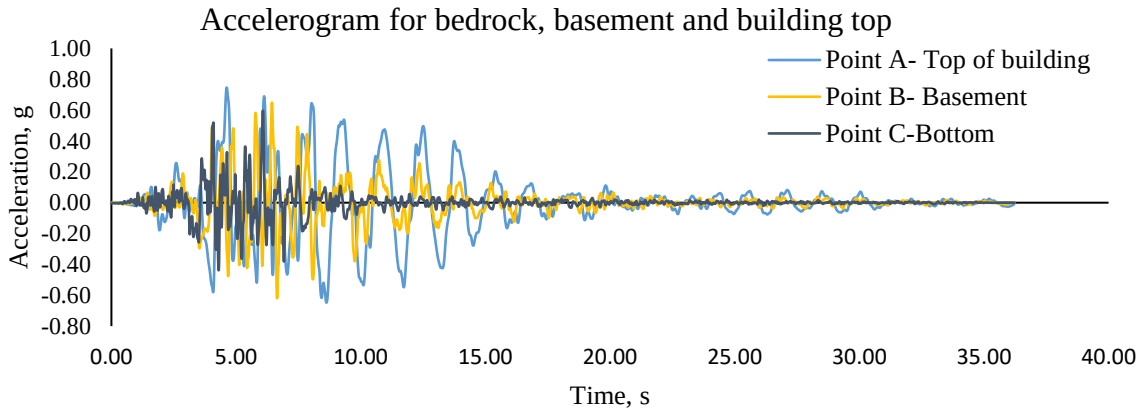

Appendix- 13 Accelerogram for bedrock, basement, and building top for Friuli input motion

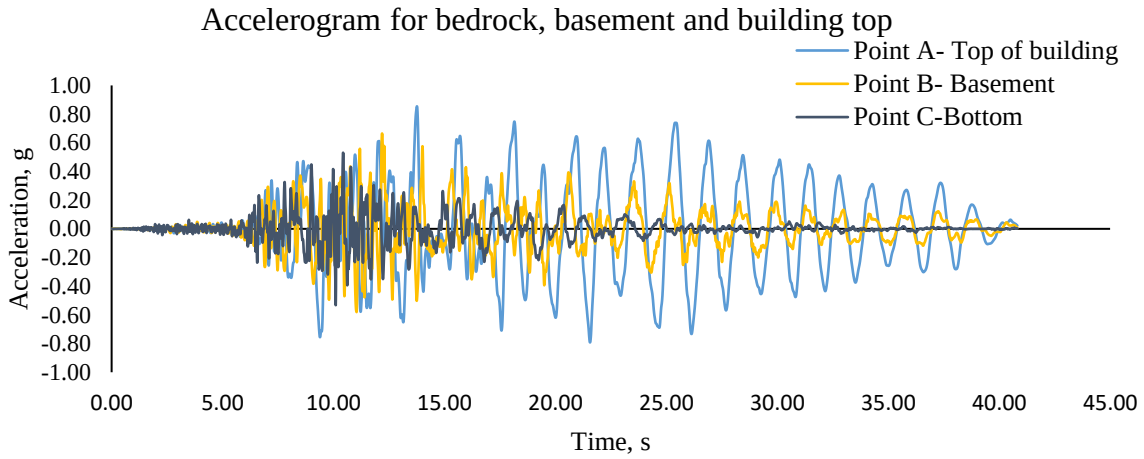

Appendix- 15 Accelerogram for bedrock, basement, and building top for Imperial Valley input motion

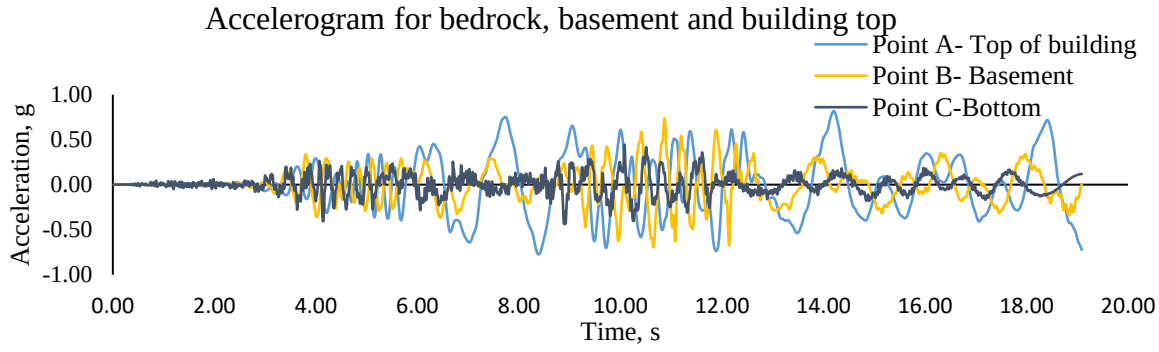

Appendix- 14 Accelerogram for bedrock, basement and building top for Nahanni input motion

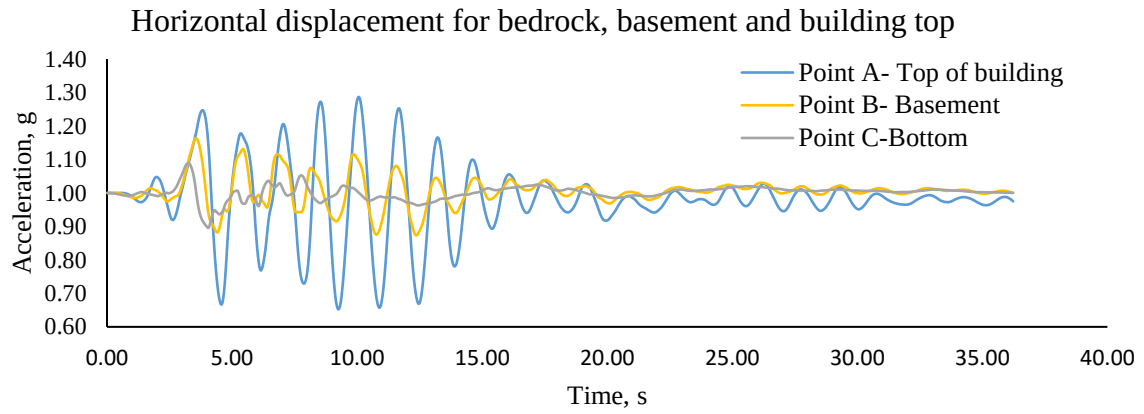

Appendix- 17 Horizontal displacement for bedrock, basement, and building top for Friuli input

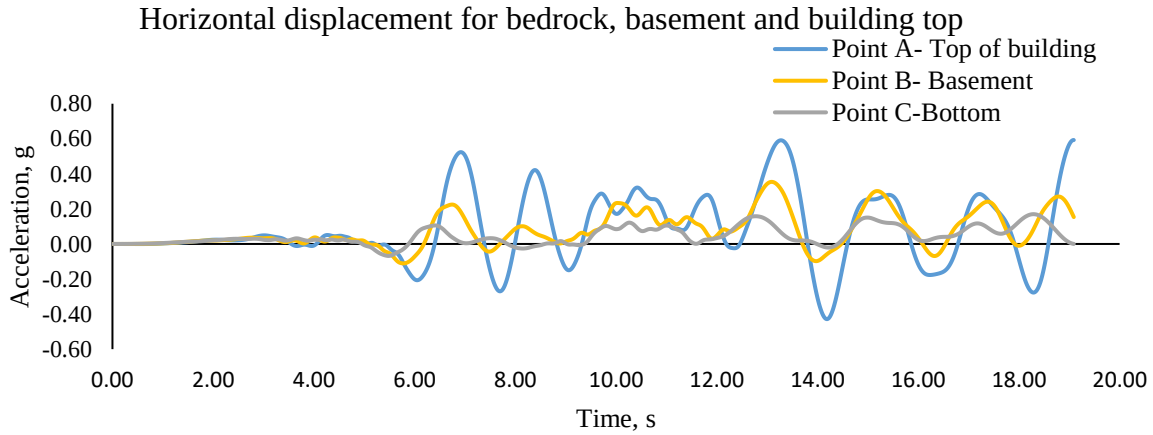

Appendix- 16 Horizontal displacement for bedrock, basement and building top for Imperial Valley input motion

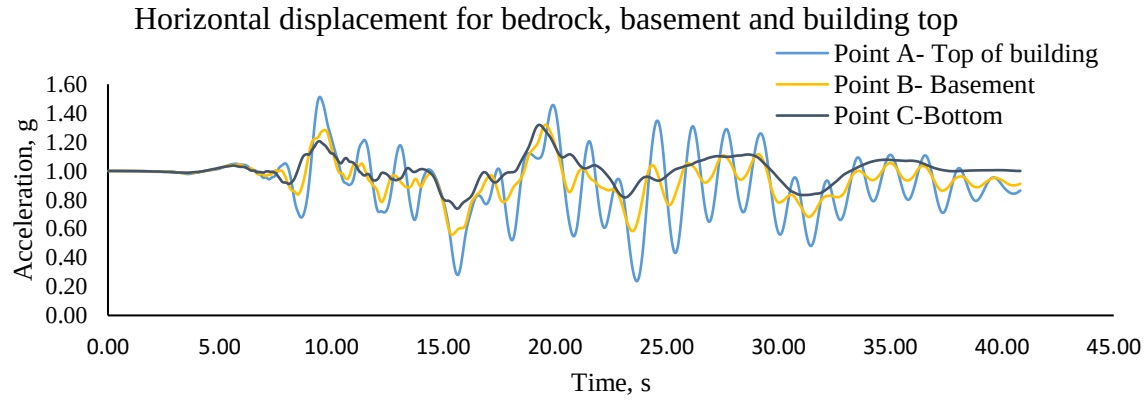

Appendix- 18 Horizontal displacement for bedrock, basement and building top for Nahanni input motion

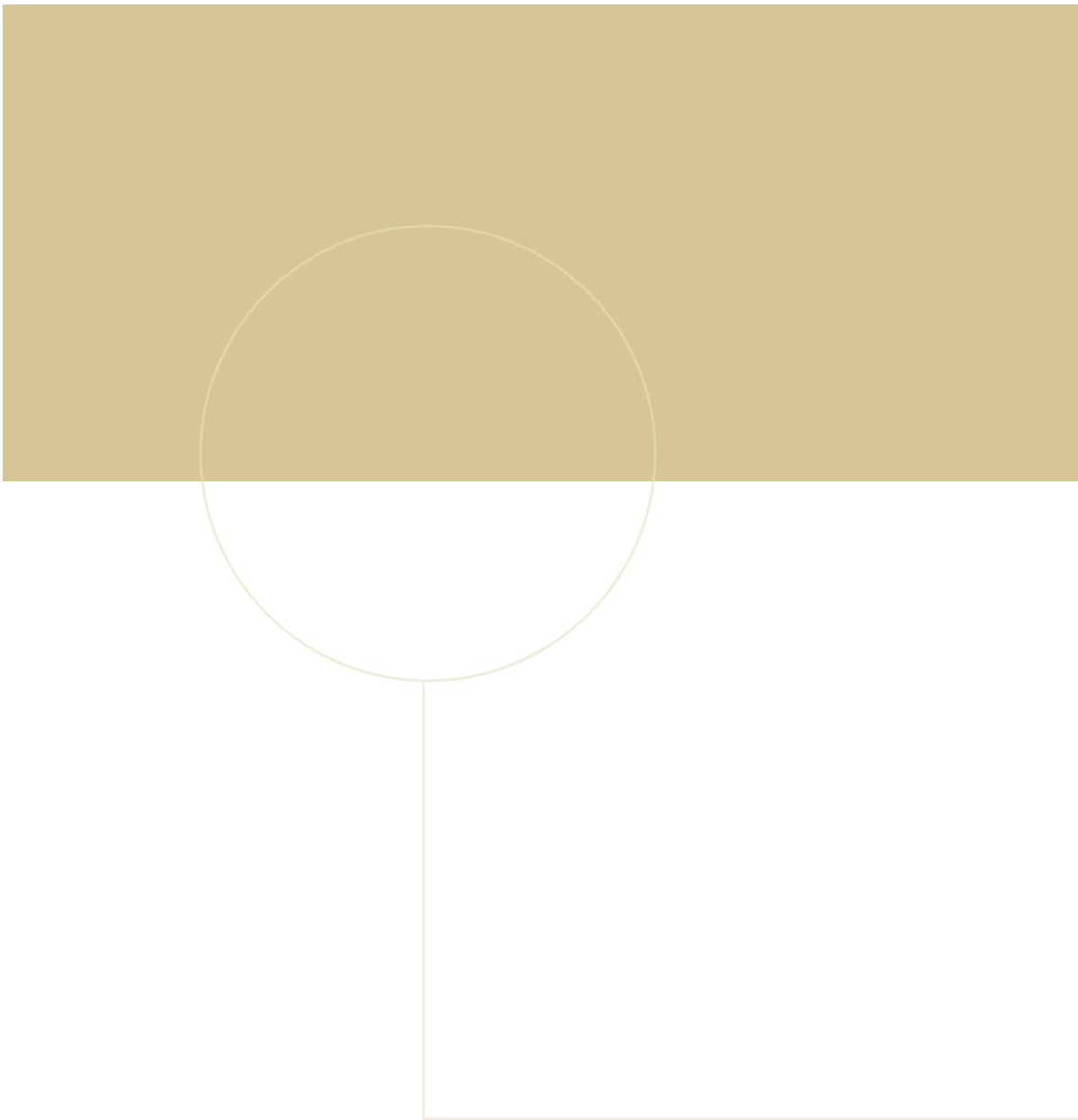

NTNU

Norwegian University of
Science and Technology